Emergent behaviors in microbial communities

by

Hyunseok Lee

Submitted to the Department of Physics
in partial fulfillment of the requirements for the degree of

Doctor of Philosophy in Physics

at the

MASSACHUSETTS INSTITUTE OF TECHNOLOGY

February 2023

Author .....
Department of Physics
November 22, 2022

Certified by .....
Jeff Gore
Professor
Thesis Supervisor

Accepted by .....
Lindley Winslow
Associate Department Head of Physics

Emergent behaviors in microbial communities

by

Hyunseok Lee

Submitted to the Department of Physics
on November 22, 2022, in partial fulfillment of the
requirements for the degree of
Doctor of Philosophy in Physics

Abstract

Physics of systems around us are often emergent, shaped by not only the fundamental constituents but their interactions, structures, and symmetries at larger scales. Microbial communities, which play indispensable roles in nature, are complex active systems that naturally pushes us to the unexplored frontier of emergent phenomena. During my PhD, I studied how some behaviors of microbial communities can be simple at emergent level despite the underlying complexity at microscopic level. First, I demonstrated that competition for resources may lead to the experimentally observed simplicity in community assembly. Even without microscopic information on the traits of microbes, trio and larger community assembly is often predictable from collections of pairwise competitions. Second, I demonstrated that slow mutants can take over expanding fronts and the resulting large-scale spatial pattern can be predicted without microscopic information. Overall, my works illustrate that, beyond qualitative explanations, we can make precise predictions for the behaviors of microbial communities without any information about microscopic details of the systems. This lens of emergent behavior allows us to discover simple descriptions of microbial communities at large scales unhindered by their complexities at small scales.

Thesis Supervisor: Jeff Gore
Title: Professor

Acknowledgments

I would like to thank Kwanjeong foundation for its financial support during early years of my PhD, and Henry W. Kendall scholarship for the support on my first year at MIT. This thesis would not have been completed if I were not lucky enough to meet many good people in the past years at MIT. My advisor Jeff has always been supportive. Even when I lost confidence in myself, Jeff's patient and confident support enabled me to keep working and realizing new possibilities from inside myself. Jeff have taught me not only microbial ecology but also the way how to do science, and I want to live up to this heritage as I stay in the academia. My thesis committee, Mehran and Nikta, have been crucial for this final step of my PhD and I sincerely appreciate their insights and efforts put into my thesis. My collaborator Kirill at Boston University has been my co-advisor, teaching me not only the theory and computation of population expansion but also how to do science. My labmates also have been crucial for my completion of PhD. My first officemates Clare and Anthony helped me getting through the transition as I initially joined the lab. My collaborators Clare, Blox, Martina, Akshit, and Sivan has been good friends and mentors and made the research enjoyable. My friends outside the lab including MIT PLS, Korean MIT graduate students, old friends from back in Korea and Caltech, and online neighbors for my blog, thank you for keeping in touch with me and supporting me even when I do not expect. My parents and brother in Korea, despite the shortage of my calls and messages I always miss you and this whole academic journey was impossible without you. Finally, my partner Jemma has been through all of this together and anything I accomplished during my PhD was based on her support. I know we will keep our journey together through whatever comes next, and I look forward to it.

Contents

Chapter 1

Introduction

1.1 Emergent phenomena and microbial community

Physics is often thought of as a search for the fundamental and universal laws. This was especially true in the first half of the 1900s with the birth of quantum mechanics, general relativity, and particle physics. Nevertheless, many physicists today do not focus on the smallest particles nor the entire universe. Instead they deal with the 'emergent phenomena' that happens at intermediate scales, such as hundreds of qubits or twisted graphene layers with thousands of carbon atoms. This is because, as pointed out in a famous article by a Nobel Laureate Philip W. Anderson 50 years ago, "More Is Different." [7] A large system may lose some symmetries of its constitutive systems or obtain a new one. A simple such example can be found in different phases of water. If we break down vapor, water, and ice to the level of a single molecule, they all become the same H_2O molecule. The immensely different behaviors of the three states originate not from the molecule itself but from how many molecules are arranged together. Therefore, understanding physics of systems around us (and what we may be able to invent) requires a holistic approach that considers not only the fundamental constituents but their interactions, structures, and symmetries at larger scales.

Biophysics is a subdivision of physics in which this concept of emergent phenomena is deeply engraved. While living systems are essentially collections of various

molecules, the particular way these molecules are arranged magically results in biological functions, conscience, and life itself [131]. Accordingly, life is an emergent phenomenon and to understand how it emerges is a central goal in biophysics.

While this field of the 'physics of life' has made significant progress over the past decades, there are a lot of questions that still remain unanswered. One major difficulty in biological physics is that many useful assumptions in conventional physics, such as the conservation of energy or thermodynamic equilibrium, no longer apply to biological systems. So a lot of effort has been put into not only studying the biological systems themselves but also inventing new theoretical and analytical tools that operate outside the realm of classical assumptions. Nevertheless, this challenge also implies that biophysics has provided a great opportunity for physicists to study the frontier of emergent phenomena where the systems' complexity defies traditional physics.

Microbial community is a particularly interesting instance of biological systems. Microbes are tiny living organisms that are too small to be seen with naked eyes, and yet they play indispensable roles in ecosystems across scales – from human gut microbiome keeping human health to marine microbiome maintaining geochemical cycles [44, 25, 99, 52, 69, 40, 14, 128, 140]. While their importance in nature is unquestionable, microbial communities also pose some interesting physics questions. Microbes are active with fast cell divisions and various modes of migration. Moreover, many microbial species coexist as a community, exchanging complex interactions mediated by acidity, contact, nutrient, toxin, and so on [95, 107, 23, 125, 83, 119]. And up to now, there is no well-established principle that governs such active and heterogeneous matter with diverse interactions. Thus, the microbial community naturally pushes us to the unexplored frontier of emergent phenomena, asking how we can ever describe collective behaviors of complex active systems.

During my PhD, I studied how some behaviors of microbial communities can be simple at emergent level despite the underlying complexity at microscopic level. In this thesis, I will discuss my two major projects which explained the simplicity emerging from competitions.

1.2 Microbial competition for resource: from diversity to patterns

Every organism needs to consume resources to survive, and microbes are no exception. Microbes require various resources such as carbon, nitrogen, and phosphate to maintain homeostasis and undergo cell division. At a larger scale, a population of microbes grows when there is sufficient resource available and perishes otherwise. Similarly, when multiple populations of microbes grow together, they compete for available resources and some may be driven extinct. This is the basic idea of microbial competition for resources. In this section, let us follow the historic development of this idea and see how my Ph.D. study contributes to the field.

Early studies of resource competitions in microbial ecology focused on a single ultimate question: why are microbial communities so diverse? Even in a very small volume of soil, we find thousands of microbial species coexisting together [66]. This highly diverse community is very puzzling, because theory of resource competition tells us that it is impossible. There is a classical 'competitive exclusion principle' that the number of species cannot exceed the number of resources [9]. The wide applicability of this theoretical principle conflicts with observed highly diverse communities. And this puzzle, 'paradox of plankton' remains a central topic in microbial ecology even up to today.

Nevertheless, the violation of the competitive exclusion principle is now accepted as a norm rather than a surprise. Studies have shown that various mechanisms including seasonality, spatial inhomogeneity, trade-off, and cross-feeding (microbes leaking out metabolites as they consume other resources) can potentially explain how the number of species may exceed the number of supplied resources [121, 30]. While the question still is pursued by many, it is now more a matter of choosing the most relevant explanation for a given diverse microcosm rather than solving the puzzle itself.

On the other hand, a relatively new trend in the field is toward understanding more than diversity. Beyond simply counting the number of species, these studies ask

how resources affect the composition of microbial communities. It is worth noting that this new direction bloomed upon the development of experimental techniques which enabled quantitative characterization of microbial communities, such as 16S ribosomal RNA sequencing.

One famous example of such study is Goldford et al. 2018 [51]. The authors sampled the microbial communities from soil and plants containing hundreds to thousands of sequence variants. The organisms were passaged after culture in low concentrations of single carbon sources and were cross-fed with each other's metabolites; then, the resulting communities were sequenced using 16S ribosomal RNA, and the outcomes were modeled mathematically. The mix of species that survived under steady conditions converged reproducibly to reflect the experimentally imposed conditions rather than the mix of species initially inoculated—although at coarse phylogenetic levels, taxonomic patterns persisted. The authors claimed this robustness of coarse-grained level composition as the 'emergent simplicity of microbial community assembly.'

1.2.1 My Ph.D. work on microbial competitions for resources

During my PhD, I have worked on several projects that involve microbial competitions for resources. In my early projects, I focused on how resource dynamics can explain the species diversity observed in laboratory experiments. In my later projects, I pursued how resource dynamics can explain not only how many but which species may survive in community assembly. While I will discuss one of my later projects in detail as it is directly related to the idea of emergent phenomena, here I will briefly discuss my PhD works on resource competition as a whole and the contributions I have made through them.

In my first paper, "Environmental fluctuations reshape an unexpected diversity-disturbance relationship in a microbial community" (2021 Elife) [96], I worked as a main theorist of the team and found how resource models can explain the observed non-monotonic trend in biodiversity as a function of disturbance. Environmental disturbances have long been theorized to play a significant role in shaping the diversity and composition of ecosystems. However, an inability to specify the characteristics

of a disturbance experimentally has produced an inconsistent picture of diversity-disturbance relationships (DDRs). Here, using a high-throughput programmable culture system, we subjected a soil-derived bacterial community to dilution disturbance profiles with different intensities (mean dilution rates), applied either constantly or with fluctuations of different frequencies. We observed an unexpected U-shaped relationship between community diversity and disturbance intensity in the absence of fluctuations. Adding fluctuations increased community diversity and erased the U-shape. All our results are well-captured by a Monod consumer resource model, which also explains how U-shaped DDRs emerge via a novel 'niche flip' mechanism. Broadly, our combined experimental and modeling framework demonstrates how distinct features of an environmental disturbance can interact in complex ways to govern ecosystem assembly and offers strategies for reshaping the composition of microbiomes.

In my second paper, "Resource-diversity relationships in bacterial communities reflect the network structure of microbial metabolism" (2021 Nature Ecology and Evolution) [30], I worked as a main theorist of the team and found how resource models can explain the observed linear trend in biodiversity as a function of supplied resources.The relationship between the number of available nutrients and community diversity is a central question in ecological research that remains unanswered. Here we studied the assembly of hundreds of soil-derived microbial communities on a wide range of well-defined resource environments, from single carbon sources to combinations of up to 16. We found that, while single resources supported multi-species communities varying from 8 to 40 taxa, mean community richness increased only one-by-one with additional resources. Cross-feeding could reconcile these seemingly contrasting observations, with the metabolic network seeded by the supplied resources explaining the changes in richness due to both the identity and the number of resources, as well as the distribution of taxa across different communities. By using a consumer–resource model incorporating the inferred cross-feeding network, we provide further theoretical support to our observations and a framework to link the type and number of environmental resources to microbial community diversity.

While both papers focused on biodiversity, the second paper addressed how the

trend in biodiversity could be understood better by looking at compositions of communities and how they are partitioned into generalists (consumes many resources) and specialists (prefers one resource). And in the paper that I will describe in Chapter 3, we focused on how community composition can be predictable under the framework of the resource competitions.

1.3 Microbial competition for space: complexity and simplicity

In ecology, the concept of space is at an interesting position: everyone believes it is important but only a few actually talk about it. While any ecosystem spans over a finite spatial scale, most ecology works consider time as the only dimension over which dynamics operate. This discrepancy is not a simple mistake of the field of ecology. In fact, it signifies a real challenge stemming from the highly context-dependent scale of spatial dynamics in ecology. Even for the restricted scope of microbial ecology, there are qualitatively different spatial behaviors that can result in different impacts of spatial dimensions.

The first case is the 'well-mixed' system in which the local communities are uniform over the space. Laboratory microcosms are often realized as a liquid culture with constant mixing, and these communities can be mostly homogeneous. Maybe for this reason, many experimental works do not consider spatial dimension and yet often manage to successfully explain their observations.

Second one is the 'motile' case, where each microbe is an active swimmer. In this case the spatial dynamics is faster than growth dynamics, and the movement of individuals can lead to non-uniform distribution of species over space via mechanisms such as chemotaxis (microbes moving toward higher nutrient concentration) [72]. Such dynamics may be dominant in swarming of bacteria, bacteria in microfluidic channels, and liquid culture without mixing. The resulting dynamic or inhomogeneous distribution of species can open up some new possibilities and lead to interesting

phenomena such as violation of the competitive exclusion principle.

Third one is the 'non-motile' case, in which each microbe does not move. In this case, unlike individuals, the whole population may still move as birth and death of microbial cells involve changes in the space that the cells occupy. For example, even on a hard surface on which each microbe is not motile, microbial colonies can expand via mechanical pushing between cells as the cells reproduce.

It is not easy to determine the impact of spatial competitions in nature. For example, in the gut microbiome, all three modes of spatial competitions may be expected: while the gut is constantly mixed, some motile bacteria there are known to drag along other non-motile bacteria, and different parts of the gut are colonized by different sets of species.

Overall, the multifaceted nature of spatial competition suggests that it adds another layer of complexity to the behavior of microbial communities. Indeed, addition of space is known to break some constraints from well-mixed assumptions and open up new possibilities for microbial communities. A well-known such example is the competitive exclusion principle that we discussed earlier. Spatial heterogeneity in the resource supply can allow more species than resources to coexist across multiple spatial patches. Also, space introduces additional traits of microbes such as motility and migration rate to affect competition outcomes. In this sense, while the impact of space is highly variable between conditions, one may expect that space generically leads to more complex behaviors of microbial communities.

In fact, this expectation does not always hold: space can sometimes make competitions simple. Especially in the expansion of microbial population into empty space, competition outcomes are often determined by a single trait of each species, the expansion speed. This simplicity originates from two mechanisms. First, a mixed microbial population tends to segregate into monoclonal sectors as it expands because of demographic fluctuations [57]. As the tips of expanding fronts have a small population size, demographic fluctuation easily drives local population at each point of the fronts to absorbing states of monoclonal population. This implies that the population away from boundaries between sectors do not experience interspecies interactions that

can involve various molecular mechanisms. Second, faster expanders can have better access to expanding front, and since the frontier provides better access to untouched resources, the advantage of faster expanders can be further amplified and they may sweep the expanding front [82, 142, 13, 134, 149, 76, 164, 45, 112, 133, 33].

This idea that fast expanders generically take over the expanding front has consistently reappeared across theoretical, experimental, and field study literatures. In comparison, fast growers in a well-mixed environment often go extinct because of their disadvantage in interspecies interactions, potentially emerging from tradeoffs between different traits [4]. Overall, while one may expect microbial competitions in space to be complex, the space can make them simpler in some perspective.

One important question left was whether fast expanders should always take over the front. And my work was the first experimental demonstration of slow expanders taking over the expanding front. In addition, I quantitatively predicted the shape of the slow expander's sector during its takeover using the emergent simplicity of large-scale patterns. I will discuss this work in more detail in Chapter 2.

Chapter 2

Resource competition explains simplicity in microbial community assembly

2.1 Overview

The work covered in this chapter is now in revision for PNAS. In this project, I worked with another graduate student Blox Bloxham and professor Jeff Gore to explain the relationship between previously discovered empirical 'Assembly rule' and resource dynamics modelling framework. competition for resources may lead to the experimentally observed simplicity in community assembly. As the first author of the paper, I conceptualized the study, performed theory calculations, ran simulations, and wrote manuscript.

Predicting the composition and diversity of communities is a central goal in ecology. While community assembly is considered hard to predict, laboratory microcosms often follow a simple assembly rule based on the outcome of pairwise competitions. Despite the empirical success of this bottom-up prediction, its mechanistic origin has remained elusive. In this study, we elucidate how resource competition can lead to simple patterns in community assembly. Our geometric analysis of a consumer-

resource model shows that trio assembly is always predictable when some species grow faster than another species on every resource. We also identify all trio assembly outcomes under three resources and find that only two outcomes violate the assembly rule. Simulations demonstrate that pairwise competitions often accurately predict trio assembly with up to 50 resources. We further show that this predictability holds for communities larger than trio and with cross-feeding between species. Our findings highlight that simple community assembly can emerge even in ecosystems with complex underlying dynamics.

2.2 Introduction

Microbes coexist in complex, multi-species communities across scales. On a small scale, the microbiome affects health and disease of its hosts, including humans [44, 25, 99, 52, 69]. On a large scale, microbial communities play crucial roles for Earth's biogeochemical cycles in oceans and soil [40, 14, 128, 140]. Understanding assembly of these communities (i.e. which species coexist and why) is a central goal in ecology that can impact agriculture, planetary science, and human health [54, 46, 157]. Predicting assembly is, however, a challenging problem: communities often have many species that interact in diverse ways, and characterizing all the potentially relevant interactions can be practically impossible [95, 107, 23, 125, 83, 119]. Similarly, theorists have found that community assembly prediction is an inherently difficult problem [35, 154, 126]. Even in simple models (e.g Lotka-Volterra model) it is difficult to construct empirical rules for community assembly, and various mechanisms such as beyond-pairwise interactions, stochasticity, and priority effects reinforce the unpredictability [156, 159, 15, 64, 50, 88, 105, 161, 115, 68]. In the end, both simple intuition and rigorous theory expect community assembly to be hard to predict. Surprisingly, observed microbial community assembly is often predictable [151, 138, 47, 52, 152, 2, 114, 49]. In particular, the assembly outcome in laboratory microcosms from an initially diverse species pool can be determined bottom-up from pairwise competitions among the species. This 'assembly rule' has

been tested in both well-mixed culture as well as in the intestine of the worm C. elegans, and also as the environment changes due to variation in dilution rate and temperature [47, 4, 84, 3, 102]. The assembly rule predicts that species A will exclude species B in community assembly if A excludes B in pairwise competition [47] (Fig. 2-1A). The rule's frequent experimental success highlights how, despite the expected complexity, community assembly can be surprisingly simple. Yet the condition for simplicity remain unclear because the assembly rule, being purely empirical, does not provide deeper explanations for why it works nor when to expect violations. A possible mechanistic origin for the empirical assembly rule is a crucial missing piece toward a better understanding of community assembly and its predictability. Competition for resources is a ubiquitous mechanism that often drives microbial community dynamics; for example, many studies have revealed how community composition depends on resource composition supplied to the environment [9, 158, 51, 49, 30, 116]. In models of resource competition, the interspecies interactions are mediated by the uptake (and potential release) of resources, introducing potentially complex dynamics and the emergence of "higher-order" interactions between species [105, 88, 113]. However, the same growth parameters govern both pairwise competitions and multispecies competitions (Fig. 2-1B). This implies the possibility of an emergent mapping between their outcomes. In this way, a bottom-up prediction from pairwise competitions to larger community assembly may be formulated under the framework of resource competition. Elucidating this bottom-up correspondence would shed light on the unexplained simplicity in community assembly (Fig. 2-1C) Here, we demonstrate that the emergent mapping between pairwise competitions and community assembly under resource competition nearly always agree with the empirical assembly rule. We first analyze a resource competition model with geometric principles and find that trio assembly always follows the assembly rule unless every species grows faster than a competitor on some resource. Moreover, we identify all possible combinations of pairwise and trio outcomes under resource competition for three resources and show that only two combinations violate the assembly rule. To verify this theoretical analysis and extend it to larger number of resources, we perform simulations of trio commu-

nities with up to 50 resources. Regardless of the number of resources, simulations of resource competition agree with the assembly rule prediction of species survival with over 90% accuracy and the list of outcomes agree with our geometric analysis. Furthermore, simulations with larger communities and with cross-feeding between species continue to be predictable by the assembly rule. Our results highlight that a complex system with many microscopic parameters can nevertheless lead to simple community assembly.

2.3 Results

2.3.1 Resource model leads to a simple mapping from pairwise outcomes to community assembly

To study community assembly under resource competition, we focus on a chemostat-like linear resource consumption model, which is a variation of MacArthur's consumer-resource model with an external resource supply and universal dilution rate [94, 89, 145, 30] (Methods). The model assumes that per-capita growth rate is the sum of growth on each resource, which is proportional to concentration of the resource. The model dynamics are:

$$\begin{aligned} \dot{n}_\mu &= \sum_{i=1,2,\ldots} r_{\mu i} c_i n_\mu - \delta n_\mu, \\ \dot{c}_i &= -\sum_{\mu=A,B,\ldots} \frac{r_{\mu i}}{Y_{\mu i}} n_\mu c_i + \delta(c_i^s - c_i), \end{aligned} \tag{2.1}$$

where n_μ is the population density of species μ, c_i is the concentration of resource i in the media, $r_{\mu i}$ is the contribution of resource i to the per-capita growth rate of species μ, $Y_{\mu i}$ is the biomass yield of species μ on resource i, δ is the dilution rate in chemostat which controls both universal mortality and resource supply rate, and c_i^s is the external supply concentration of resource i. In this paper, we will assume that relative biomass yields between resources are the same for all species (i.e. $Y_{\mu i} = a_\mu y_i$). Under this assumption, each competition converges to a single equilibrium independent of initial

population densities (i.e. multi-stability is not possible).

The population dynamics under this model have been studied using a graphical approach in the space of resource concentrations [143, 89, 98]. This approach utilizes each species' Zero Net Growth Isocline (ZNGI), which is the set of resource concentrations for which growth of a species exactly keeps up with the dilution rate (Fig. 2-2). Notably, the equilibrium resource concentration satisfies two geometric principles. First, equilibrium concentrations must lie on the innermost ZNGIs such that all species' populations are either constant or going extinct. A species survives if the equilibrium resource concentration is on its ZNGI. Second, for resource consumption to balance supply, the supply must fall within the convex hull of the surviving species' resource consumptions at the equilibrium [121]. Geometrically, this can be determined by drawing resource consumption vectors originating from all ZNGI intersections (Fig. 2-1B). The first principle dictates whether species can ever coexist, and the second principle tells whether they coexist under a particular resource supply. Fig. 2-1B illustrates these geometric principles for pairwise and trio competitions. Between species A and species B, A's ZNGI is always inside B's ZNGI, so, by the first geometric principle, if only A and B are present any fixed point will have A surviving and B being driven extinct. By contrast, both A and C's ZNGIs and B and C's ZNGIs intersect, so the first principle suggests both these pairwise competitions may lead to coexistence. However, the second geometric principle now becomes relevant: the resource supply lies between A and C's consumption but not between B and C's consumption. Thus, while A and C coexist, B and C cannot because no population composition can balance the resource supply and keep the resource concentrations at the intersection of B and C's ZNGIs. In the trio competition, the same two principles apply: B cannot survive because its ZNGI is never one of the innermost while A and C again coexist because the resource supply lies between their resource consumption. This trio outcome also matches the assembly rule. The graphical approach identifies conditions for resource competition to follow the assembly rule. Remarkably, for trio communities, resource competition outcomes always match with the assembly rule predictions when not all the ZNGIs cross. For example, when A's ZNGI is below B's

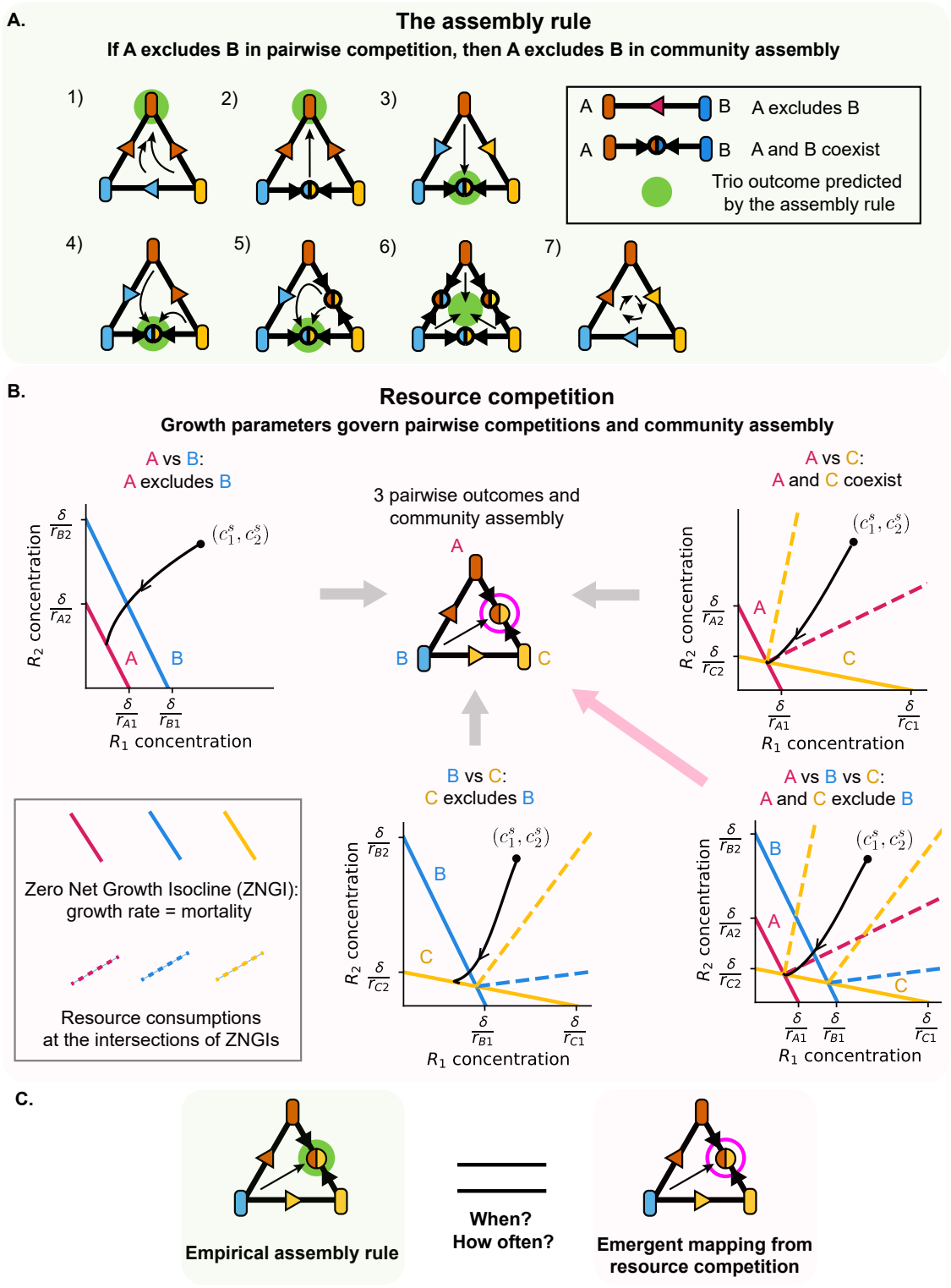
A.
The assembly rule
If A excludes B in pairwise competition, then A excludes B in community assembly
1)
2)
3)
4)
5)
6)
7)
A B A excludes B
A B A and B coexist
Trio outcome predicted by the assembly rule
B.
Resource competition
Growth parameters govern pairwise competitions and community assembly
A vs B:
A excludes B
3 pairwise outcomes and community assembly
A vs C:
A and C coexist
B vs C:
C excludes B
A vs B vs C:
A and C exclude B
R_2 concentration
R_1 concentration
(c_1^s, c_2^s)
Zero Net Growth Isocline (ZNGI): growth rate = mortality
Resource consumptions at the intersections of ZNGIs
C.
Empirical assembly rule
When?
How often?
Emergent mapping from resource competition

Figure 2-1

Figure 2-1: Assembly rule may emerge from resource competitions. (A) Assembly rule predicts trio competition outcomes based on pairwise competition outcomes. The assembly rule predicts that if species A excludes species B in pairwise competition then A excludes B in community assembly. Equivalently, the assembly rule assumes that a species invades a community if and only if it can invade every member of the community. The rule predicts exactly one trio outcome for each combination of pairwise competitions except for the rock-paper-scissors case for which no trio outcome is predicted. (B) In resource competition models, growth parameters govern both pairwise competitions and community assembly. Each competition is represented in the space of resource concentrations using ZNGIs (Zero Net Growth Isocline: the set of resource concentrations on which a species' growth rate equals its mortality rate and thereby the species maintains a nonzero population size) and resource consumptions at the intersections of ZNGIs (i.e. lines from each intersection $(c_1^{\int}, c_2^{int})$ in the direction of $(\frac{r_{\mu 1}}{Y_{\mu 1}} c_1^{\int}, \frac{r_{\mu 2}}{Y_{\mu 2}} c_2^{int})$. The black dots represent resource supply (c_1^s, c_2^s) and the black curves represent trajectories of resource concentrations until the population reaches an equilibrium. Under this graphical representation, equilibrium concentrations must lie on the innermost ZNGIs and resource consumption must balance with resource supply at equilibrium. Followingly, for the illustrated example, A excludes B (top left), A and C coexist (top right), C excludes B (bottom center), and in trio competition A and C exclude B (bottom right). Finally, all the three pairwise outcomes and community assembly are represented on a simplex (top center). Geometric analysis of each competition is detailed in Results. Notably, this trio community follows the assembly rule. (C) The emergent mapping from resource competition in Fig. 1B agrees with the assembly rule. Elucidation on when and how often this agreement holds may explain the origin of simple empirical rule's successful predictions.

ZNGI without crossing, then A excludes B in both pairwise competition and community assembly. This is a sufficient condition for the assembly rule to be obeyed in any trio that contains A and B. Fig. 2-2A illustrates this agreement: while both pairwise and trio competition outcomes shift depending on the resource supply, every set of pairwise and trio outcomes follow the assembly rule.

Resource competition outcomes can violate the assembly rule when all ZNGI pairs cross. In Fig. 2-2B, while the assembly rule is obeyed for most resource supply concentrations, a few violations are permitted. In the violation V1 (with two coexisting pairs and one excluding pair), species A and C survive while the assembly rule expects B to survive instead of A. While B excludes A in pairwise competition, because A's and B's ZNGIs cross, A could exclude B under a different resource supply. By coexisting with C, A maintains the resource concentration on which it outgrows B, resulting in an unexpected trio outcome. Similarly, in the other violation V2 (with three coexisting pairs), species A and C survive while the assembly rule expects A, B, and C to all coexist. As in the previous case, by coexisting, A and C both maintain the resource concentration on which they outgrow B, resulting in the unexpected exclusion of B. In fact, when all pairs coexist in a two-resource environment their community assembly always results in a two-species survival, unless parameters are fine-tuned to have a mutual intersection of all ZNGIs [121]. More generally, all-species coexistence requires all-pair coexistence but not vice versa (Fig. S2). Overall, these violations highlight that resource competition inherently involves higher-order interactions; interaction between a pair can be altered by the third species as it modifies the resource environment.

So far, we have investigated how resource competitions among some trios may follow or violate the assembly rule depending on the resource supply. Extending this procedure to all possible trios and resource supplies would identify the complete list of resource competition outcomes (Fig. 2-3A). While this may sound formidable, there are only a few topologically distinct ways that 3 ZNGIs can intersect. By enumerating all the possible phase diagrams, we identify all pairwise and trio outcomes under two and three resources (Fig. 2-3B, SI Appendix I & II). Interestingly, the only possible

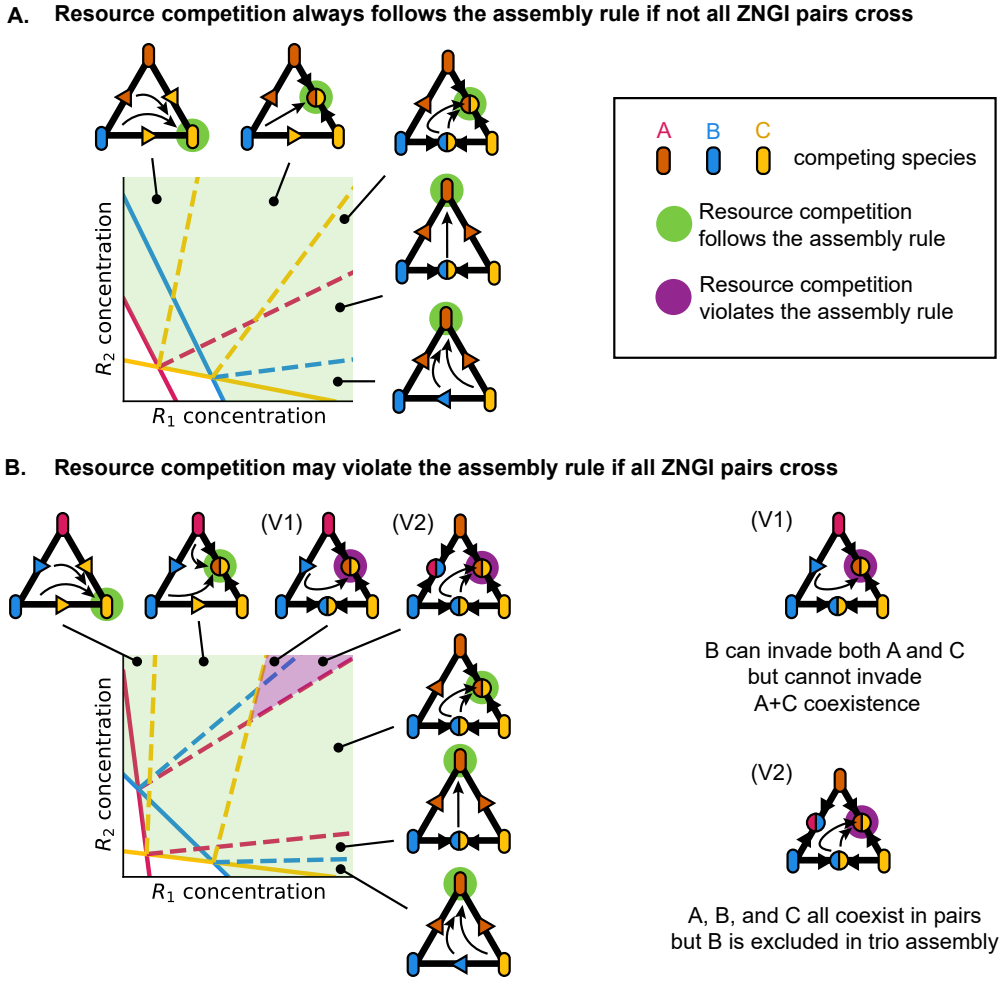
A. Resource competition always follows the assembly rule if not all ZNGI pairs cross
R_2 concentration
R_1 concentration
A B C
competing species
Resource competition follows the assembly rule
Resource competition violates the assembly rule
B. Resource competition may violate the assembly rule if all ZNGI pairs cross
(V1)
(V2)
R_2 concentration
R_1 concentration
(V1)
B can invade both A and C but cannot invade A+C coexistence
(V2)
A, B, and C all coexist in pairs but B is excluded in trio assembly

Figure 2-2

Figure 2-2: Geometric analysis of resource competition model reveals the conditions for assembly rule agreement and violation. (A) Resource competition of trio community always follows the assembly rule if not all ZNGI pairs cross. In the illustrated example, species A's ZNGI is inside species B's ZNGI. Then A always outgrows B under any resource concentration, and thus B is excluded by A in both pairwise competition and community assembly. As a result, the community assembly follows the pairwise competition between A and C, and the assembly rule is always obeyed. In the illustrated example, while competition outcomes shift as the resource supply changes, each combination of pairwise and trio outcomes under any resource supply follows the assembly rule (Fig. S1). (B) Resource competition of trio community may violate the assembly rule if all ZNGI pairs cross. In the illustrated example, each pair's ZNGIs intersect. Then any species can outcompete its competitor at some resource concentration, and a third species may shift the competition outcome between a pair by modifying the resource environment. The illustrated example exhibits two violations (Fig. S1). In the violation V1 (with two pairwise coexistence and an exclusion), A and C survive in the community assembly while the assembly rule expects B to survive instead of A. By coexisting with C, A maintains the resource concentration on which it outgrows B, which results in the unexpected exclusion of B in community. In the violation V2 (with three pairwise coexistence), only A and C survive while the assembly rule expects all A, B, and C to survive. As in the previous case, by coexisting, both A and C maintain the resource concentration on which they outgrow B, resulting in the unexpected exclusion of B. In a generic resource competition, all-species coexistence requires all-pair coexistence but not vice versa (Fig. S2).

violations of the assembly rule are the two previously identified cases (Fig. 2-2B). All other resource competition outcomes follow the assembly rule. The list of possible resource competition outcomes has several notable features (Fig. 2-3C). First, resource competition can realize every outcome predicted by the assembly rule. Second, while resource competition can violate the assembly rule, both violations have been experimentally observed [47]. Strikingly, one of the two violations in the model (two-species survival under all-pair coexistence) is the most frequently observed violation in experiments [47]. Third, resource competition excludes many possible assembly rule violations, including the violations allowed under the Lotka-Volterra model [165]. In addition, rock-paper-scissors pairwise outcome, for which assembly rule prediction does not exist, is impossible in our resource competition model. In the end, the overall agreement between resource competition and the assembly rule prediction suggests that resource competition often results in simple community assembly.

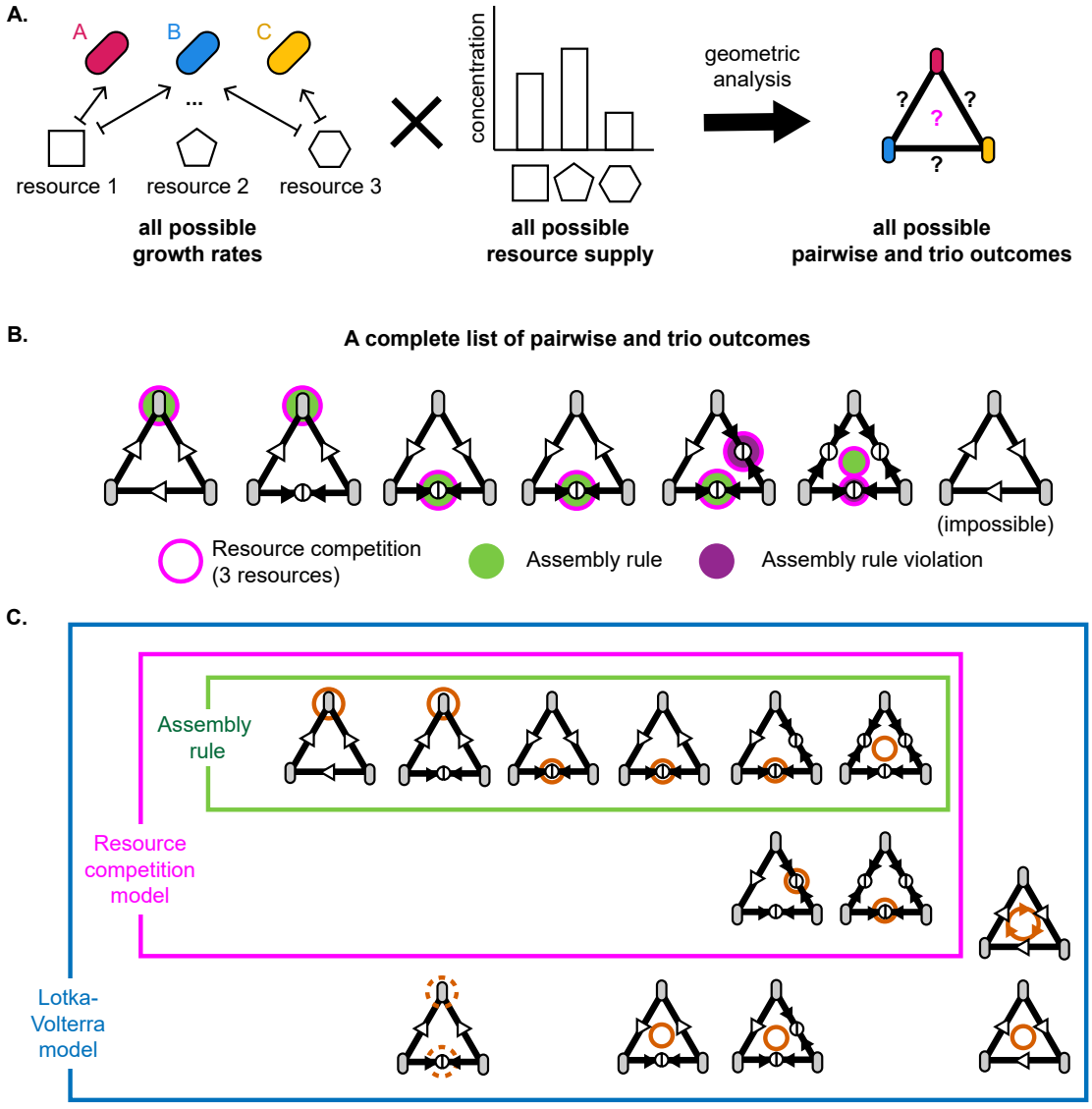

Figure 2-3: A complete list of pairwise and trio outcomes under resource competition for three resources. (A) We find all possible pairwise and trio outcomes under resource competition by investigating outcomes under all possible growth rates and resource supply. Geometric analysis simplifies this procedure because there are only a few distinct arrangements of ZNGIs under 1, 2, and 3 resources. (B) A complete list of pairwise and trio outcomes under resource competition for three resources (SI Appendix I & II). (C) Trio outcomes under the assembly rule, resource competition model, and Lotka-Volterra model. Dotted circles imply bistable community assembly. Resource competition model can lead to all assembly rule predictions plus only two assembly rule violations. Rock-paper-scissors pairwise outcome, for which assembly rule prediction does not exist, is impossible in our resource competition model.

2.3.2 Resource competition in complex ecosystems often follows the assembly rule

To augment the geometric analysis of resource competition under two and three resources, we simulated resource competition across different numbers of supplied resources from 1 to 50 (Fig 2-4A, Methods). We compared the simulated community assembly with three different predictions: 'Everyone survives' that always predicts all three species to survive, 'Fastest grower survives' that predicts the best grower under the resource supply to exclude other two species, and the assembly rule (Methods). Overall, the assembly rule agreed remarkably well with the simulated resource competition for any number of supplied resources, with prediction accuracy above 90% (Fig 2-4B). When only one resource was supplied, the fastest grower excluded all other species, and the assembly rule was always successful (Fig 2-4C). In the other limit, where 50 resources were supplied, the number of available niches became much greater than the number of species. Therefore, species mostly survived in all pairwise and trio competitions, and the assembly rule was again successful. In the end, the assembly rule worked almost perfectly on both few-resource and many-resource limits. With an intermediate number of supplied resources, resource competitions no longer perfectly agreed with the assembly rule. However, any simulated violation was one of the two outcomes expected from our geometric analysis, suggesting that increasing the number of supplied resources did not enable new unexpected outcomes (Fig. S3). Similarly, violations never occurred when some ZNGI pairs did not cross (Table S1). Moreover, even when violations occurred, the average agreement between the assembly rule and resource competition never dropped below 90% (minimum at 10 resources, with accuracy 90.13% $\pm$ 0.01%, SEM, N=500). This uniformly high accuracy of the assembly rule prediction highlights the simplicity and predictability of resource-competing communities.

In addition to competition for many resources, we also considered another axis of complexity: competition among more than three species. We note that the assembly rule is applicable to communities larger than trio (Fig 2-5A). We simulated commu-

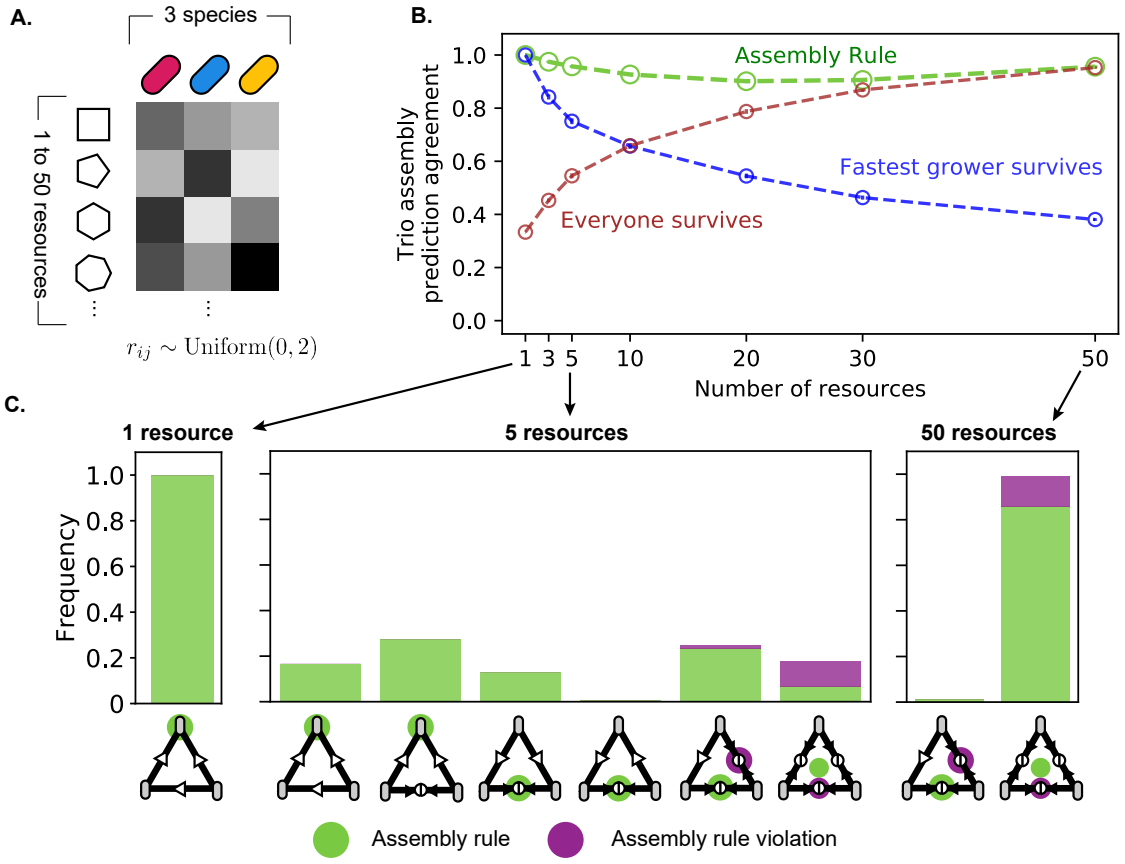

Figure 2-4: Simulations of resource competition typically followed the assembly rule. (A) We simulated resource competition of trio community under variable number of resources from 1 to 50. The growth rates were sampled from a discretized uniform distribution from 0 to 2 (Methods). (B) In simulations, community assembly often followed the assembly rule. We compared the simulated resource competitions with three different predictions: in addition to the assembly rule, 'Everyone survives' always predicts all three species' survival, and 'Fastest grower survives' predicts the best grower under the resource supply to exclude other two species. We quantified prediction agreements by fraction of species in each trio that matched each prediction. Overall, across all numbers of supplied resources, the agreement between resource competition and the simple assembly rule was maintained above 90%. 'Fastest grower survives' prediction failed in many-resource regime and 'Everyone survives' prediction failed in few-resource regime. (C) Distributions of simulated outcomes under 1, 5, and 50 supplied resources. The bar plots show observed frequency of each set of pairwise outcomes and community assembly. Community assembly that followed the assembly rule is marked in green, and violations are marked in violet. With single supplied resource, fastest grower on the single resource excluded others in all competitions. With 5 supplied resources, the outcomes became diverse and the assembly rule was no longer perfect. Nevertheless, simulations agreed with geometric analysis; all expected outcomes including the two violations were observed, and no unexpected outcome was observed (Fig. 2-3B). With 50 supplied resources, due to the large number of available niches, species almost always coexisted in both pairwise and trio competitions. Simulations with other numbers of supplied resources showed the same trend (Fig. S3).

nity assembly among 3, 5, 7, and 10 species along with the corresponding pairwise competitions (Fig 2-5B). Despite the substantial increase in complexity, the communities assembled under resource competition continued to closely match the assembly rule prediction (Fig 2-5C). Even in the most complex simulations of 10 resources and 10 species, species survival in the resource competition simulations agreed with the assembly rule prediction with a high accuracy (81.46% ± 0.01%, SEM, N=500). This agreement highlights how a model with hundreds of parameters, representing an ecosystem with highly complex consumer-resource interactions, still leads to predictable community assembly that follows a simple and experimentally established rule.

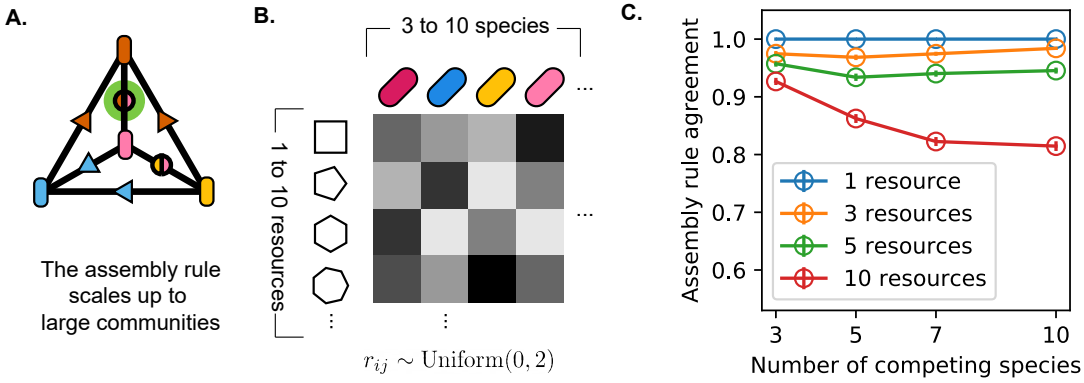

Figure 2-5: Resource competition of multispecies communities often follow the assembly rule. (A) Assembly rule scales up to large communities. For example, in the illustrated 4-species competition, since species B and C are both excluded by A in pairwise competitions, they are also excluded in 4-species competition. (B) We simulated resource competition of variable number of species (from 3 to 10) under variable number of resources (from 1 to 10). The growth rates were sampled from a discretized uniform distribution from 0 to 2 (see Methods) (C) Resource competitions of multispecies communities often followed the assembly rule. Even when 10 species competed for 10 resources, despite the complexity with a large number of microscopic parameters (100 growth rates and 10 supply resource concentrations), the assembly rule worked with 81.46% accuracy (± 0.01%, SEM, N=500).

2.3.3 Community assembly in the presence of cross-feeding typically follows the assembly rule

So far, we have assumed that species always consume resources and thereby all interactions are antagonistic. In nature, however, microbes often produce metabolic byproducts that are consumed by another species. This cross-feeding increases the number of available niches and increases the number of species that could potentially coexist in community [66, 94, 9, 51, 93]. To test whether simplicity and predictability in assembly are maintained under the presence of cross-feeding, we implemented conversions from one resource to another that are proportional to consumption of the first resource (Fig 2-6A, Methods). We also assumed that the cross-feeding reduces the efficacy of the first resource as its energy content is leaked out [51]. The link between each resource pair was established with probability p, and l is the conversion rate from consumption of a complex resource to production of a simpler "metabolite" resource (Fig 2-6B, Methods). As cross-feeding became stronger, the number of species surviving in community assembly tended to increase due to the creation of additional niches (Fig 2-6C). Compared to the case where all 10 resources are externally supplied, a cross-feeding community could reach the same biodiversity with sufficiently large cross-feeding strength l. Also, as l increased, the assembly rule agreement of communities with cross-feeding approached to the case where all 10 resources were externally supplied (Fig 2-6D). Overall, assembly rule prediction accuracy stayed above 90% (minimum at l=0.4, prediction accuracy 91.73% $\pm$ 0.01%, SEM, N=500). Thus, the simplicity of community assembly under resource competition was maintained even when cross-feeding complicated the underlying dynamics.

2.4 Discussion

In this study, we demonstrated that competition for resources may lead to the experimentally observed simplicity in community assembly. Trio assembly is always predictable from pairwise competitions if a species grows better than another species

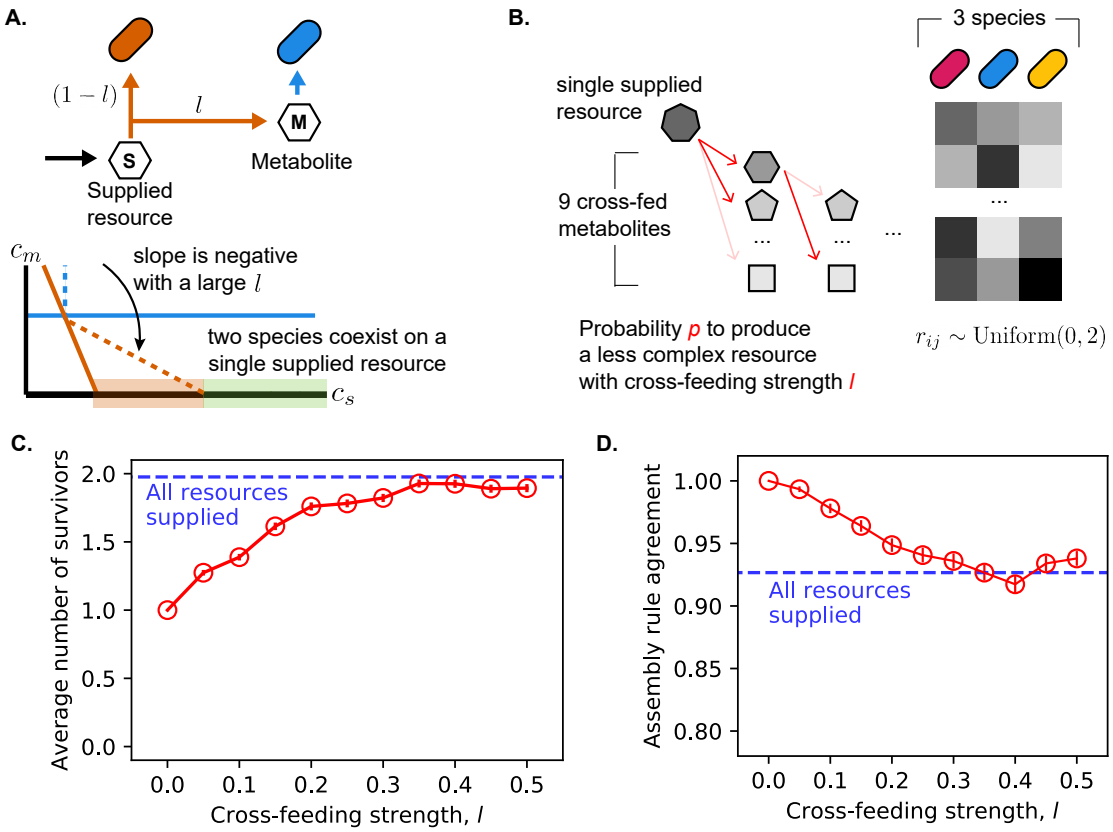

Figure 2-6: Resource competition with cross-feeding is often simple. (A) Cross-feeding enables coexistence of two species under single supplied resource. As a species consumes a resource, fraction l of the resource can be leaked out as metabolic byproducts which others can consume. This increases the number of niches in the environment and allows for more species to coexist. (B) We ran simulations of trio competing under cross-feeding. Only the most complex resource was supplied, but cross-feeding could allow coexistence as 9 other resources could appear as metabolites. Each trio shared a cross-feeding network in which each resource may cross-feed simpler resources with probability p and cross-feeding strength l (see Methods). For simplicity, we fixed $p = 0.5$ and varied l in simulations. (C) Number of survivors in trio competitions increased with cross-feeding strength. With $l = 0$, only one species survived in trio competition as expected. The number of survivors could reach, but could not exceed, the number of survivors with all 10 resources being supplied. (D) Prediction accuracy of the assembly rule was still high for cross-feeding communities. The prediction accuracy could approach, but could not be significantly lower than, the prediction accuracy with all 10 resources being supplied.

on every supplied resource. Otherwise, resource competition may violate the assembly rule, but only via two rare and specific scenarios. This predictability holds for communities with large number of species and resources and in the presence of cross-feeding. The simplicity that emerges from our resource competition model is at odds with the model's complexity. Compared to the Lotka-Volterra model with 6 pairwise interactions for a trio, our resource competition model for multiple resources has more parameters and allows for higher-order interactions in which a third species affects pairwise competition between others. Yet resource competition leads to a more constrained set of outcomes than the Lotka-Volterra model. This is because, in the resource competition model, how each species interacts with the environment is independent of its competitor. This invariance over different competitions enables a simple emergent mapping despite the underlying complexity. Geometric analysis provides insights on the simple community assembly. The relative ordering between ZNGIs determines a competitive hierarchy between species, and simple arrangement of ZNGIs leads to simple community assembly. Specifically, when a ZNGI does not cross with another ZNGI, then the trio community always follows the assembly rule. This competitive hierarchy also explains why resource competitions are often transitive and rock-paper-scissors pairwise outcome is impossible. In addition, geometric principles impose hierarchy between coexistences such that coexistence of many species require coexistence of all pairs between them: A, B, and C coexist as a trio community only if A-B, A-C, and B-C pairs all coexist, but not vice versa . These geometric hierarchies provide a way to understand the agreement between bottom-up assembly rule prediction and resource competition. Like in laboratory experiments, community assembly under resource competition sometimes deviates from the bottom-up assembly rule prediction. Strikingly, such violations may strengthen the connection between experimentally observed community assembly and resource competition. For example, we find that the most frequently observed violation in the experiment is the most frequently observed violation in simulations [47]. Our resource model analysis also clarifies conditions for the bottom-up prediction's failure in terms of growth rates and resource supply. Experiments aided with metabolomics may

verify the criteria and further improve the predictive power [42]. While we focused on a simple linear consumption model, there are many other models for ecological interactions [147]. For example, the Lotka-Volterra model allows more community assembly outcomes from the pairwise competitions compared to our resource competition model. While our resource competition model and the assembly rule successfully describe laboratory microcosms, further work will be necessary to determine the rules of community assembly in other systems. In addition, our assumption of uniform relative biomass yields means that all communities in our model has a single stable equilibrium. How our results hold in the presence of alternative stable states and dynamical phases such as limit cycles is a question that remains to be answered [65, 24, 73, 130, 6, 160, 101]. Finally, we acknowledge that linear resource consumption is not the only possible mechanism for resource competition, and different models such as Monod model or diauxic model may be more appropriate in some systems. Interestingly, we found that diauxic model also leads to community assembly that is often predicted by the same assembly rule [18] (Fig. S4). Future work is required to explore the extent of possible mechanistic origins behind the simplicity of community assembly. Our approach highlights that, even when one uses mechanistic models, direct measurement of microscopic parameters is not always necessary for predictive power. This is a significant advantage of the empirical approach that has attracted many ecologists [34, 59, 130, 132, 27, 8, 68]. In the case of resource competition, fully characterizing the metabolism of each microbial species is a formidable experimental challenge due to many complications such as cross-feeding, diauxie, and co-utilization of resources. Our results illustrate how mechanistic insights can guide simple experimental predictions while circumventing the full microscopic complexity.

2.5 Methods and Materials

2.5.1 Simulations of linear resource consumption model

We used simulations to complement our geometric approach with our resource competition model. The model we studied is described in 2.1 in the main text. For each condition, we simulated 500 communities and numerically solved outcomes of all pairwise competitions and the all-species competition for each community. For each simulation of 500 communities with S species and R resources, growth rates and supplied resource concentrations were drawn randomly in the following way. Growth rates $r_{\mu i}$ on each resource were sampled from an array of length $500S$ and approximately unit mean, $(2/500S, 4/500S, ..., 2)$ without replacement. This ensured finite differences between growth rates of different species on a same resource and prevented numerical artifacts. Note that growth rates on different resources were drawn independently, and there was no trade-off in growth rates. Supplied resource concentrations were drawn from uniform distribution between 0.1 and 1, and then were normalized to a fixed total concentration $R_0 = 10$. Biomass yields were set to 1 and dilution rate was set to $\delta = 0.02$. $\delta/\langle r_{\mu i}\rangle \ll R_0$ implied that supplied resource concentrations were far from ZNGIs and any extinction was driven by competition, not by dilution outpacing monoculture growth. We implemented convex optimization to solve for the equilibrium of each competition [97, 98]. Species with population fraction $< 10^{-4}$ were considered extinct.

2.5.2 Quantification of agreement between simulation and prediction

In trio community simulations without cross-feeding, we compared the simulated community assembly with three different predictions: 'Everyone survives' that always predicts all three species to survive, 'Fastest grower survives' that predicts the best grower under the resource supply to exclude other two species, and the assembly rule. We quantified how well the simulated competitions agreed with each prediction by

calculating the fraction of species in each trio that either survives while predicted to survive or goes extinct while predicted to go extinct. For example, if prediction tells that only A would survive and simulation results in only B surviving, the agreement is 0 for A, 0 for B, and 1 for C, resulting in an average 1/3 agreement for the trio. In larger-community simulations and trio community simulations with cross-feeding, we compared the simulated community assembly to the assembly rule. The quantification followed the same protocol described above.

2.5.3 Simulations of linear resource consumption model with cross-feeding

To implement simulations with cross-feeding, we considered the following equations:

$$\begin{aligned}\dot{n}_\mu &= (1-l)\sum_{i=1,2,\ldots} r_{\mu i}c_i n_\mu - \delta n_\mu,\\ \dot{c}_i &= -\sum_{\mu=A,B,\ldots}\frac{r_{\mu i}}{Y_{\mu i}}n_\mu c_i + l\sum_{\mu=A,B,\ldots}\sum_{i=1,2,\ldots}\frac{r_{\mu i}}{Y_{\mu i}}n_\mu CF_{ij}c_j + \delta(c_i^s - c_i),\end{aligned} \tag{2.2}$$

where l is the strength of cross-feeding, and CF_{ij} is the cross-feeding chain between resources. $CF_{ij} = 1$ if consumption of j-th resource produces i-th resource; $CF_{ij} = 0$ otherwise. We assumed that species in a community shared same CF_{ij}. We assumed that each resource had probability p to cross-feed a less complex metabolite; $CF_{i<j} = Binomial(1, p)$ and $CF_{i\geq j} = 0$. All other parameters were drawn in the same way as the simulations without cross-feeding. We implemented the same convex optimization to solve for the equilibrium of each competition.

Chapter 3

Slow expanders invade by forming dented fronts in microbial colonies

3.1 Overview

The work covered in this chapter is published as "Slow expanders invade by forming dented fronts in microbial colonies" (Lee et al, PNAS 2021) [85]. In this project, I worked with professor Kirill Korolev at Boston University and professor Jeff Gore to explain spontaneous formation of dents on expanding biofilm of a soil isolate *Raoultella planticola*. We discovered that the dented pattern were signatures of slowly expanding mutants that nevertheless take over the front because of their advantage in local competition. We explained the quantitative shape of pattern using geometric theory and verified with additional experiment and numerical simulations. As the first author of the paper, I set up and performed experiments, analyzed data, performed theory calculations, ran simulations, and wrote manuscript.

Most organisms grow in space, whether they are viruses spreading within a host tissue or invasive species colonizing a new continent. Evolution typically selects for higher expansion rates during spatial growth, but it has been suggested that slower expanders can take over under certain conditions. Here, we report an experimental observation of such population dynamics. We demonstrate that the slower mutants win not only when the two types are intermixed at the front but also when they are

spatially segregated into sectors. The latter was thought to be impossible because previous studies focused exclusively on the global competitions mediated by expansion velocities but overlooked the local competitions at sector boundaries. We developed a theory of sector geometry that accounts for both local and global competitions and describes all possible sector shapes. In particular, the theory predicted that a slower, but more competitive, mutant forms a dented V-shaped sector as it takes over the expansion front. Such sectors were indeed observed experimentally and their shapes matched up quantitatively with the theory. In simulations, we further explored several mechanism that could provide slow expanders with a local competitive advantage and showed that they are all well-described by our theory. Taken together, our results shed light on previously unexplored outcomes of spatial competition and establish a universal framework to understand evolutionary and ecological dynamics in expanding populations.

3.2 Introduction

Population dynamics always unfold in a physical space. At small scales, microbes form tight associations with each other, substrates, or host cells [53, 31]. At large scales, phyto- and zooplanktons form complex patterns influenced by ecological interactions [37, 12, 90] and hydrodynamics [1, 120]. Between these two extremes, populations constantly shrink and expand in response to changing conditions, and there is still a great deal to be learned about how spatial structure affects ecology and evolution [136, 87, 60, 91, 110]. Better understanding of these eco-evolutionary dynamics is essential for management of invasive species [106, 127], controlling the growth of cancer [80], and preserving biodiversity [61, 67].

It is particularly important to understand how natural selection operates at the edge of expanding populations. These expansion frontiers are hot spots of evolution because mutations that arise at the edge can rapidly establish over large areas via allele surfing or sectoring [10, 74, 58, 56]. Furthermore, numerous studies argue that selection at the expansion front favors faster expanders and therefore makes

population control more difficult [82, 142, 13, 134, 149, 76, 164, 45, 112, 133, 33]. Indeed, organisms that expand faster have a head start on growing into a new territory and may face weaker competition or better access to nutrients. A well-known example is the evolution of cane toads which increased the expansion speed by 5 fold over 50 years [118]. Yet, despite substantial empirical evidence across many systems [142, 134, 13, 149, 164, 45, 112, 133, 33], it has been suggested that the simple intuition of "faster runner wins the race" does not always hold.

Two theoretical studies have found that slower dispersal could evolve in populations with a strong Allee effect, i.e a negative growth rate at low population densities [146, 141, 77]. Slow mutants nevertheless can take over the populations because they are less likely to disperse ahead of the front into regions with low densities and negative growth rates. In a different context, both theory and experiments have shown that slow cheaters could invade the growth front of fast cooperators [76, 32]. In this system, the production of public goods allowed cooperators to expand faster, but made them vulnerable to the invasion by cheaters.

The examples above show that slower expanders succeed in the presence of a tradeoff between local and global fitness. The global fitness is simply the expansion rate of a given species in isolation, which determines how quickly it can colonize an empty territory. When two species are well-separated in space, their competition is determined solely by the global fitness. In contrast, when the two species are present at the same location, their competition could involve differences in growth rates, production of public goods [5, 11], or secretion of toxins [139]. We refer to such local competitive abilities as local fitness. It is natural to assume that slow expanders can win only if they are superior local competitors, but it is not clear a priori if this is actually feasible or how to integrate local and global fitness under various scenarios of spatial competition.

Our interest in the interplay between local and global competition was sparked by an unusual spatial pattern in colonies of *Raoultella planticola* grown on agar plates. These colonies repeatedly developed depressions or dents along the edge. We found that dents were produced by a spontaneous mutant that expanded slower than the

wildtype, when in isolation. Thus, we discovered a convenient platform to explore the fate of slower expanders in spatial competition and to elucidate the tension between local and global fitness.

In our experiment, the slower mutant took over the colony either while increasing in frequency homogeneously along the front or while forming pure, mutant-only, sectors. When mutant sectors formed, they had an unusual "dented" or "V" shape. To explain this spatial pattern, we developed a theory that describes all possible sector geometries. Our theory unifies local and global competitions without assuming any particular mechanism for growth and dispersal. Although mechanism-free, the theory makes quantitative predictions, which we confirmed experimentally. We also simulated specific microscopic models to demonstrate that the takeover by mutant with a slower monoculture expansion velocity is generic and could occur due to multiple ecological mechanisms. These simulations further confirmed that sector shape prediction from geometric theory is universal. Taken together, our results establish a new framework to understand evolutionary and ecological dynamics in expanding populations with arbitrary frequency- and density-dependent selection.

3.3 Results

3.3.1 Experimental observation of slow mutants taking over the front

The strains used in our experiment were derived from a soil isolate of *Raoultella planticola*, a Gram-negative, facultatively anaerobic, non-motile bacterium that is found in soil and water and can occasionally lead to infections [36, 38]. We grew *R. planticola* on a hard LB agar plate (1.5% agar) and noticed the formation of V-shaped dents along the front. Such dents were reproducibly observed in biological replicates (Fig. S1). Suspecting that dents were caused by a mutation, we isolated cells from the smooth parts of the colony edge (wildtype) and from the dents (mutant) (Fig. 3-1A).

We first characterized the expansion dynamics of the two strains in isolation by inoculating each culture at the center of a hard agar plate. Both strains formed smooth, round colonies, which expanded at a constant velocity (Fig. 3-1B, Fig. S2). The wildtype had about 50% larger expansion velocity compared to the mutant. Thus, the evolved strain expanded slower when in isolation.

Our observations seemed paradoxical given numerous observations of invasion acceleration due to genetic changes that increase expansion velocities [135, 118]. However, range expansions are known to produce high genetic drift [155, 17] and, therefore, allow for the fixation of deleterious mutations [58, 39, 124, 137, 21]. So, we next investigated whether the mutant has a selective advantage in competition with the wildtype within the same colony.

We competed the two strains by inoculating an agar plate with a drop containing a 99:1 mixture of the wildtype and the mutant. We used two wildtype strains (and their respective mutants) with different fluorescent labels and the spatial patterns were analyzed with fluorescence microscopy (see Methods). After about 48 hours of growth, a ring of mutant completely encircled the wildtype (Fig. 3-1C). Only the mutant ring continued to expand, while the expansion of the wildtype ceased (Fig. S3). Thus the mutant not only localized to the front but also achieved a greater population size. This is quite different from other microbial systems where a strain with poor motility localized to the front without suppressing the growth of faster strain and without producing a larger biomass [163, 162]. Thus, our experiments strongly suggest that the mutant has a competitive advantage when in contact with the wildtype despite its lower expansion velocity in isolation.

3.3.2 Experimental observation of mutants invading while forming dented fronts

Our initial competition experiments did not exhibit the dents that sparked our initial interest in the strains. The mutant took over uniformly across the expansion front, producing a rotationally invariant spatial pattern (Fig. 3-1C). In fact, one might even

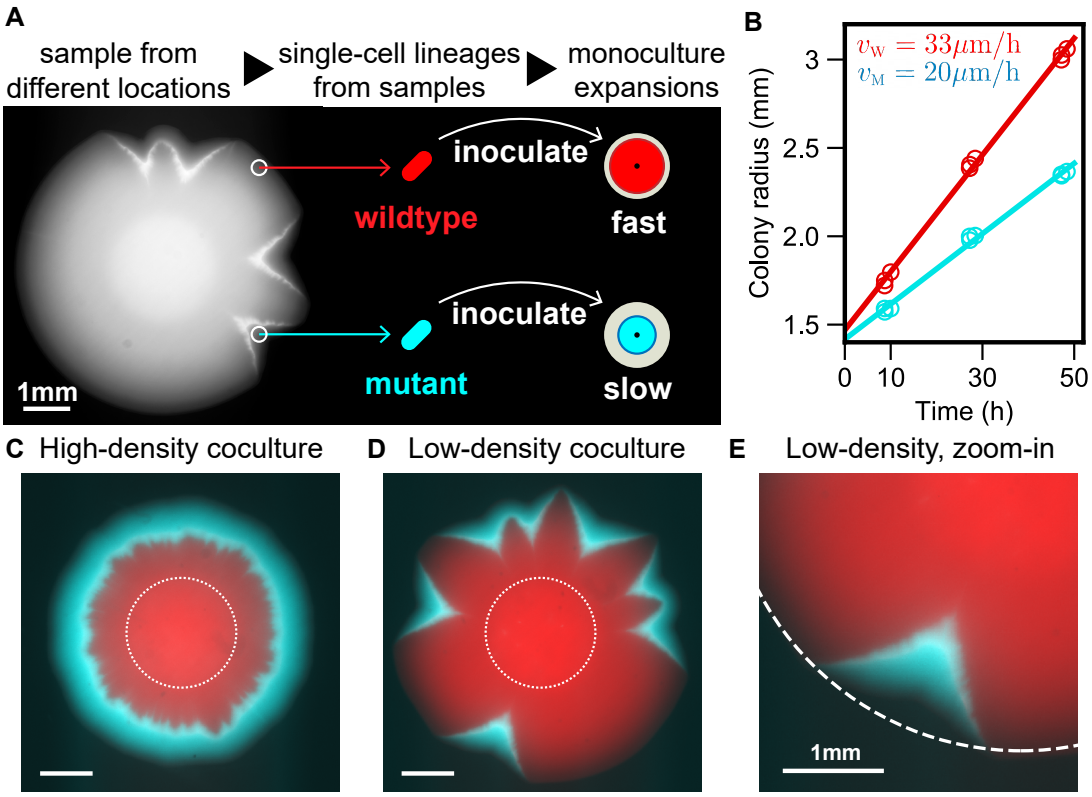

Figure 3-1: Slow mutant takes over the front with and without sector formation. (A) We found that wildtype *R. planticola* colonies develop V-shaped indentations; a bright-field image is shown. We sampled cells from the dents and non-dented regions and then developed strains descending from a single cell (see Methods). (B) The mutant expanded more slowly than the wildtype when in isolation. The data points come from two technical replicates, and the line is a fit. (C, D) Despite its slower expansion on its own, the mutant wins in coculture. Fluorescence images show the spatial patterns 48 hours after inoculation with a 99:1 mixture of the wildtype and mutant. A ring of mutant (cyan) outrun and encircled wildtype (red) when the mixed inoculant had a high density (OD_{600} of 10^{-1}). Mutant sectors emerged and widened over the front when the mixed inoculant had a low density (OD_{600} of 10^{-3}). Images are taken 48 hours after inoculation, and dotted lines represent initial inoculant droplets. (E) A zoomed image of a V-shaped sector (from the bottom of D). Dotted circle is a fit from wildtype expansion. The advantage of the mutant and its slower expansion away from the wildtype is evident from the lateral expansion of the cyan sector.

argue that the success of the mutant could have been entirely due to the transient growth dynamics, and the wildtype would prevail if allowed to somehow spatially segregate from the mutant. To address both of these concerns, we sought to alter the experiments so that the mutant and the wildtype grow as distinct sectors within the same colony.

In microbial colonies, sectors emerge due to genetic drift at the growing edge. The magnitude of demographic fluctuations varies widely in different systems, depending on the organism, the growth conditions, and the duration of the experiment [57, 78]. To test for the effects of sectoring, we needed to increase stochasticity without altering other aspects of the competition. Reducing the cell density of the initial inoculant accomplished this goal. By lowering the inoculant density (from 10^{-1} OD_{600} to 10^{-3} OD_{600}), we increased the separation between cells that localized to the colony edge following the drying of the inoculation drop. This in turn dramatically increased the formation of monoclonal sectors (Fig. 3-1D).

Sectoring spatially segregated the two strains and, thus, allowed the wildtype to to take advantage of its higher expansion velocity as a monoculture. Nevertheless the mutant still outcompeted the wildtype (Fig. 3-1D, Fig. 3-1E). The takeover of mutant was robust under different choices of initial density, initial mutant fraction, and fluorescent label (Fig. S4, Fig. S5). The takeover by the mutant also produced the characteristic V-shaped dents at the colony edge. These dents are the exact opposite of the bulges or protrusions that one usually observes for beneficial mutations [79]. Typically, the advantageous mutants have a greater expansion velocity and, therefore, outgrow the ancestors at the front. For our strains, however, the winning mutant had a lower expansion velocity away from the wildtype, and this lower expansion velocity produced the opposite of the bulge—the dent.

3.3.3 Mechanism-free theory of sector geometry

Our experiments unambiguously demonstrated that a mutant that expands more slowly on its own can indeed outcompete a faster wildtype with and without sectoring. Still, we need a careful theoretical description of the spatial dynamics to reconcile

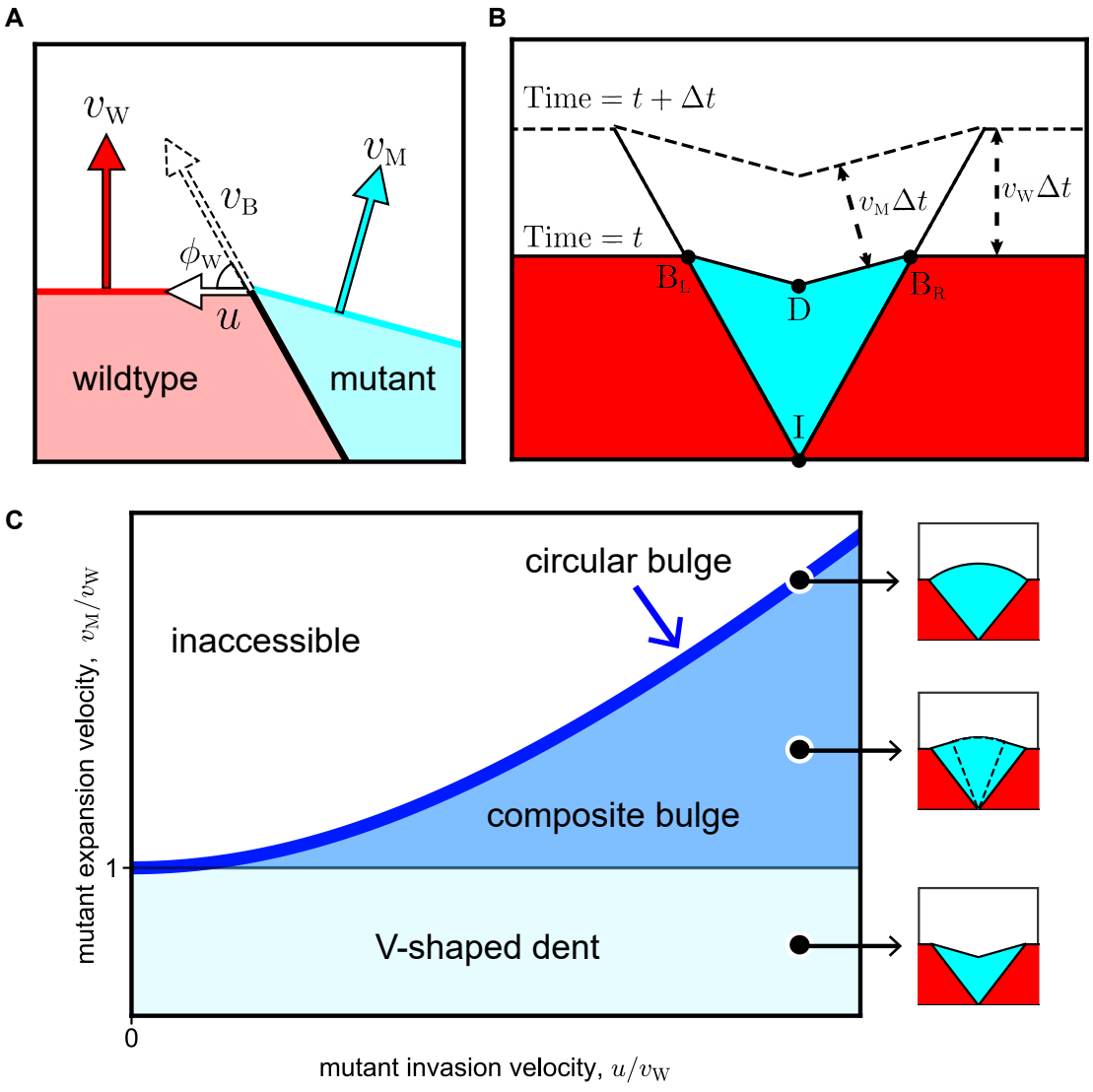
A
v_W
v_B
v_M
ϕ_W
u
wildtype
mutant
B
Time $= t + \Delta t$
Time $= t$
$v_M \Delta t$
$v_W \Delta t$
B_L
D
B_R
I
C
circular bulge
inaccessible
composite bulge
V-shaped dent
mutant expansion velocity, v_M/v_W
1
0
mutant invasion velocity, u/v_W

Figure 3-2

Figure 3-2: Geometric theory predicts sector shapes as a function of local and global fitness. Flat-front initial conditions are illustrated here, and the corresponding results for circular fronts are shown in the SI. (A) Global fitness of mutant and wildtype are defined with speeds v_{W} and v_{M} with which their fronts advance away from sector boundary. Local fitness is characterized by movement of mutant along the sector boundary, which advances with speed v_{B} at angle ϕ_{W} with the wildtype front. We use lateral invasion speed u to describe the local fitness, and the equivalence among v_{B}, ϕ_{W}, and u is explained in SI I. (B) The shape of the mutant sector can be derived from geometric considerations. During a time interval Δt, the boundary points $\mathrm{B_L}$ and $\mathrm{B_R}$ move upward by $v_{\mathrm{W}}\Delta t$ and laterally outward by $u\Delta t$. The position of the dent D is obtained from the requirement that both $\overline{\mathrm{DB_L}}$ and $\overline{\mathrm{DB_R}}$ shift by $v_{\mathrm{M}}\Delta t$; the directions of the shifts are perpendicular to $\overline{\mathrm{DB_L}}$ and $\overline{\mathrm{DB_R}}$ respectively. Point I labels the origin of the sector. (C) The geometric theory predicts sector shapes as a function of u/v_{W} and $v_{\mathrm{M}}/v_{\mathrm{W}}$. When $v_{\mathrm{M}} < v_{\mathrm{W}}$ and $u > 0$, the mutant forms a V-shaped dented front; note that all boundaries are straight lines. When $v_{\mathrm{M}} > v_{\mathrm{W}}$ and $u > \sqrt{v_{\mathrm{M}}^2 - v_{\mathrm{W}}^2}$, the mutant forms a bulged front. The shape of the bulge consists of two regions. It is an arc of a circle near the middle and two straight lines near the two boundaries between the mutant and the wildtype. The circular region grows and the linear region shrinks as $v_{\mathrm{M}}/v_{\mathrm{W}}$ increases at constant u/v_{W}. The bulge becomes completely circular when $v_{\mathrm{M}}/v_{\mathrm{W}}$ reaches its maximal value of $\sqrt{1 + u^2/v_{\mathrm{W}}^2}$ on the boundary of the accessible region. See SI for derivation and exact mathematical expressions of all sector shapes.

the apparent contradiction between the slow global expansion of the mutant and its superior performance in local competition. We could approach this question by simulating a specific ecological mechanism that could be responsible for the tradeoff between local and global fitness. However, it is much more useful to first ask what can be said about spatial competition generically and determine the range of possible sector shapes without relying on any specific mechanism.

One way to understand the origin of the dented fronts is to consider the motion of the sector boundary. The mutant clearly expands further along the sector boundary than it expands outward away from the sector boundary. In other words, the mutant expands faster in the presence of the wildtype, and the dented shape of sector is the result of this velocity enhancement of the mutant in the vicinity of the wildtype.

To formalize this idea, we follow the approach similar to geometric optics in physics [22, 62, 92] which relies on a few standard assumptions. The expansion velocities of the two strains in isolation (v_{W} and v_{M}) are assumed to be time-independent both to simplify the calculations and to reflect experimental observation (Fig. 3-1B). We also assume, consistent with past studies [81, 108, 104], that there is little growth

behind the front so that the spatial pattern remains once established as in our experiments. Finally, we neglect long-range interactions due to the diffusion of nutrients, toxins, or signaling molecules[1] [123, 103, 28].

The nontrivial aspect of our work is how we capture the effect of local competition between strains. This can be done in a number of ways. One approach is to consider the velocity of the boundary between the strains v_{B}, which cannot be inferred solely from v_{W} and v_{M} because it depends on the interaction between the wildtype and the mutant. Another approach, which is equivalent to the first one, is to define a velocity u as the projection of the boundary velocity v_{B} on the wildtype front. In other words, u is the rate at which the length of the front dominated by the wildtype shrinks. The connection between these approaches is illustrated in Fig. 3-2A.

The knowledge of the three velocities v_{W}, v_{M}, and u is sufficient to simulate how the shape of the colony changes with time. In some situations, colony shapes can also be obtained analytically by comparing the position of the front at two times t and $t+\Delta t$. We derive the equations for sector shapes by requiring that all distances between the corresponding points of the two fronts are given by Δt times the appropriate velocity (Fig. 3-2B). The details of these calculations are provided in the SI (Fig. S9).

We found that all possible sector shapes fall into three classes. Without loss of generality, we take u to be positive by calling the mutant the strain that invades locally. The shape of the sector is then largely determined by $v_{\mathrm{M}}/v_{\mathrm{W}}$. When this ratio is less than one, sectors have a dented shape. In the opposite case, sectors bulge outwards. The exact shape of the front of course depends on all three velocities. Overall, there are the two broad classes discussed above and a special limiting case when $u = \sqrt{v_{\mathrm{M}}^2 - v_{\mathrm{W}}^2}$ which is discussed below. In all cases, we obtained sector shapes analytically for both circular and flat initial fronts (SI Fig. S10, Fig. S11). The latter are summarized in Fig. 3-2C and are used to test the theoretical predictions.

The geometrical theory provides a concrete way to define local fitness advantage, u/v_{W}, and global fitness advantage, $v_{\mathrm{M}}/v_{\mathrm{W}} - 1$. These two types of fitness can

[1]The addition of long-range interactions would provide greater modelling flexibility and therefore make it easier to observe novel spatial patterns such as a V-shaped sector. Our works shows that this extra flexibility is unnecessary and dented fronts can appear in purely local models.

take arbitrary values, even with opposite signs. The only condition is that a positive u needs to be larger than $\sqrt{v_{\rm M}^2 - v_{\rm W}^2}$ when the mutant is faster than the wildtype. This constraint arises because, for large $v_{\rm M}/v_{\rm W}$, the gaining of new territory due to the large global fitness advantage outpaces the gain in the new territory due to a smaller local fitness advantage. The constraint on u is not relevant to dented fronts, so we relegate this discussion to the SI (Fig. S8).

3.3.4 Experimental test of the geometric theory

How can we test whether the theory of sector geometry described above indeed applies to our experiments? The theory utilizes three velocities $v_{\rm W}$, $v_{\rm M}$, and u to predict the shape of the sector boundary and the sector front. The absolute values of the velocities determine how quickly the colony grows overall and its shape depends only on two dimensionless parameters: $v_{\rm M}/v_{\rm W}$ and $u/v_{\rm W}$. The first parameter can be obtained from the direct measurements of expansion velocities in monocultures. The second parameter can be inferred by fitting the shape of the sector boundary to the theory. This leaves the shape of the sector front as an independent measurement that can be compared to the theoretical prediction.

The linear expansion geometry greatly simplifies all the steps involved in testing the theory because the shapes of both the sector boundary and the dent are determined by their opening angles. Qualitative agreement with this theoretical prediction is quite clear from the experimental images (Fig. 3-3A), which indeed show that mutant sectors are bounded by straight lines on all sides. The opening angle of the sector boundary determines $u/v_{\rm W}$ and the opening angle of the dent serves as a testable prediction (Fig. 3-3B).

Our experiments proceeded as follows. We first measured expansion velocities in monocultures by tracking the colony radius as a function of time; see Fig. 3-1B. Then, the data on sector shapes were collected from plates inoculated along a straight line with a low-density (10^{-3} $\rm OD_{600}$) 99:1 mixture of the wildtype and the mutant. After two days of growth, five well-isolated sectors were analyzed to determine $\phi_{\rm B}$ and $\phi_{\rm D}$ (see Methods). Since each side of the angle can be used, we

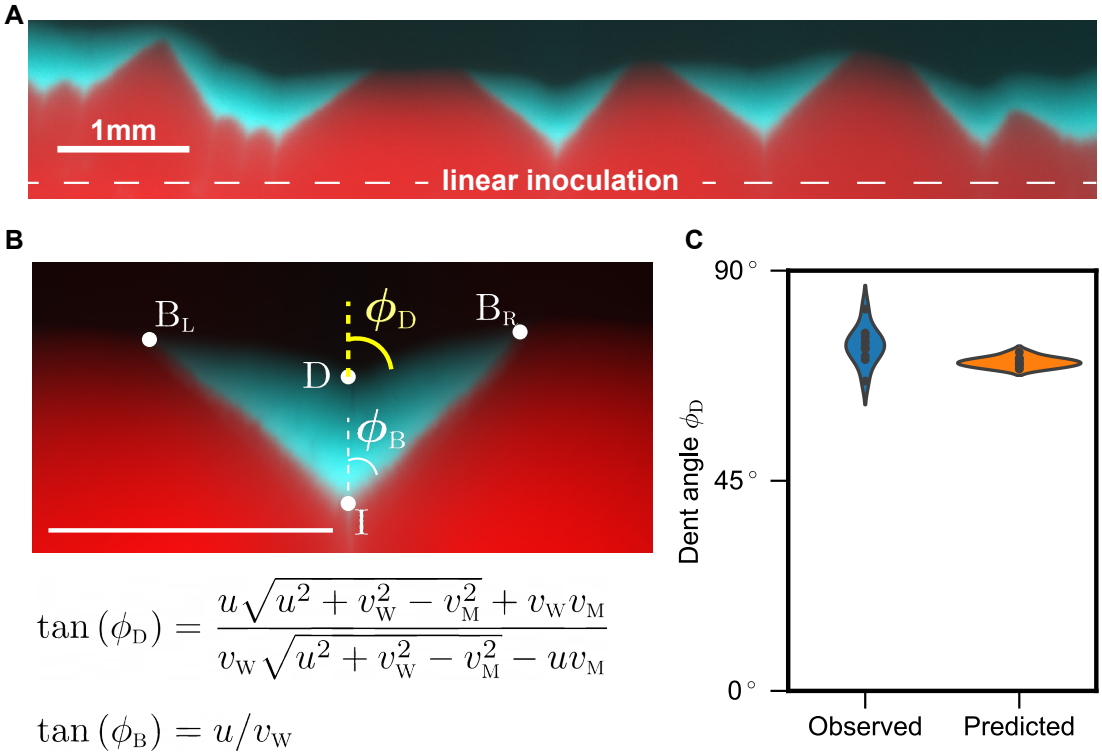

Figure 3-3: Empirical test of predicted sector shapes. (A) We used linear inoculations with low density and low fraction of the mutant and grew the colonies for 48 hours. (B) Top: Zoom-in image of one of the sectors. The shape of mutant sector is quantified by two opening angles: one between the two sector boundaries $2\phi_B$ and one between the two parts of the expansion front that meet at the dent $2\phi_D$. Bottom: The theory predicts ϕ_B and ϕ_D as functions of the three velocities: v_W, v_M, and u. We used ϕ_B to determine u/v_W and predict ϕ_D; v_M/v_W is measured from monoculture expansions. (C) The observed and predicted values of ϕ_D are very close to each other.

effectively obtained ten measurements. Figure 3-3C shows that observed ϕ_{D} is 73.93° (SD=3.81°, SEM=1.21°, n=10). Predicted ϕ_{D} is 70.39° (SD=1.02°, SEM=0.32°, n=10). This is an excellent agreement given other sources of variability in our experiment including variations in velocity between replicates and potential systematic errors in fitting sector shapes. Thus the geometric theory not only provides an explanation of the novel sector shape, but also describes it quantitatively.

Another experimental verification of our theory comes from Ref. [79] that studied sector shapes in yeast colonies. Instead of dents, their strains produced circular bulges (the special case with $v_{\text{M}} = \sqrt{v_{\text{W}}^2 + u^2}$). For this special case, our results fully agree with both their theoretical and experimental findings (see Eq. 12, Table 1, and Figure S8 in Ref. [79]). As far as we know, the intermediate case of composite bulge (see Fig. 3-2C) has not been observed yet. Perhaps engineered strains with a tunable tradeoff between local and global fitness would enable the observation of all sector shapes in a single system.

3.3.5 Concrete mechanisms of fitness tradeoff

The geometric theory integrates local and global competition and quantitatively predicts the shape of mutant sector in our experiment. Yet, the theory does not provide a tangible mechanism behind the takeover by a mutant with a slower monoculture expansion velocity. To show that dented fronts emerge readily under different ecological scenarios we used the flexible framework of reaction-diffusion models, which are also known as generalized Fisher-Kolmogorov equations [43, 75, 109]. A general model can be written as:

$$\begin{aligned} \partial_t n_{\text{W}} &= \left(\nabla^2 \left(D_{\text{W}} n_{\text{W}}\right) + r_{\text{W}} n_{\text{W}}\right)\left(1 - n_{\text{W}} - n_{\text{M}}\right), \\ \partial_t n_{\text{M}} &= \left(\nabla^2 \left(D_{\text{M}} n_{\text{M}}\right) + r_{\text{M}} n_{\text{M}}\right)\left(1 - n_{\text{W}} - n_{\text{M}}\right). \end{aligned} \tag{3.1}$$

Here, n_{W} and n_{M} are the population densities of the wildtype and the mutant normalized by the shared carrying capacity; D_{W}, r_{W} and D_{M}, r_{M} are their respective dispersal and per capita growth rates.

The factor of $(1 - n_W - n_M)$ ensures that there is no growth or movement behind the front. In the growth term, this is a standard assumption that ensures finite carrying capacity [109]. In the dispersal term, the factor of $(1 - n_W - n_M)$ has rarely been studied in mathematical biology because it is specific to microbial range expansions, where there is no movement behind the front [79, 81, 108, 104]. In the SI, we demonstrate that dented fronts also occur with standard density-independent dispersal and therefore could be relevant for range expansions of macroscopic organisms (SI appendix II.

The non-spatial limit of Eq. 3.1 is obtained by dropping the dispersal term. This limit is analyzed in the appendix III. As population grows from any initial condition, the relative abundance of the faster grower increases until the total population density reaches the carrying capacity. At this point there is no further change in n_W and n_M. This neutral coexistence between the two strains ensures that the population is frozen behind the front and the competition unfolds only at expansion frontier. The simplest

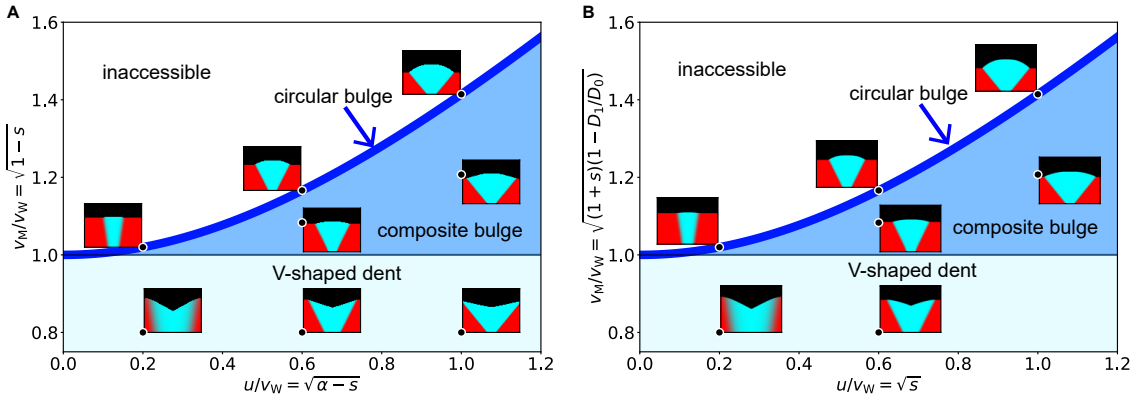

Figure 3-4: Sector shapes from microscopic simulations recapitulate phase diagram from the geometric theory. (A) Simulation of cooperator-cheater model (Eq. 3.2) is compared with the geometric theory. By varying s (benefit from cooperation) and α (strength of cheating), we explored sector shapes for different values of v_M/v_W and u/v_W. The locations of various sector shapes match the predictions of the geometric theory. In particular, V-shaped dents are observed when a cheater expands more slowly than a cooperator when in isolation ($s > 0$), but has a sufficiently large advantage from cheating ($\alpha > s$). (B) Simulations of growth-dispersal tradeoff model (Eq. 3.3) also agree with the geometric theory. Different sector shapes were obtained by varying the the growth advantage s and and the dispersal disadvantage D_1. See Methods for simulation parameters.

spatial model takes all growth and dispersal rates to be independent of population

density. It is then easy to show that there is no difference between local and global fitness; see Fig. S6 and Ref. [79]. Most of the previous work focused on this special case of so-called "pulled" waves [16] and thus could not observe the takeover by the slower expander.

Many organisms, however, exhibit some density dependence in their growth or dispersal dynamics [86, 26, 100, 70, 117], which can lead to a tradeoff between local and global fitness. One commonly-studied case is found in the interaction between cooperators and cheaters [111, 76, 163, 29]. To model this ecological scenario, we take

$$\begin{aligned} &D_{\mathrm{W}} = D_{\mathrm{M}} = D, \\ &r_{\mathrm{W}} = r\left(1 - \alpha\frac{n_{\mathrm{M}}}{n_{\mathrm{W}} + n_{\mathrm{M}}}\right), \quad r_{\mathrm{M}} = r\left(1 - s + \alpha\frac{n_{\mathrm{W}}}{n_{\mathrm{W}} + n_{\mathrm{M}}}\right). \end{aligned} \tag{3.2}$$

The benefit of cooperation is specified by s, which is the difference in the growth rate of cooperators and cheaters when grown in isolation. The benefit of cheating is controlled by α; the growth rate of cheaters increases by up to α provided cooperators are locally abundant. For simplicity, we chose a symmetric linear dependence of the growth rates on the mutant frequency and assumed that the diffusion constants are equal.

Numerical simulations of this model reproduced a V-shaped dented front (Fig. 3-4A). The dents flattened when there was no benefit to cooperate ($s = 0$) and were replaced by bulges when cooperators grew slower than cheaters when in isolation ($s < 0$). We were also able to test whether these transitions in sector shape matched the predictions of the geometric theory. For this comparison between the theory and simulations, we need a mapping between the microscopic parameters of the model and the three velocities that enter our geometric theory. Fortunately, in this model, all three velocities can be calculated analytically: $v_{\mathrm{W}} = 2\sqrt{rD(1+s)}$, $v_{\mathrm{M}} = 2\sqrt{rD}$, and $u = \sqrt{(\alpha - s)rD}$. Therefore, we could overlay individual simulations on the phase diagram predicted by the geometric theory. The result, shown in Fig. 3-4A, shows the expected agreement and provides further validation for the geometric theory.

The geometric description is generic and should transcend the specifics of the

cooperator-cheater model discussed above. To further illustrate that different ecological interactions can produce identical spatial patterns, we simulated a completely different mechanism for the tradeoff between local and global fitness. This time, we assumed that the wildtype loses the local competition because it reproduces slower than the mutant, but this slower growth is more than compensated by a much higher dispersal rate. This growth-dispersal tradeoff may be common in nature [144, 19, 45, 55], and is captured by the following set of parameters:

$$\begin{aligned} D_{\text{W}} &= D_{\text{M}} = D_0 - D_1 \frac{n_{\text{M}}}{n_{\text{W}} + n_{\text{M}}}, \\ r_{\text{W}} &= r, \quad r_{\text{M}} = r\,(1+s)\,. \end{aligned} \tag{3.3}$$

Here, the growth rates are density-independent, but the dispersal rates change with the local community composition. We chose $D_{\text{W}} = D_{\text{M}}$ to reflect the collective nature of movement in colonies of non-motile microbes [41, 153], which are pushed outward by mechanical stressed generated by all cells behind the front. In addition, this simplifying assumption enables us to calculate the velocities analytically and construct a quantitative phase diagram similar to Fig. 3-4A. In the SI, we show that dented front can also be observed in models with $D_{\text{W}} \neq D_{\text{M}}$ (Fig. S7).

Our simulations again exhibited dented fronts and all shape transitions in full agreement with the geometric model (Fig. 3-4B). Thus, the geometric description is universal, i.e. a wide set of growth-dispersal dynamics converges to it. This universality, however, makes it impossible to determine the specifics of ecological interactions from spatial patterns alone. In other words, the observation of a dented front indicates the existence of a tradeoff between local and global fitness, but does not hint at any specific mechanism that is responsible for this tradeoff. For example, both models (Eq. 3.2 and Eq. 3.3) produce identical sector shapes (Fig. 3-4) and both would provide a perfect fit to our experimental data. Indeed, each model has four parameters, which is more than sufficient to specify the three velocities that control all aspects of spatial patterns. Such fits of course would not provide a meaningful insight into the mechanism. To determine the mechanism, one would have to perform a different kind of experiments that could probe population dynamics on the spatial

scale of local competition.

3.4 Conclusion

This study used a simple and well-controlled laboratory microcosm to elucidate the factors that influence spatial competition. We found a stark contradiction to the intuitive expectation that the faster runner wins the race [33]. A mutant that expanded more slowly on its own nevertheless took over the expansion front when inoculated with the wildtype. This spatial takeover accompanied V-shaped sectors, which are a characteristic signature of the mismatch between local and global competition. To explain these observations, we developed a theory that integrates local and global competition and predicts all possible sector shapes. We then confirmed the validity of the theory using both further experiments and simulations.

Our experimental results unequivocally demonstrate that a mutant with grows slower in isolation can nevertheless win in competition. Under low genetic drift conditions, the mutant took over the front uniformly across the colony. This outcome can be described by one-dimensional models because the competition occurs primarily along the radial direction. In contrast, stronger genetic drift resulted in sector formation and produced fully two-dimensional growth dynamics. Even under these less favorable conditions, the mutant still outcompeted the wildtype.

Previously, slower expanders were found to be successful only in one-dimensional models [146, 77, 32], and only buldged sectors of faster expanders were reported for two-dimensional growth [79]. The latter was true even when there was a tradeoff between local and global fitness [150], presumably because local fitness advantage was not sufficiently large. Our experiments not only confirm the predictions of one-dimensional models, but also expand the set of conditions under which the unusual takeover by a slower mutant can be observed. In fact, the slower expanders could be successful in many settings not only because the theory and simulations strongly support this claim, but also because we relied on evolved mutants from natural isolates rather than genetic engineering to obtain the strains.

The observation of dented fronts clearly shows that the existing theoretical understanding of sector growth is incomplete. Previously, it was assumed that the spatial pattern depends only on the mutant and wildtype velocities in monocultures [79]. We found, however, that the outcome of the competition also depends on the interaction between the species at sector boundaries. When the mutant expands much faster in the presence of the wildtype than in isolation, the boundary velocity could tilt towards the region dominated by the wildtype and result in a positive velocity u that describes how quickly the mutant takes over along the wildtype front. Our theory integrated both local and global competition and showed that the sector shapes are completely determined by the three velocities (v_{M}, v_{W}, u). These results enabled us to make quantitative inferences from experimental data and test our theory.

The geometric theory is not without limitations. This phenomenological theory cannot predict whether the fast or the slow mutant wins in a given system. To answer that question, one needs to consider a mechanistic model and derive how the invasion velocity u depends on microscopic parameters, which we have done for specific models. The universal nature of the geometric theory also precluded us from identifying the mechanism responsible for the growth dynamics observed in our experiments. We left this fascinating question for future works, and instead, focused on several common tradeoffs between local and global fitness. The simulations of these tradeoffs not only confirmed the validity of the geometric theory, but further highlighted that slower expanders could establish by a wide range of mechanisms.

The geometric theory also relies on a few technical assumptions such as constant expansion velocities, negligible stochasticity, and the absence of long-range interaction due to chemotaxis or nutrient depletion. Relaxing these assumptions could lead to certain quantitative changes in sector shapes, but the main conclusions, including the existence of the dented front, should not be affected. In particular, the strain that grows more slowly on its own could nevertheless prevail in competition.

Our work opens many directions for further investigation. We clearly showed that the expansion velocity cannot be the sole determinant of the spatial competition. Therefore, it will be important to examine how local interactions influence the

eco-evolutionary dynamics during range expansions. Such future work would bring about a more detailed description of ecological and biophysical processes in growing populations. It would also greatly enhance our understanding of the tradeoffs among different life-history traits and shed light on the incredible diversity of successful strategies to navigate spatial environments [144, 19, 45, 55]. The geometric theory developed here provides a convenient way to integrate these various aspects of population dynamics. It abstracts the main features of spatial growth and should facilitate the analysis of both experiments and simulations.

3.5 Methods and Materials

3.5.1 Strains

Wildtype *Raoultella planticola* strains were isolated from a soil sample (MIT Killian Court, Cambridge, MA) [71] and were tagged with two different fluorescent proteins mScarlet-I (red) and mTurquois2 (cyan) by insertion of plasmids pMRE145 and pMRE141 respectively [129]. As we grew wildtype colonies on agar plates, they reproducibly developed dents after several days as shown in Fig. 3-1A and Fig. S1. We sampled the cells from either inside the dent or on the smooth edge using inoculation loops, streaked on small plates, and grown in 30°C for two days. Then we sampled single colonies, grew them overnight in LB growth media, and stored as a -80°C glycerol stock.

3.5.2 Growth media preparation

We prepared hard agar plates with 1X Luria-Bertani media (LB, 2.5% w/v; BD Biosciences-US) and 1.5% w/v of agar (BD Bioscience-US). We also added 1X Chloramphenicol (Cm, 15mg/L, prepared from 1000X solution) for constitutive expression of fluorescence. For each agar plate, 4mL of media was pipetted into a petri dish (60X15mm, sterile, with vents; Greiner Bio-one), and was cooled overnight (15 hours) before inoculation.

3.5.3 Expansion experiment

For each strain, $-80°$C glycerol stock was streaked on a separate plate and grown for 2 days. Then a colony from each strain was picked up and put into a 50mL Falcon Tube filled with 5 mL of liquid media (1X LB and 1X Cm). Bacterial cultures were grown overnight at 30°C under constant shaking 1350 rpm (on Titramax shakers; Heidolph). We then diluted and mixed the cultures to desired total density and mutant fraction, measured in optical density (OD_{600}) using a Varioskan Flash (Thermo Fisher Scientific) plate reader. For circular expansions, we gently placed a droplet of 1.5 μL inoculant at the center of an agar plate. For linear expansions, we dipped a long edge of a sterile cover glass (24X50mm; VWR) gently into the culture and touched the agar plate with the edge. After inoculation, each colony was grown at 30°C for 48 hours.

3.5.4 Imaging

At fixed times after inoculation, each plate was put on a stage of Nikon Eclipse Ti inverted light microscope system. 10X magnification was used for whole-colony images, and 40X magnification was used for single sector images. Fluorescent images were taken using Chroma filter sets ET-dsRed (49005) and ET-CFP (49001) and a Pixis 1024 CCD camera.

We used scikit-image [148] for image processing in Python. Images from different fluorescent channels were integrated after background subtraction and normalization by respective maximum intensity. The sector boundaries were identified as the furthest points from inoculation plane where both strains' FL intensities were above respective thresholds. The codes for image analysis are available via GitHub (https://github.com/lachesis2520/dented_front_public.git).

3.5.5 Numerical simulation

Numerical simulations were performed by solving the corresponding partial differential equations on a square grid using a forward-in-time finite difference scheme that is

second order accurate in space and first order accurate in time [122]. Python codes are available via GitHub (https://github.com/lachesis2520/dented_front_public.git).

For cooperator-cheater model simulation, we used the following set of values for parameters (s, α): $(-0.04, 0)$, $(-0.36, 0)$, $(-1, 0)$, $(-0.173, 0.187)$, $(-0.457, 0.543)$, $(0.36, 0.4)$, and $(0.36, 0.72)$.

For growth-dispersal tradeoff model simulation, we used (s, D_1) of $(0.04, 0)$, $(0.36, 0)$, $(1, 0)$, $(0.36, 0.147)$, $(1, 0.271)$, $(0.04, 0.385)$, and $(0.36, 0.529)$.

Chapter 4

Conclusion

4.1 How my works fit into today's microbial ecology

During my PhD study in microbial ecology from 2018 to 2022, there has been a growing trend of studying microbial communities in the lens of emergent phenomena. Many significant works in resource competition demonstrated that microbial communities' behaviors are often explained not by microscopic characterization but by taking appropriate coarse-grained description [51, 63].

I have pursued understanding emergent simplicity in microbial communities competing for resource and space. As all microbes consume resources and occupy space, the two modes of competition I studied can be relevant to a wide range of microbial communities in nature. Not to mention, the two axes are both highly active areas of research in the field.

Both of my major projects share one feature that is not always found in other studies of emergent behaviors of microbial communities. They both demonstrate that, beyond qualitative explanations, we can make precise predictions for the behaviors of microbial communities without any information about microscopic details of the systems. In my work on resource competition, I have shown that individual species' survival in community assembly can be predicted without any information about the supplied resources of the system or growth rates of the microbes. In my work on spatial competition, I have shown that the large-scale pattern can be predicted

without any information about the growth rates and migration rates of microbes or the interspecies interactions between them.

Finally, my PhD works point toward exciting future directions ahead in the field of microbial ecology. In resource competitions, we have focused on a limited scope of a particular resource model and future work is required to explore the extent of possible mechanistic origins behind the simplicity of community assembly. In terms of spatial competition, it will be important to examine how local interactions influence the eco-evolutionary dynamics during range expansions. In the end, it will be interesting to push toward the limit of how the lens of emergent behavior allows us to discover simple descriptions of microbial communities at large scales unhindered by their complexities at small scales.

4.2 Emergent phenomena in complex systems

In my PhD, I have studied emergent phenomena in microbial communities. The studies have demonstrated that for microbial communities, we can find simple governing principles at emergent level. Now, the question is whether we can find more general governing principles that are applicable for any complex systems. While most artificial systems are pure, natural systems are often heterogeneous mixtures of diverse components: intracellular fluid contains diverse proteins and organelles, tissues contain diverse cells, and interstellar matter consists of diverse molecules. In these systems, some conventional physics may break down and totally new behaviors may emerge. Nevertheless both new and unbroken features in complex systems remain unclear.

My PhD was limited as I could not find a general principle or approach that is applicable for a wide range of complex systems which do not have without conservation of energy, conservation of number of particles, nor a single scale of interaction over the system. As I plan to pursue this idea during my postdoctoral work, I propose two themes that may be hint toward understanding physics of complex systems better.

The first concept is duality. Duality, such as AdS/CFT correspondence, is an

equivalence between two completely different theories that enables one to utilize advantages of both theories []. In my selected work on competition for resource, I demonstrated a correspondence between mechanistic model of resource competition and empirical simple rule of microbial community assembly. In this example, the duality across scales is a powerful tool that extracts simple principles emerging from a microscopic model. It would be very interesting to find such duality between microscopic model of other - or generic - complex systems and a simple theory at emergent level.

The second concept is a dynamic phase. Recent studies have discovered multiple mechanisms that lead to 'dynamic phase' in complex systems during which spontaneous dynamics persist by interactions between components without any external drive. A microbial community may sustain persistent fluctuation in its composition when it has sufficiently many different species, and a binary mixture with nonreciprocal interaction may stay in a chiral or swap phase during which the system's order parameter keeps rotating or flipping [63, 48]. Both of these examples suggest that spontaneously driven persistent dynamics may be a feature of complex systems in general that is not possible in simple (passive, single-type) systems. It would be interesting to understand a general principle governing such dynamic phase and explain important phenomena in nature with this concept.

Overall, this is the right moment to expand the language of physics. While we still do not have a good understanding of the physics of complex systems, recent advances in the fields of ecology and active matter suggest potential ways to achieve it. It would be exciting to integrate all the interdisciplinary progress into a universal understanding of the emergent phenomena in complex systems.

Appendix A

Appendix for Chapter 2

A.1 Supplementary figures

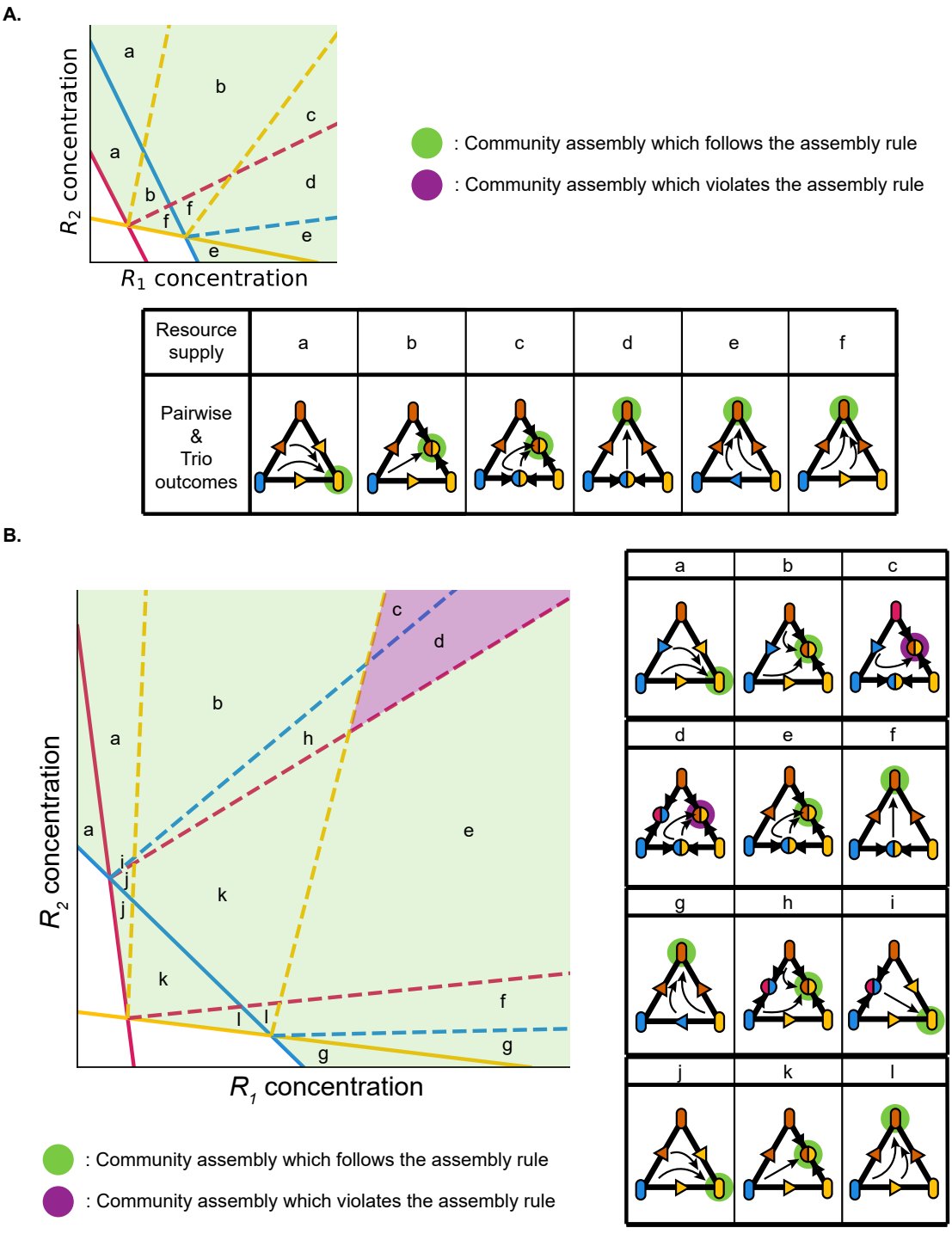
A.
a
b
c
a
d
b
f
f
e
e
R_2 concentration
R_1 concentration
: Community assembly which follows the assembly rule
: Community assembly which violates the assembly rule
Resource supply
a
b
c
d
e
f
Pairwise & Trio outcomes
B.
c
d
b
a
h
e
a
i
j
k
j
k
f
l
l
g
g
R_2 concentration
R_1 concentration
: Community assembly which follows the assembly rule
: Community assembly which violates the assembly rule
a
b
c
d
e
f
g
h
i
j
k
l

Figure A-1

Figure A-1: Community assembly of trios in Fig. 2 agrees with the assembly rule under most of resource supply concentration. A. All 6 outcomes for the trio in Fig. 2A. Note that outcomes change only when resource supply moves over a resource consumption vector. All the outcomes follow the assembly rule. B. All 12 outcomes for the trio in Fig. 2B. Outcomes violate the assembly rule when resource supply is inside region c or d.

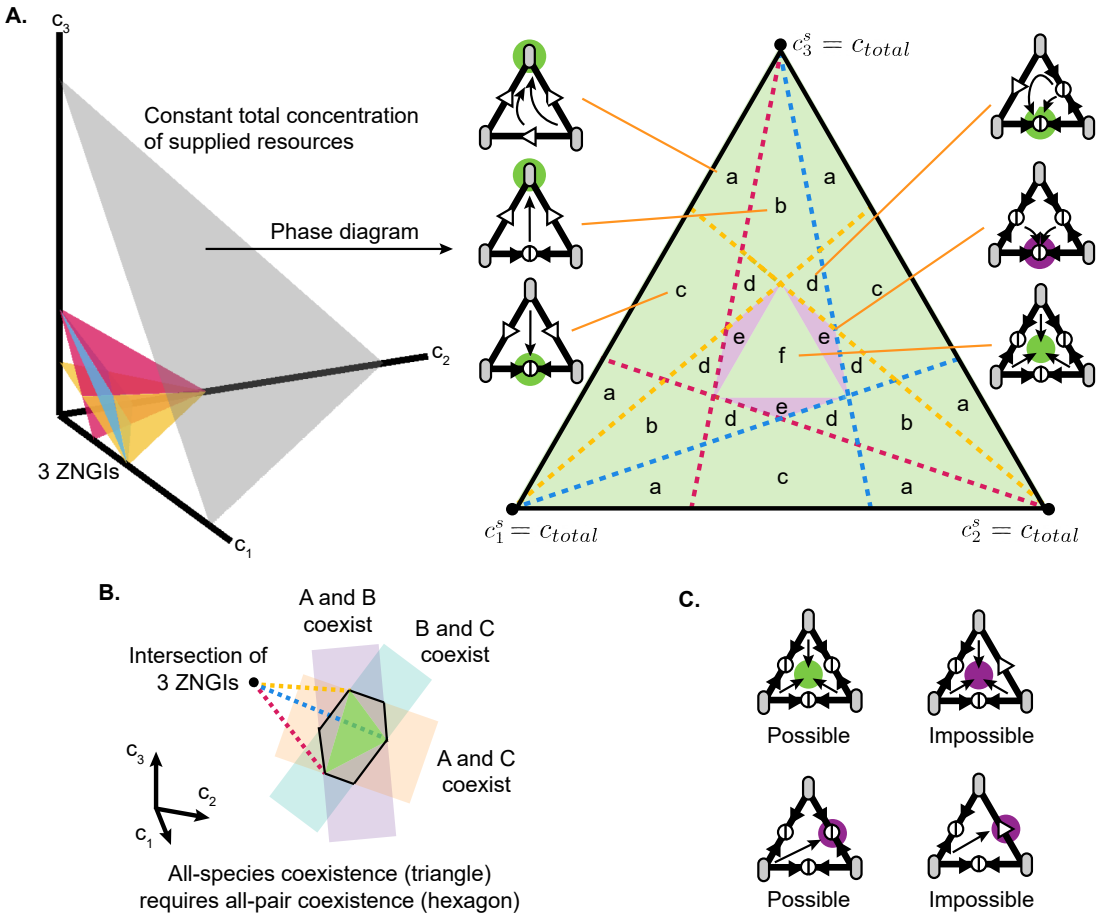
A.
c3
Constant total concentration
of supplied resources
Phase diagram
c2
3 ZNGIs
c1
$c_3^s = c_{total}$
$c_1^s = c_{total}$
$c_2^s = c_{total}$
a
b
c
d
e
f
B.
A and B
coexist
B and C
coexist
Intersection of
3 ZNGIs
A and C
coexist
c3
c2
c1
All-species coexistence (triangle)
requires all-pair coexistence (hexagon)
C.
Possible
Impossible
Possible
Impossible

Figure A-2

Figure A-2: All-species coexistence requires all-pair coexistence, but not vice versa. A. Geometric analysis of trio community competing for three resources illustrates all-pair coexistence both with and without all-species coexistence. In the 3-dimensional space of three resource concentrations, it is often useful to consider a simplex on which the total concentration of supplied resources is kept constant. The phase diagram of outcomes in the case of three ZNGIs intersecting at a point, projected on the simplex, is qualitatively same as the example illustrated on the right. We can see that the region where three species coexist in trio competition (region f) is inside the region where all pairs coexist (region e & f). B. Generically, the resource supply supporting all-species coexistence always supports all-pair coexistence as well, but not vice versa. This is because the convex hull of three resource consumption vectors, which is the region of all-species coexistence, is always included in the intersection of every region for each pairwise coexistence. C. This geometric constraint dictates that when a pair does not coexist it can never coexist in community assembly. This implies that the two outcomes on the left are possible while the other two on the right are impossible.

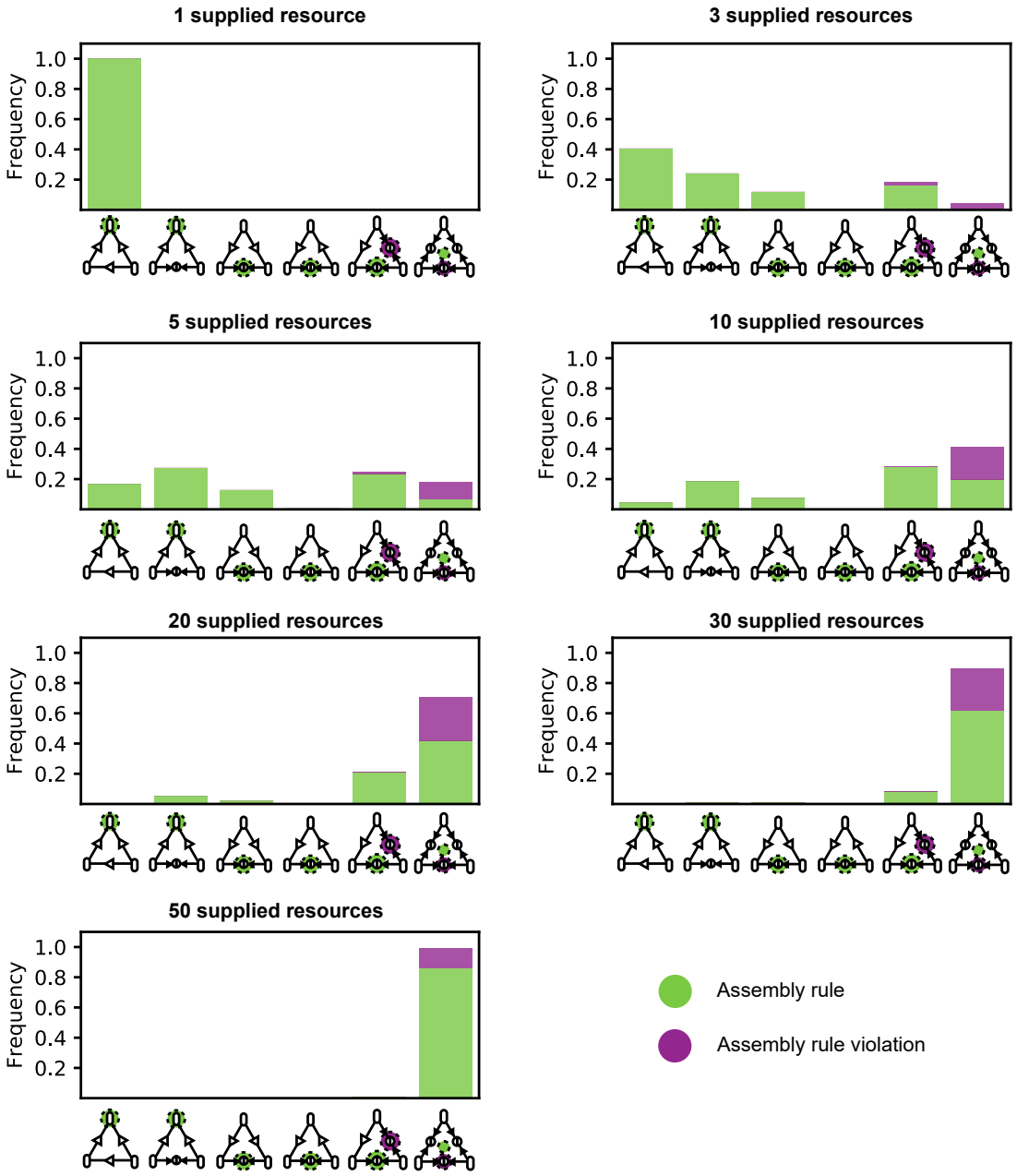

Figure A-3

Figure A-3: Trio community assembly outcomes for each number of supplied resources do not exhibit unexpected assembly rule violations. In addition to 1, 5, and 50 resources cases shown in Fig. 4, here we show the distribution of outcomes under all number of resources that we have simulated. As the number of resources increase, species tend to coexist. Also, any violation observed in simulations is one of two violations that are expected from geometric analysis.

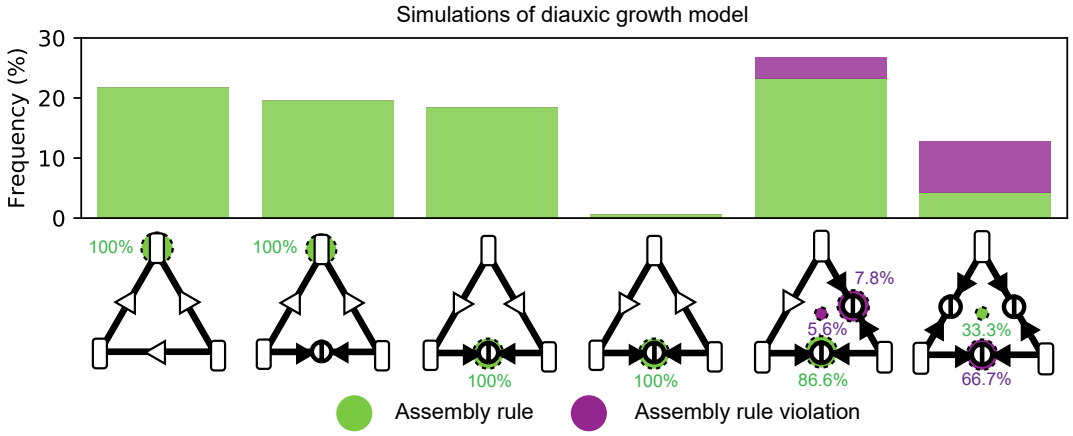

Figure A-4

Figure A-4: Trio community outcomes in diauxic growth model often agree with the assembly rule. While our chemostat-like model in the main text assumes that species consume all resources simultaneously, microbes in nature often exhibit diauxic growth in which each resource consume one resource at a time, starting with its top preference and then moving on to its next remaining preference after each resource depletion. We tested how the assembly rule works under such growth dynamics by implementing a diauxic growth model used in Bloxham et al. [18]. Across 1000 simulated communities of three species growing on three resources, the assembly rule often predicted trio outcomes accurately from pairwise outcomes. (For each simulated community, each component of the resource supply was uniform-randomly sampled from 0 to 1 and the total resource supply was then normalized to 1, while growth rates were uniform-randomly sampled from 0 to 1. Each species' resource preference order matched the ordering of its growth rates such that each species first consumed whichever resource it grew fastest on. A dilution factor of 10 was used. Diauxic lags were assumed to be zero so that species instantly starts consuming the next preferred resource upon depletion of the previous resource.)

Number of resources	Communities with a non-intersecting ZNGI pair	Assembly rule prediction accuracy (%)	Communities without non-intersecting ZNGI pair	Assembly rule prediction accuracy (%)
1	500	100	0	-
3	278	100	222	94.29
5	82	100	418	94.90
10	3	10	497	92.62
20	0	-	500	90.13
50	0	-	500	90.6
100	0	-	500	95.6

Table A.1: Assembly rule prediction always works perfectly for trio communities with non-intersecting ZNGI pairs. From geometric analysis, we stated that the assembly rule should perfectly predict trio community assembly when any pair of ZNGI does not intersect. By inspecting the growth rates in each simulated community, we divide the dataset used in Fig. 4 into communities with and without non-intersecting ZNGI pairs. Here we show the number of communities in the two subsets and average assembly rule accuracy in each of the subsets. The assembly rule indeed perfectly works for simulated communities with non-intersecting ZNGI pairs, verifying our statement from geometric analysis.

A.2 Trio community assembly under two supplied resources

In this appendix, we find all cases of 3-species community assembly under two resource supply. Assuming biomass yields are uniform or have the structure $Y_{\mu i} = a_\mu y_i$ (as in the Main Text), all possible scenarios for trio community can be categorized by how their ZNGIs intersect. There are 6 different ways for three lines (each with positive intercepts on both axes) to intersect on the quarter-plane of two positive resource concentrations. And for each topology of ZNGIs, we obtain a phase diagram of how different region of supplied resource concentrations lead to different pairwise and trio outcomes.

We also note that there are some important constraints on the resource consumption vectors:

First, two consumption vectors of a species from different points of its ZNGI can never cross. To see this, let us consider any two points (c_1^a, c_2^a) and (c_1^b, c_2^b) on a single ZNGI, Then consumption vectors from them have slopes $\frac{Y_{\mu 1} r_{\mu 2}}{Y_{\mu 2} r_{\mu 1}} \frac{c_2^a}{c_1^a}$ and $\frac{Y_{\mu 1} r_{\mu 2}}{Y_{\mu 2} r_{\mu 1}} \frac{c_2^b}{c_1^b}$, respectively. The slope will always be steeper for the point with larger $\frac{c_2}{c_1}$, and since the two points lie on the same line with a negative slope, the two consumption vectors will never intersect.

Second, by assuming that the biomass yield $Y_{\mu i} = a_\mu y_i$, we find a similar relation between consumption vectors of different species. Following the same analysis, we can see that the slopes will be steeper for larger $\frac{r_{\mu 2}}{r_{\mu 1}} \frac{c_2}{c_1}$. Thus by inspecting the slopes of ZNGIs and the points of intersections, we can tell whether two consumption vectors may or may not intersect.

For the sake of clarity, here we show the phase diagrams for all 6 topologies. For each arrangement of ZNGIs, a phase diagram with the maximum number of outcomes is shown.

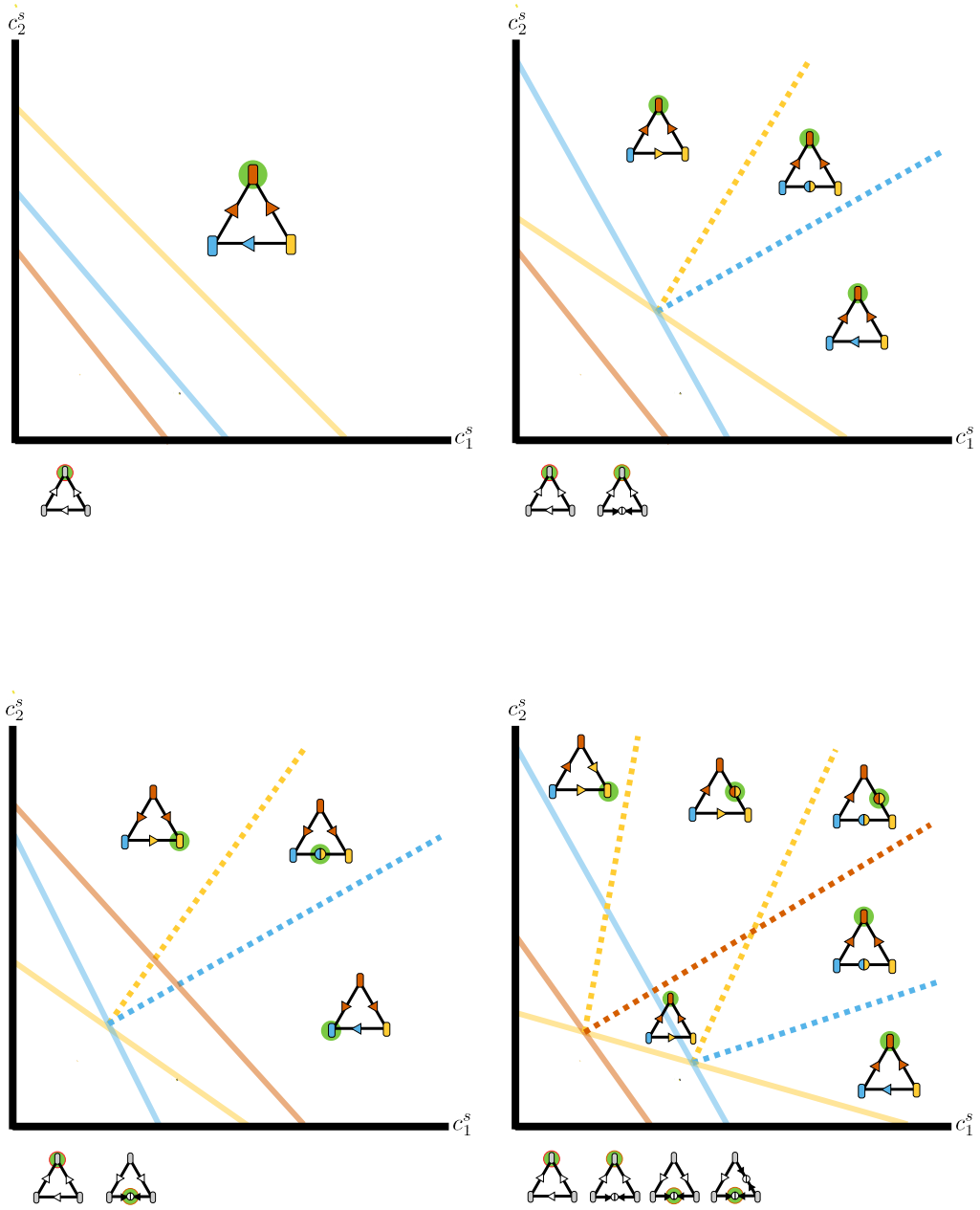

Figure A-5

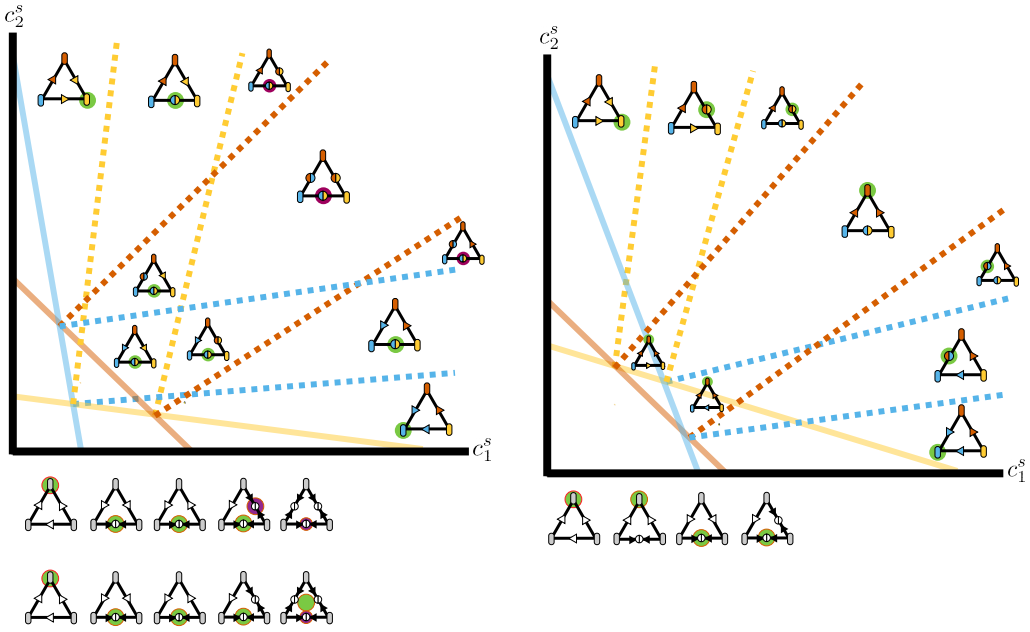

Figure A-5: Phase diagrams for all ZNGI topologies of 3 species on 2 resources. The bottom left diagram can lead to two distinct violations (one of which appears twice due to symmetry). All other cases always follow the assembly rule.

A.3 Trio community assembly under three supplied resources

In this appendix, we find all cases of 3-species community assembly under three resource supply. Similar to the previous case, we identify all possible ZNGI arrangements and corresponding phase diagrams. As each ZNGI is a plane in this three-dimensional case, two ZNGIs intersect along a line and three ZNGIs at a single point may intersect. By counting such intersections that either lie on the innermost ZNGIs or lie outside them, we find all 7 possible ZNGI arrangements and possible community assembly under each of them (While we do not present a mathematically rigorous proof but instead focus on providing a more intuitive understanding, we are unaware of any other community assembly being possible).

Remarkably, many ZNGI arrangements in 3D are equivalent to 2D arrangements; one may find an axis along which all 2D slices of ZNGI planes have the same arrangements (such that rotating the 2D slice about the axis does not change the qualitative arrangement of the ZNGI projections on the slice). When this happens, as in the illustrated example on the left, since the 3D ZNGI arrangements is equivalent to a trivial extension of 2D arrangement along a new axis, the set of pairwise and trio outcomes is the same as its equivalent 2-resource competition's.

Given this, let us examine each of all 7 phase diagrams.

Overall, we expect 8 possible 3-species community assembly, as shown in Fig. 4B in the main text.

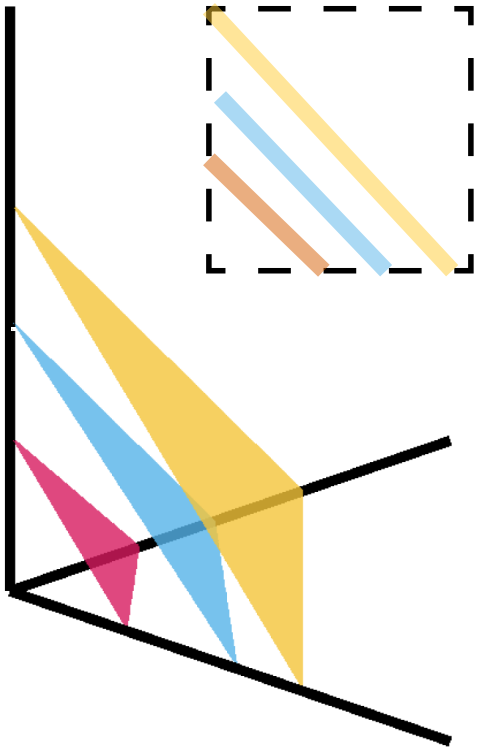

Figure A-5: 0 ZNGI intersections: This case is equivalent to the 2-resource case with no ZNGI intersections. Fast grower excludes others in all competitions, and only one set of pairwise and trio outcome is possible.

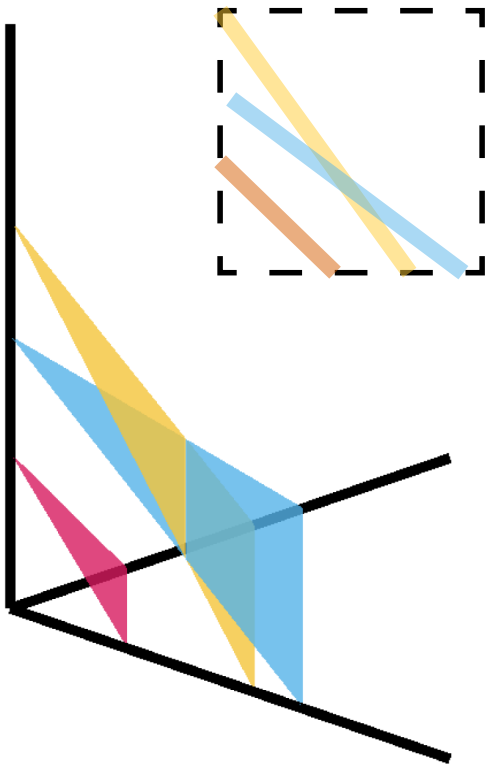

Figure A-5: 0 intersection on innermost ZNGIs, 1 intersection outside: This case is equivalent to the 2-resource case with one ZNGI intersection outside the innermost ZNGI. The fastest grower (red) excludes others, and the others may coexist or exclude one another depending on resource supply.

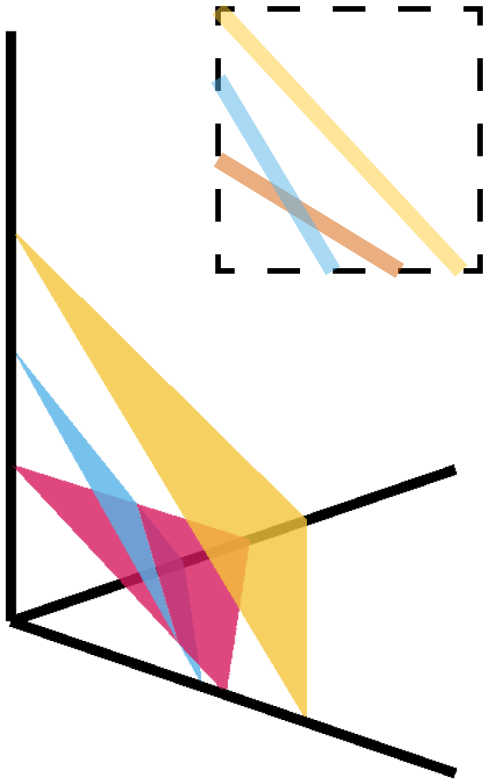

Figure A-5: 1 intersection on innermost ZNGIs, 0 intersection outside: This case is equivalent to the 2-resource case with two innermost ZNGIs intersecting. The slowest grower (yellow) is excluded by others, and the others may coexist or exclude one another depending on resource supply.

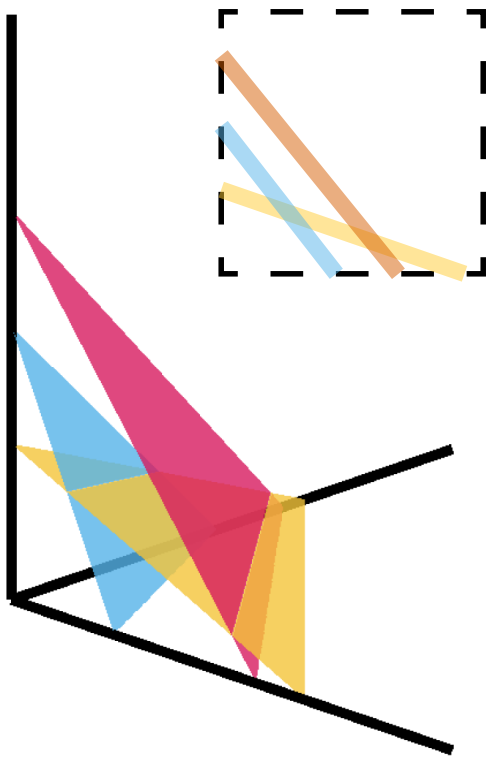

Figure A-5: 1 intersection on innermost ZNGIs, 1 intersection outside: This case is equivalent to the 2-resource case with one ZNGI intersecting with the other two.

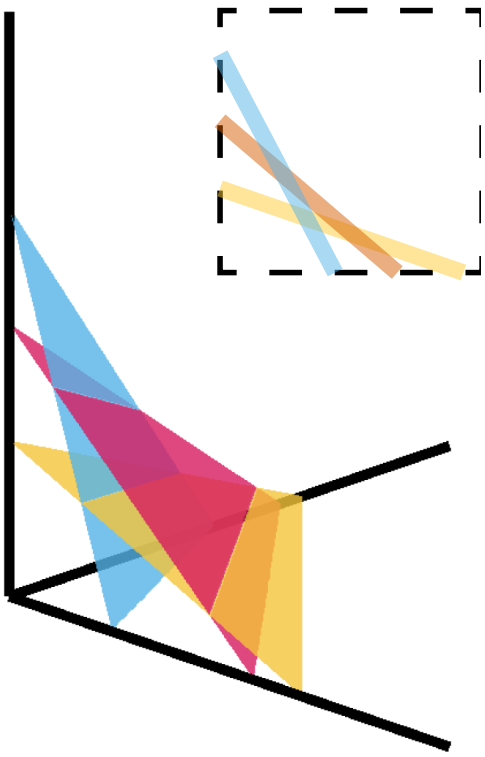

Figure A-5: 1 intersection on innermost ZNGIs, 2 intersections outside: This case is equivalent to the 2-resource case with all ZNGI pairs intersecting, with innermost ZNGIs consisting of two ZNGIs.

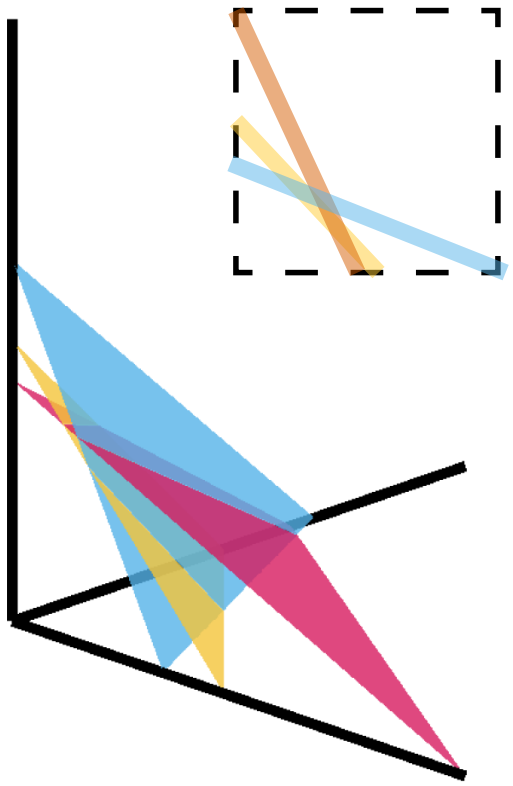

Figure A-5: 2 intersections on innermost ZNGIs, 1 intersection outside: This case is equivalent to the 2-resource case with all ZNGI pairs intersecting, with innermost ZNGIs consisting of three ZNGIs.

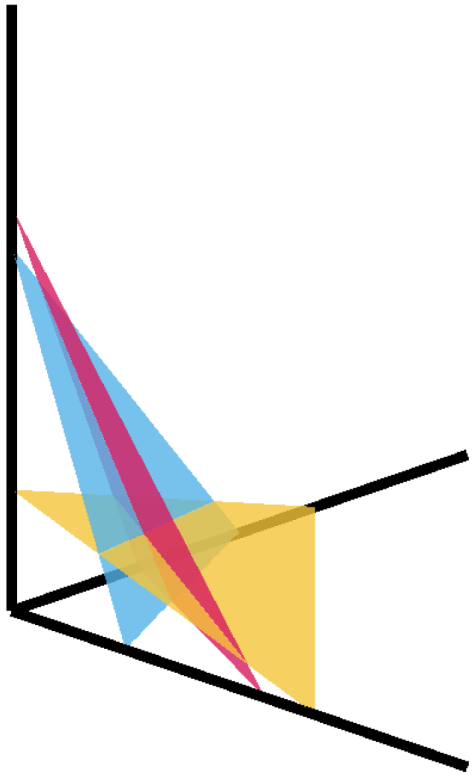

Figure A-5: 7. Three ZNGIs intersect at a point: This case is not equivalent to any of 2-resource cases, which we can immediately see from the fact that three ZNGIs cannot intersect at a point on a plane in general. Remarkably, this is the only case where all three species can coexist. The phase diagram of outcomes for this arrangement is illustrated in Fig. S2.

Appendix B

Appendix for Chapter 3

Supplementary figures

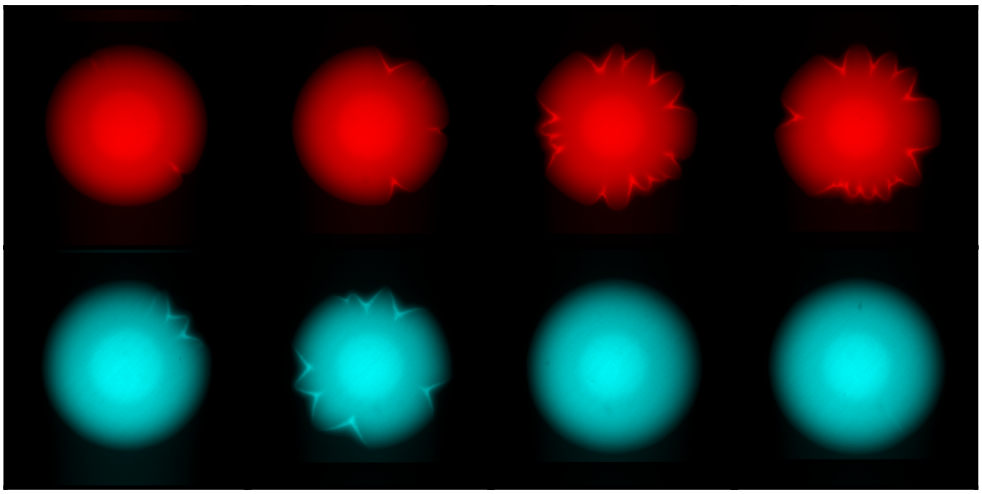

Figure B-1: Emergence of dents in wildtype colonies was reproducible. Wildtype colonies were grown for 48 hours. Top: wildtype strains constitutively expressing mScarlet-I. Bottom: wildtype strains constitutively expressing mTurquois-2.

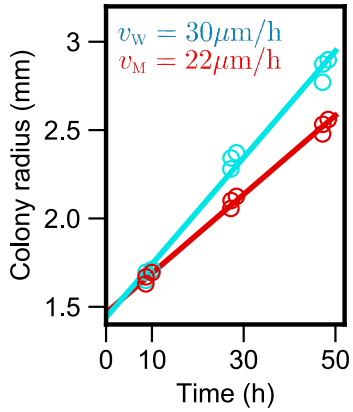

Figure B-2: Mutant expands more slowly regardless of the choice of fluorescent labels. Wildtype with mTurquoise-2 fluorescence protein expanded with $v_W = 30\ \mu m/h$ while mutant with mScarlet-I fluorescence protein expanded with $v_M = 22\ \mu m/h$.

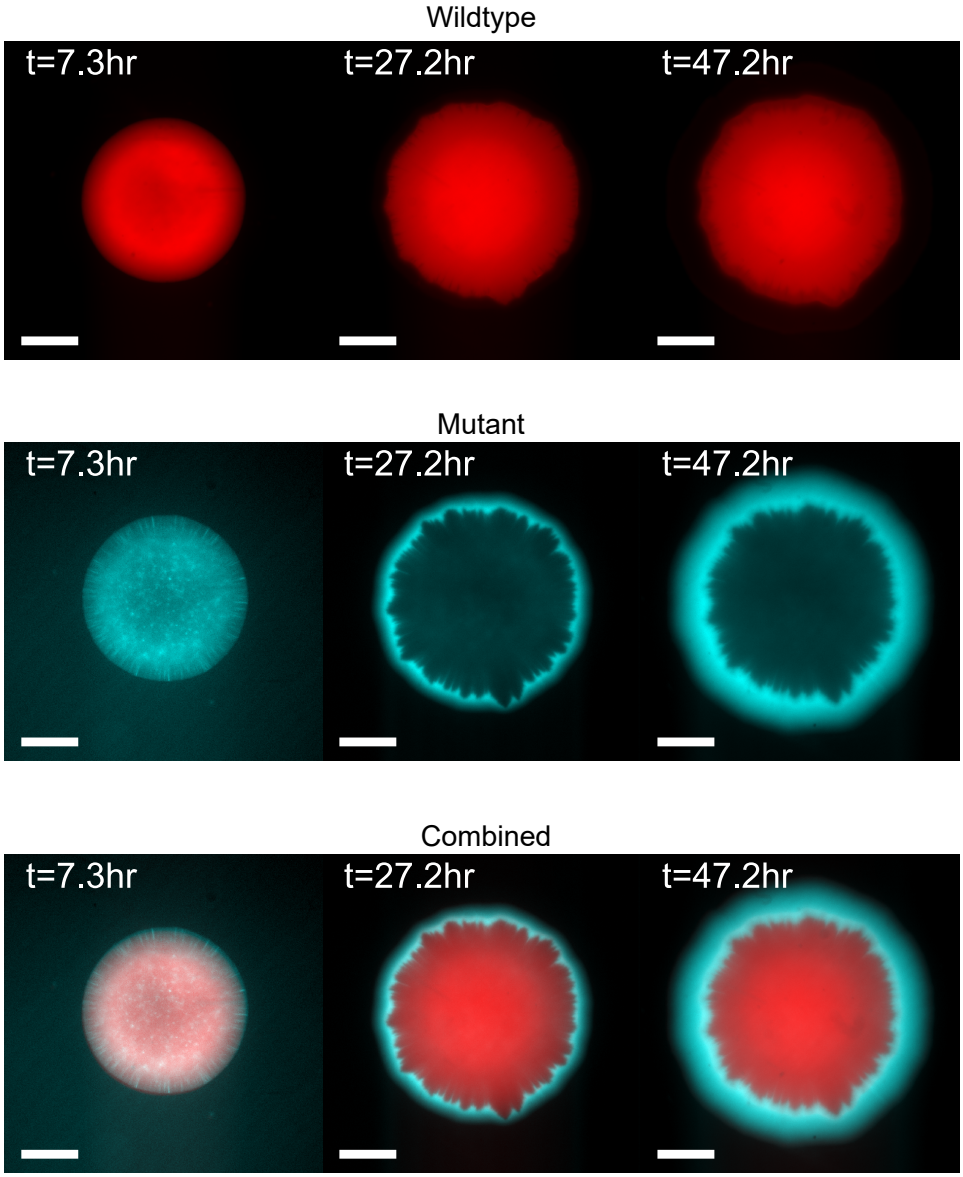

Figure B-3: In co-culture experiment, wildtype did not expand after a day while mutant kept expanding. Top: Fluorescence images of wildtype cells during expansion. Middle: Fluorescence images of mutant cells during expansion. Bottom: combined.

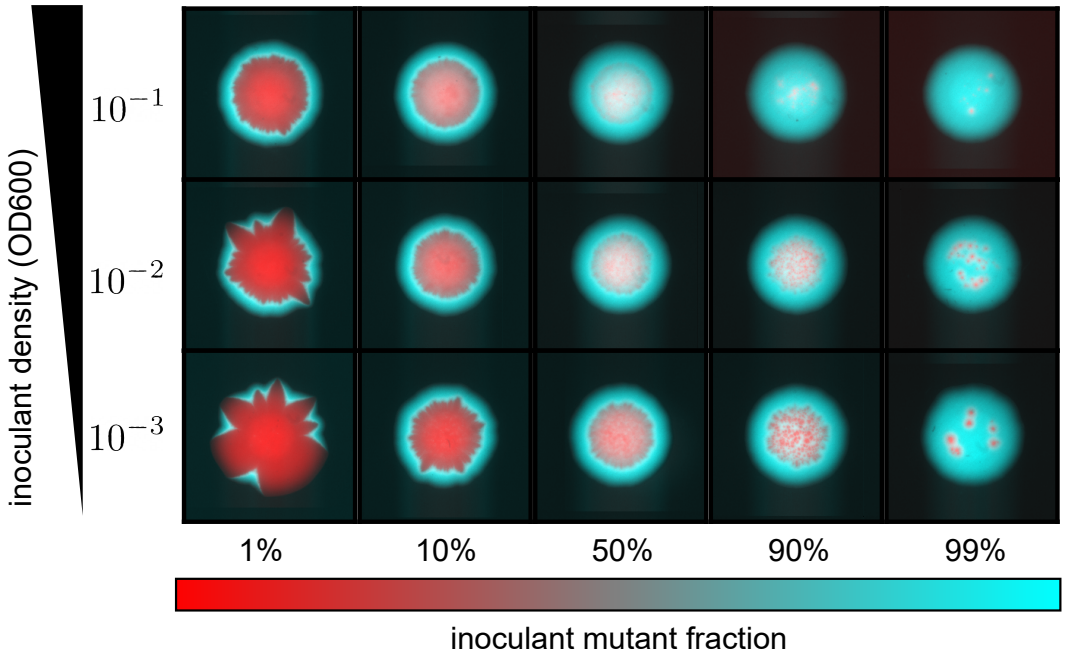

Figure B-4: Mutant outcompetes wildtype under a wide range of inoculant densities and initial mutant fractions.

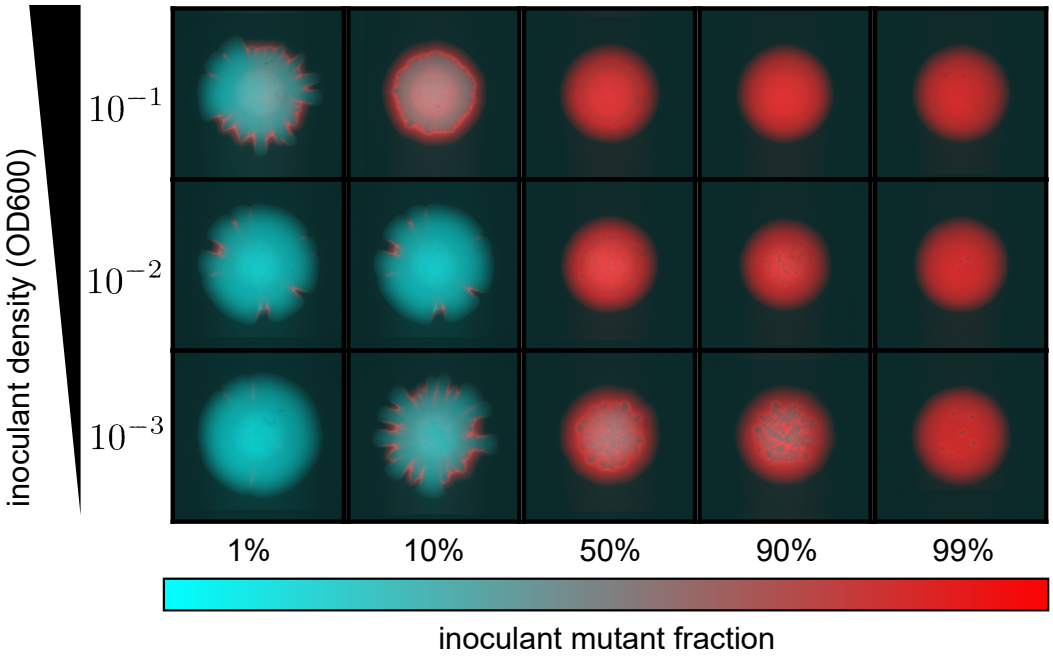

Figure B-5: Mutant outcompetes wildtype under a different choice of fluorescent labels of wildtype and mutant.

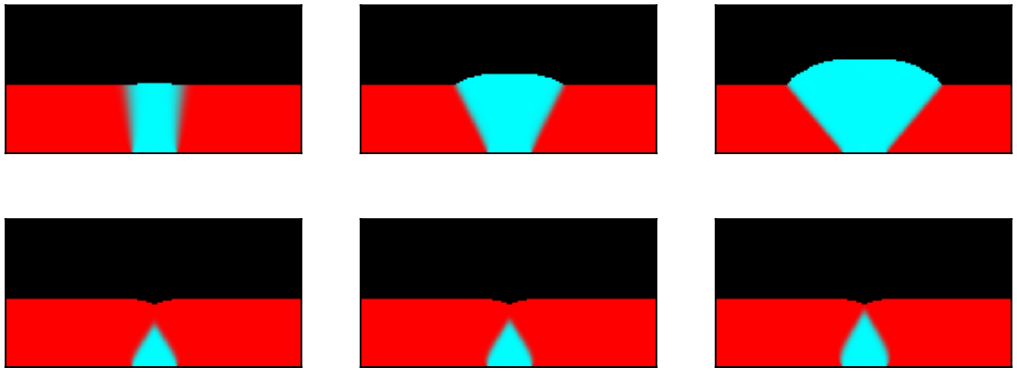

Figure B-6: No dented fronts occur in simulations with density-independent growth and dispersal. In each column, the growth advantage $r_{\mathrm{M}}/r_{\mathrm{W}} - 1$ is the same (Left: 0.04, Middle: 0.36, Right:1). Simulations in top row have $D_{\mathrm{W}} = D_{\mathrm{M}}$, so that the ratio of the expansion velocities varies with the growth rates ($v_{\mathrm{M}} = v_{\mathrm{W}}\sqrt{r_{\mathrm{M}}/r_{\mathrm{W}}}$). For the bottom row, we used $D_{\mathrm{M}} = \frac{0.64 r_{\mathrm{W}}}{r_{\mathrm{M}}} D_{\mathrm{W}}$ so that $v_{\mathrm{M}} = 0.8 v_{\mathrm{W}}$. We observed no expanding mutant sectors when its expansion velocity was less than that of the wildtype.

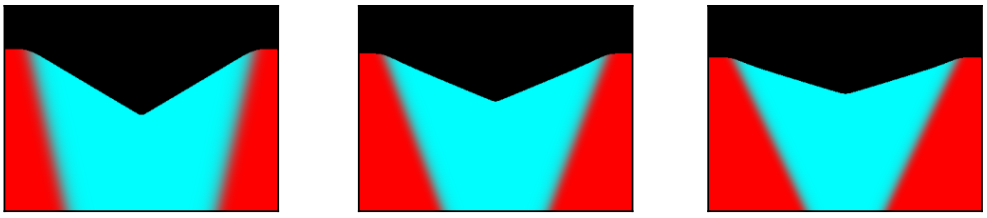

Figure B-7: Dented fronts occur in simulations with $D_{\mathrm{M}} \neq D_{\mathrm{W}}$. We used a variation of cheater-cooperator model (Eq. 2) in which dispersal of wildtype and mutant is no longer identical. In all cases of $D_{\mathrm{M}} = 0.9D_{\mathrm{W}}$, $D_{\mathrm{M}} = D_{\mathrm{W}}$, and $D_{\mathrm{M}} = 1.1D_{\mathrm{W}}$ mutant developed a dented front with only quantitative changes in sector shapes. These simulations used parameters $s = 0.4$ and $\alpha = 0.6$.

B.1 Geometric theory and sector shapes

B.1.1 Introduction

During spatial growth in microbial colonies or other cellular aggregates, mutants appear and compete with each other. Previous studies [79] and common intuition suggest that advantageous mutants should form a sector that bulges out of the expansion front. In the main text, we reported experiments showing that this is not always the case. Here, we identify all possible shapes that can result from competition between two types in a growing colony.

To make progress, we make a number of approximations and work in the so-called geometrical optics limit. This limit assumes that the expansion front and the boundary between the types can be treated as thin lines. Neglecting sector and boundary widths is justified when these length scales are much smaller than the colony size. In small colonies, thin boundaries require strong genetic drift and slow motility. Furthermore, we assume that the expansion velocity of each type remains fixed. In particular, we neglect the effects of spatial variation in nutrient concentration due to protrusions of one type ahead of the other. This approximation is valid for high nutrient concentrations and when the size of the protrusions is small compared to the size of the mutant sector.

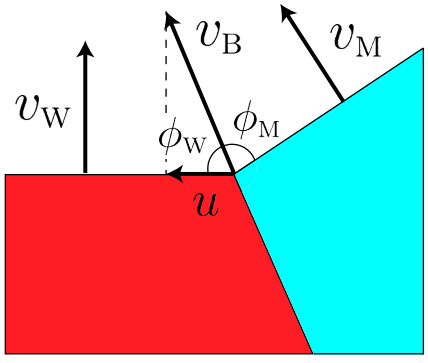

Figure B-8: Geometry of the competition.

In the geometric-optics limit, the competition between two types is described by three velocities: the velocity of mutant v_M, the velocity of wildtype v_W, and the

velocity of the boundary v_{B}, which are shown in Fig. B-8. (Note $v_{\text{B}} \neq u$) Previous work [79] focused on the regime when v_{B} was determined by v_{M} and v_{W}; in contrast, we make no assumptions about the relative magnitude of these three velocities.

To avoid confusion we want to reiterate that the velocity of the wildtype v_{W} is defined in isolation, away from the mutant. Similarly, the velocity of the mutant v_{M} is defined in isolation, away from the wildtype. For brevity, we refer to wildtype as fast and mutant as slow even though this terminology is not applicable at the sector boundary where the mutant may expand faster than the wildtype.

In the close vicinity of the sector boundary, the two expansion fronts can be approximated as straight lines. Their position (Fig. B-8) is determined by requiring that the expansion along the boundary with velocity v_{B} results in the same displacement of the fronts as moving perpendicular to them with velocities v_{M} and v_{W} respectively:

$$v_{\text{W}} = v_{\text{B}} \sin \phi_{\text{W}}, \tag{B.1}$$

$$v_{\text{M}} = v_{\text{B}} \sin \phi_{\text{M}}. \tag{B.2}$$

For linear inoculations, the above equations are sufficient to completely specify sector shapes because, as we show below, the expansion fronts are straight lines even away from the sector boundary. For circular initial conditions, Eqs. (B.2) provide information only about the local orientation at the sector boundary, and further calculations are necessary. One way to obtain global shape is to write down partial differential equations that specify how the position of the front changes and use Eqs. (B.2) as the boundary conditions. A much simpler approach is to use an equal time argument from Ref. [79].

This method traces the ancestral lineage from each point along the front and requires that the time traveled on that lineage is equal to the current time t. The location of the ancestral lineage is such that it takes the shortest time to reach the initial population starting from a given point without entering the space occupied by the other type. The details of these calculations are provided below.

Before proceeding, we note that, here and in the main text, we typically parameterize the problem with velocity u rather than v_{B}. Since u is defined as the velocity of the boundary point along the front of wildtype, we can obtain it by projecting the boundary velocity on the expansion front of the wildtype:

$$u = v_{\text{B}} \cos \phi_{\text{W}}. \tag{B.3}$$

From this equation and Eq. (B.2), it follows that

$$v_{\text{B}} = \sqrt{v_{\text{W}}^2 + u^2}. \tag{B.4}$$

In the following, we assume that mutant takes over the front, i.e. $u > 0$. Mutants with negative u immediately become extinct at least in the deterministic model considered here.

Finally, we observe that Eqs. (B.2) impose constraints on the values of the three velocities. In particular, since sines are always less than one, the boundary velocity v_{B} must be greater or equal than both v_{M} and v_{W}. In terms of u, this implies that

$$v_{\text{M}} \leq \sqrt{u^2 + v_{\text{W}}^2}. \tag{B.5}$$

B.1.2 Linear inoculation

Sector boundary

Linear expansion geometry, the simplest situation to consider, allows us to explain the essence of the equal time argument. This geometry is illustrated in Fig. B-9. Initially ($t = 0$), the colony front is located at $y = 0$, and expansion proceeds in the upper half-plane. Mutant is only present at a single point, which we put at $x = 0$; the rest of the front is occupied by the wildtype.

As the expansion proceeds, the region near $x = 0$ is affected by the competition between the types. From the definition of u, the extent of this region is given by $x \in (-ut, ut)$. Regions further away are however unaffected and expand as if

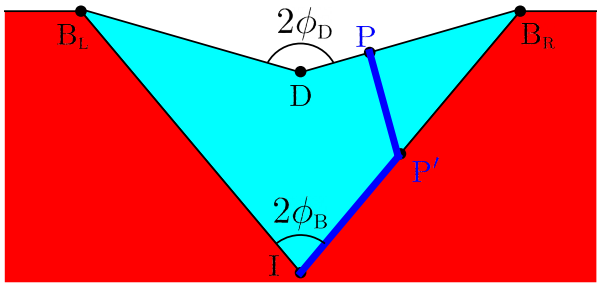

Figure B-9: Sector shape for linear inoculation and $v_M < v_W$. Sectors of faster wildtype (red) and slower mutant (cyan) meet at sector boundary $\overline{IB}_L$ and $\overline{IB}_R$. It takes the shortest time for the mutant to go from its initial location at I to a point on the front P by first following $\overline{IP'}$ and then $\overline{P'P}$ (blue path). The resulting geometry can be characterized by two opening angles: $2\phi_B$ for the sector boundary and $2\phi_D$ for the expansion front.

only wildtype is present. Thus, for $|x| \geq ut$, the front is located at $y = v_W t$. From these considerations, we can further conclude that the sector boundary is described by $(ut, v_W t)$. Note that, below, we consider only the right side of the expansion; the left side is described by the mirror image with respect to the y-axis. Thus,

$$\tan \phi_B = \frac{u}{v_W}. \tag{B.6}$$

Note that, $\phi_B = \phi_W - \pi/2$, which is clear from Figs. B-8 and B-9.

The shape of the front for $|x| < ut$ depends on the relative values of v_M, v_W, and u.

$v_M \leq v_W$

When mutant is slower than wildtype, we find that front has a V-shaped dent with an opening angle $2\phi_D$ as shown in Fig. B-9. To derive this result, we take a point P on the front with yet unknown coordinates (x_p, y_p). Note that $x_p \in (0, ut)$. Then, we should obtain the location of the ancestral lineage that connects this point to the initial location of the mutant: point I. Because the ancestral lineage is located so that to minimize the travel time, it must be a union of straight lines. Indeed, it is a well-known fact from geometrical optics that light rays travel on straight lines except where the value of the refraction index changes [20]. In our case, this means that the ancestral lineages of mutant can consist of straight lines within the mutant sector

and regions of the boundary. Obviously, the ancestral lineage of the mutant cannot penetrate the region occupied by the wildtype.

The equal time argument then offers us two possibilities: a direct connection $\overline{IP}$ and an indirect connection $I\widehat{P'P}$ via a point P' on the sector boundary. The times to traverse these paths are

$$T_{PI} = |PI|/v_{\text{M}}, \tag{B.7}$$

$$T_{PP'I} = |PP'|/v_{\text{M}} + |P'I|/v_{\text{B}}. \tag{B.8}$$

To complete the analysis, we need to choose the path with the lowest travel time and determine all locations of P for which the travel time equals t. For the direct connection, it is clear that P must lie on an arc of a circle with the radius of $v_{\text{M}}t$ centered at I. For the indirect connection, we first need to determine the location of P', which must minimize the travel time.

Since P' lies on the sector boundary its coordinates are given by $(ut', v_{\text{W}}t')$ with an unknown t'. The travel time is then given by

$$T_{PP'I} = \frac{\sqrt{(x_p - ut')^2 + (y_p - v_{\text{W}}t')^2}}{v_{\text{M}}} + \frac{\sqrt{u^2 + v_{\text{W}}^2}t'}{v_b}. \tag{B.9}$$

Upon minimizing $T_{PP'I}$ with respect to t', we find that

$$t' = \frac{u\sqrt{u^2 + v_{\text{W}}^2 - v_{\text{M}}^2} + v_{\text{M}}v_{\text{W}}}{(u^2 + v_{\text{W}}^2)\sqrt{u^2 + v_{\text{W}}^2 - v_{\text{M}}^2}} \left(x_p + \frac{uv_{\text{W}} - v_{\text{M}}\sqrt{u^2 + v_{\text{W}}^2 - v_{\text{M}}^2}}{u^2 - v_{\text{M}}^2} y_p \right), \tag{B.10}$$

and the travel time equals

$$T_{PP'I} = \frac{(uv_{\text{M}} - v_{\text{W}}\sqrt{u^2 + v_{\text{W}}^2 - v_{\text{M}}^2})x_p + (v_{\text{M}}v_{\text{W}} + u\sqrt{u^2 + v_{\text{W}}^2 - v_{\text{M}}^2})y_p}{(u^2 + v_{\text{W}}^2)v_{\text{M}}}, \tag{B.11}$$

which is smaller than T_{PI} as long as $v_{\text{M}} < v_{\text{W}}$. Thus, the ancestral lineages takes an

indirect path that first connects point P to the sector boundary and then follows the sector boundary until I. The shape of the front is determined by setting $T_{PP'I}$ from Eq. (B.11) equal to t. This results in a segment of a straight line, and a straightforward calculation shows that

$$\phi_{\text{D}} = \arctan\left(\frac{u\sqrt{v_{\text{W}}^2 + u^2 - v_{\text{M}}^2} + v_{\text{M}}v_{\text{W}}}{v_{\text{W}}\sqrt{v_{\text{W}}^2 + u^2 - v_{\text{M}}^2} - uv_{\text{M}}}\right). \tag{B.12}$$

Because the front and the sector boundaries are straight, the result above also directly follows from Eqs. (B-8). Indeed, a simple geometric argument shows that $\phi_{\text{D}} = \phi_{\text{M}} + \phi_{\text{W}} - \pi/2$.

Note that, for $v_{\text{M}} = v_{\text{W}}$, the angle $\phi_{\text{D}} = \pi/2$ and the whole front is flat as it should if the expansion rates of the strains are identical.

$v_{\mathbf{M}} = \sqrt{v_{\mathbf{W}}^2 + u^2}$

In the limiting case of maximal allowed v_{M}, the shape of the sector is also simple and immediately follows from the calculations above. Now, as we compare the two alternative paths, we find that T_{PI} is always smaller than $T_{PP'I}$. Thus, the shape of the sector is an arc of a circle of radius $v_{\text{M}}t$ around I that connects to the flat front of the wild type at the sector boundary.

Previous work that used the equal time argument to describe competition in microbial colonies only considered $v_{\text{M}} = \sqrt{v_{\text{W}}^2 + u^2}$ and missed other possible front shapes [79]. While it might appear that $v_{\text{M}} = \sqrt{v_{\text{W}}^2 + u^2}$ is a very special case, this relationship between the velocities holds across a wide set of conditions. Specifically, $v_{\text{M}} = \sqrt{v_{\text{W}}^2 + u^2}$ whenever local competition between the types is not strong enough to alter the priority effects due to different expansion velocities.

$v_{\mathbf{W}} < v_{\mathbf{M}} < \sqrt{v_{\mathbf{W}}^2 + u^2}$

The remaining possibility is the hybrid of the two cases considered so far. Depending on how far P is from the sector boundary, the quickest path from P to I may be either the direct or the indirect connection. We find that the front around $x = 0$ is a

semicircle of radius $v_{\rm M}t$, but it is a straight line near the sector boundaries. The two segments joint smoothly. The angular half-width of the central arc, $\phi_{\rm transition}$, and the slope of the linear segment (see Fig. B-10) are given by

$$\phi_{\rm transition} = \arctan\left(\frac{uv_{\rm M} - v_{\rm W}\sqrt{v_{\rm W}^2 + u^2 - v_{\rm M}^2}}{v_{\rm M}v_{\rm W} + u\sqrt{v_{\rm W}^2 + u^2 - v_{\rm M}^2}}\right), \tag{B.13}$$

$$\text{slope} = -\frac{uv_{\rm M} - v_{\rm W}\sqrt{v_{\rm W}^2 + u^2 - v_{\rm M}^2}}{v_{\rm M}v_{\rm W} + u\sqrt{v_{\rm W}^2 + u^2 - v_{\rm M}^2}}. \tag{B.14}$$

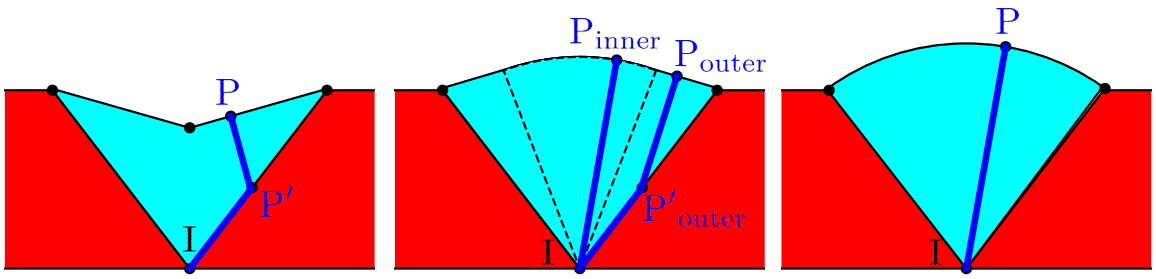

Figure B-10: Possible sector shapes for linear inoculation. Left: $v_{\rm M} < v_{\rm W}$. The mutant sector emerging from point I has a dented front. The front consists of two straight lines. The shortest-time path follows the sector boundary and also enters the sector interior. Middle: $v_{\rm W} < v_{\rm M} < \sqrt{v_{\rm W}^2 + u^2}$. The mutant sector is a composite bulge. The front consists of two straight lines and an arc. To reach a point P_{outer} on straight part of the expansion front, the shortest-time path first follows the sector boundary before entering the sector interior. To reach a point P_{inner} on the arc, the shortest-time path follows a straight line from I to P_{inner}. Right: $v_{\rm M} > \sqrt{v_{\rm W}^2 + u^2}$. The front is an arc. To reach a point P on the front, the shortest-time path follows a straight line from I to P.

B.1.3 Circular inoculation

We assume that the expansion starts at $t = 0$ when wildtype colony fills the circle with radius $r \le r_0$, and the mutant is present only at $I = (r_0, 0)$ in polar coordinates.

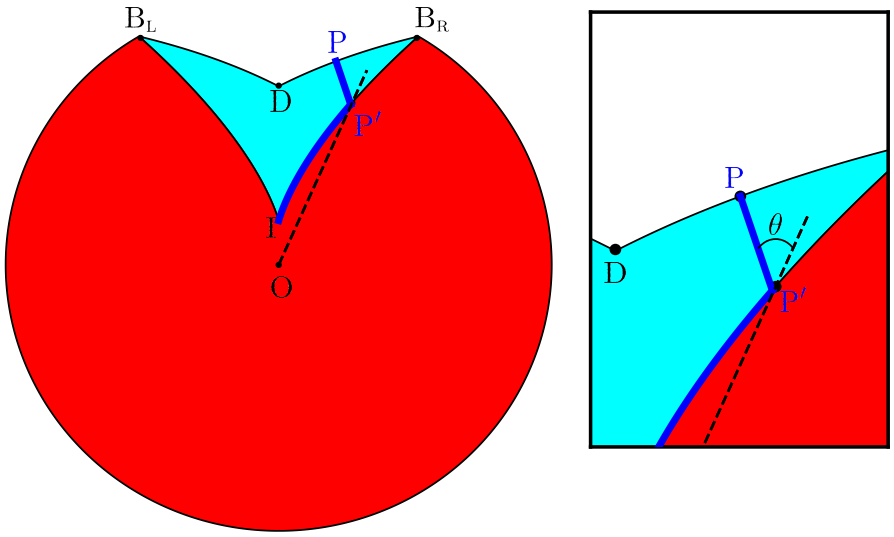

Figure B-11: Circular colony with a dented front, $v_{\text{W}} > v_{\text{M}}$. The path of the shortest time follows the sector boundary from I to P' and then a straight line connecting P' and P. Note that $\overline{P'P}$ and $\overline{OP'}$ always intersect at angle θ.

Sector boundary

The boundary between the mutant and the wild type moves with linear velocity u along the front.In polar coordinates, the position of the sector boundary $(r_{\text{B}}, \phi_{\text{B}})$ then obeys the following equation

$$\frac{d\phi_{\text{B}}}{dt} = \frac{u}{r_{\text{B}}}. \tag{B.15}$$

We can eliminate time by using $dr_{\text{B}}/dt = v_{\text{W}}$ to obtain

$$\phi_{\text{B}}(r_{\text{B}}) = \frac{u}{v_{\text{W}}} \ln(\frac{r_{\text{B}}}{r_0}). \tag{B.16}$$

We also find that the length of boundary at time t is $\sqrt{v_{\text{W}}^2 + u^2}t$, and thus

$$v_{\text{B}} = \sqrt{v_{\text{W}}^2 + u^2} \tag{B.17}$$

just as in the linear case.

$v_{\mathrm{M}} < v_{\mathrm{W}}$

Let us consider a point $P = (r_p, \phi_p)$ on a mutant patch with $\phi_p > 0$ for simplicity. As described before, we first find $T_{PP'I}$ by minimizing $\frac{|PP'|}{v_{\mathrm{M}}} + \frac{|\widehat{P'I}|}{v_{\mathrm{W}}}$ over points P' on the sector boundary. The point $P' = (r_{P'}, \phi_{P'})$ should satisfy two equations:

$$\phi_{P'}(r_{P'}) = \frac{u}{v_{\mathrm{W}}} \ln(\frac{r_{P'}}{r_0}), \tag{B.18}$$

$$\frac{d}{dr_{P'}} \left(\frac{r_{P'} - r_0}{v_{\mathrm{W}}} + \frac{\sqrt{(r_p \cos\phi_p - r_{P'} \cos\phi_{P'})^2 + (r_p \sin\phi_{P'} - r_{P'} \sin\phi_{P'})^2}}{v_{\mathrm{M}}} \right) = 0. \tag{B.19}$$

Here, the first equation constrains P' to be on the sector boundary, and the second equation minimizes $T_{PP'I}$ over P'. Since there are two unknowns and two equations, we can solve for $(r_{P'}, \phi_{P'})$. The solution is conveniently written in an implicit form:

$$\begin{aligned} &\frac{r_{P'} \sin\phi_{P'} - r_p \sin\phi_p}{r_{P'} \cos\phi_{P'} - r_p \cos\phi_p} = -\tan(\theta - \phi_{P'}), \\ &\theta = \arctan\left(\frac{u v_{\mathrm{M}} - v_{\mathrm{W}} \sqrt{v_{\mathrm{W}}^2 + u^2 - v_{\mathrm{M}}^2}}{v_{\mathrm{M}} v_{\mathrm{W}} + u \sqrt{v_{\mathrm{W}}^2 + u^2 - v_{\mathrm{M}}^2}} \right). \end{aligned} \tag{B.20}$$

This tells that $\overline{PP'}$ is parallel to $(1, \theta - \phi_{P'})$; the angle between $\overline{PP'}$ and $\overline{P'O}$ is a constant θ independent of r_p, ϕ_p. Note that $\theta > 0$ for $v_{\mathrm{M}} < v_{\mathrm{W}}$, and thereby every point P on mutant front with ϕ_p has its corresponding P' on sector boundary $\widehat{IB}$.

The next step toward identifying the front position at time T is to find all points P such that $T_{PP'I} = T$. Using the mapping between P and P' described above, we find P by first moving along sector boundary and then moving in a straight line parallel to $(1, \theta - \phi_{P'})$. By varying the time t' spent along the sector boundary while keeping the total time T fixed, we obtain a parametric expression for $P(T) = (x_p(T), y_p(T))$ in Cartesian coordinates:

$$x_p(T;t') = (v_{\mathrm{w}}t' + r_0)\sin(\frac{u}{v_{\mathrm{w}}}\ln(\frac{r_0+v_{\mathrm{w}}t'}{r_0})) + v_{\mathrm{M}}(T-t')\sin(\frac{u}{v_{\mathrm{w}}}\ln(\frac{r_0+v_{\mathrm{w}}t'}{r_0}) - \theta),$$
$$y_p(T;t') = (v_{\mathrm{w}}t' + r_0)\cos(\frac{u}{v_{\mathrm{w}}}\ln(\frac{r_0+v_{\mathrm{w}}t'}{r_0})) + v_{\mathrm{M}}(T-t')\cos(\frac{u}{v_{\mathrm{w}}}\ln(\frac{r_0+v_{\mathrm{w}}t'}{r_0}) - \theta). \tag{B.21}$$

It is also possible to get a non-parametric, explicit expression by solving an equivalent partial differential equation using the method of characteristics:

$$\begin{aligned}
&\phi_p(t,r) = \frac{u}{v_{\mathrm{w}}}\ln\left(1+\frac{v_{\mathrm{w}}t}{r_0}\right) + F\left(\frac{r}{r_0+v_{\mathrm{w}}t}\right) - F(1), \quad \text{where} \\
&F(\rho) = \frac{u}{2v_{\mathrm{w}}}\ln\left((\rho^2 v_{\mathrm{w}}^2 - v_{\mathrm{M}}^2)\frac{\sqrt{\rho^2 - \frac{v_{\mathrm{M}}^2}{v_{\mathrm{w}}^2+u^2}} - \frac{uv_{\mathrm{M}}}{v_{\mathrm{w}}\sqrt{v_{\mathrm{w}}^2+u^2}}}{\sqrt{\rho^2 - \frac{v_{\mathrm{M}}^2}{v_{\mathrm{w}}^2+u^2}} + \frac{uv_{\mathrm{M}}}{v_{\mathrm{w}}\sqrt{v_{\mathrm{w}}^2+u^2}}}\right) \\
&+ \arctan\left(\frac{\sqrt{v_{\mathrm{w}}^2+u^2}}{v_{\mathrm{M}}}\sqrt{\rho^2 - \frac{v_{\mathrm{M}}^2}{v_{\mathrm{w}}^2+u^2}}\right).
\end{aligned} \tag{B.22}$$

$v_{\mathrm{M}} > v_{\mathrm{w}}$

In this regime, $\theta < 0$ and thereby some points P on the mutant front do not have a corresponding P' on the sector boundary. In other words, the straight path $\overline{IP}$ takes the shortest time. We find that, when P is near the top of the bulge, the minimal path is a straight line $\overline{IP}$ while, When P is further from the top, the minimal path is a straight line $\overline{P'P}$ followed by a curved path $\overset{\frown}{IP'}$ along the sector boundary.

Note that the straight path is tilted by a fixed angle θ from $\overline{OP'}$, pointing inwards to the center of the sector compared to the tangent line except when $v_{\mathrm{M}} = \sqrt{v_{\mathrm{w}}^2+u^2}$. In the latter case, $\theta = -\arctan\left(\sqrt{\frac{v_{\mathrm{M}}^2}{v_{\mathrm{w}}^2}-1}\right)$, and the straight path is tangent to the sector boundary, as described in [79].

The boundary between the two regions of the front lies angle $\phi_{\text{transition}}$ way from the center. This angle is given by

$$\phi_{\text{transition}} = \arctan\left(\frac{uv_{\mathrm{M}} - v_{\mathrm{w}}\sqrt{v_{\mathrm{w}}^2+u^2-v_{\mathrm{M}}^2}}{v_{\mathrm{M}}v_{\mathrm{w}} + u\sqrt{v_{\mathrm{w}}^2+u^2-v_{\mathrm{M}}^2}}\right). \tag{B.23}$$

Thus, the bulge is an arc of a circle near the center and is described by Eq. (B.21) near the sector boundary.

B.2 Dispersal without carrying capacity

In the main text, we considered two mechanistic models that produce all possible sector shapes. For both models, we assumed that the dispersal term has a factor of $(1 - n_{\mathrm{W}} - n_{\mathrm{M}})$ so that the dispersal ceases when population reaches the carrying capacity. Without the carrying capacity factor, any spatial patterns should eventually vanish because the populations continue to intermix behind the expanding front. Accordingly, sectors exist only in the transient timescale between expansion and diffusion. Nevertheless, the $(1-n_{\mathrm{W}}-n_{\mathrm{M}})$ factor does not affect the ratios between three velocities v_{W}, v_{M} and u, and since these ratios determine the sector shape in geometric theory, we expect that the absence of the $(1 - n_{\mathrm{W}} - n_{\mathrm{M}})$ factor does not affect the sector shape observed in transient timescales. To verify this idea, we simulated a microscopic model without carrying capacity on diffusion:

$$\begin{aligned}
\partial_t n_{\mathrm{W}} &= D\nabla^2 n_{\mathrm{W}} + r\left(1 - \alpha\frac{n_{\mathrm{M}}}{n_{\mathrm{W}} + n_{\mathrm{M}}}\right) n_{\mathrm{W}}(1 - n_{\mathrm{W}} - n_{\mathrm{M}}), \\
\partial_t n_{\mathrm{M}} &= D\nabla^2 n_{\mathrm{M}} + r\left(1 - s + \alpha\frac{n_{\mathrm{W}}}{n_{\mathrm{W}} + n_{\mathrm{M}}}\right) n_{\mathrm{M}}(1 - n_{\mathrm{W}} - n_{\mathrm{M}}).
\end{aligned} \tag{B.24}$$

The simulation demonstrated that the sector shape was not affected by carrying capacity factor from dispersal (Fig. B-12). The sector boundaries were blurred by the nonzero dispersal behind the front, but the overall shape of the sector remained the same.

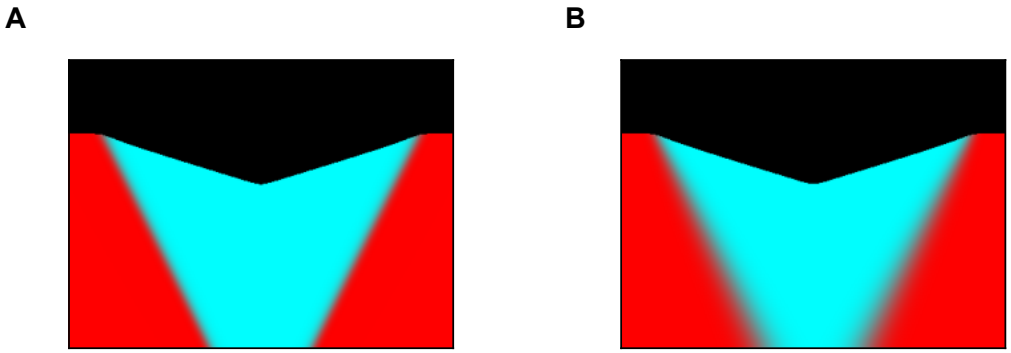

Figure B-12: Dented front in a model with density-independent dispersal. Formation of dented sectors in simulations with different models of dispersal. (A) The model from the main text Eq. 1. (B) A model with density-independent dispersal Eq. B.24. Note the blurry sector boundaries due to continued intermixing after growth ceases behind the front.

B.3 Nonspatial limit for mechanistic models

In the main text, we considered two mechanistic models that produce all possible sector shapes. Here, we analyze these models in the nonspatial, i.e. well-mixed, limit, which describes local competition.

B.3.1 Cheater-cooperator model

The model reads

$$\begin{aligned}\partial_t n_{\mathrm{W}} &= \left(D\nabla^2 n_{\mathrm{W}} + r\left(1-\alpha\frac{n_{\mathrm{M}}}{n_{\mathrm{W}}+n_{\mathrm{M}}}\right)n_{\mathrm{W}}\right)(1-n_{\mathrm{W}}-n_{\mathrm{M}}),\\ \partial_t n_{\mathrm{M}} &= \left(D\nabla^2 n_{\mathrm{M}} + r\left(1-s+\alpha\frac{n_{\mathrm{W}}}{n_{\mathrm{W}}+n_{\mathrm{M}}}\right)n_{\mathrm{M}}\right)(1-n_{\mathrm{W}}-n_{\mathrm{M}}).\end{aligned} \tag{B.25}$$

In the well-mixed limit, the partial differential equations above reduce to a set of ordinary differential equations:

$$\begin{aligned}\frac{dn_{\mathrm{W}}}{dt} &= r\left(1-\alpha\frac{n_{\mathrm{M}}}{n_{\mathrm{W}}+n_{\mathrm{M}}}\right)n_{\mathrm{W}}(1-n_{\mathrm{W}}-n_{\mathrm{M}}),\\ \frac{dn_{\mathrm{M}}}{dt} &= r\left(1-s+\alpha\frac{n_{\mathrm{W}}}{n_{\mathrm{W}}+n_{\mathrm{M}}}\right)n_{\mathrm{M}}(1-n_{\mathrm{W}}-n_{\mathrm{M}}).\end{aligned} \tag{B.26}$$

We only consider $s < 1$ and $-1 < \alpha < 1$ and assume that initial populations densities are positive and their sum is below the carrying capacity. With these assumptions, it is clear that the population densities remain positive for any $t \geq 0$ since $\frac{dn_{\mathrm{W}}}{dt}$ and $\frac{dn_{\mathrm{M}}}{dt}$ are positive. The monotonic increase of the population densities also ensures that $\lim_{t\to\infty} n_{\mathrm{W}} + n_{\mathrm{M}} = 1$ because both time derivatives switch sign when $n_{\mathrm{W}} + n_{\mathrm{M}}$ exceeds unity. In fact, it follows directly from Eqs. (B.26) that any pair of positive n_{W} and n_{M} that sum up to one is a fixed point.

This line of fixed points is a direct consequence of our assumption that population dynamics are frozen behind the front. In a generic Lotka-Volterra system, the differences in the competitive abilities at high population densities would break this degeneracy and lead to the takeover by one of the types (stable coexistence is also

possible) [109, 79]. Microbial populations however grow only until the nutrients are exhausted, and the two types could, therefore, remain at an arbitrary ratio once the growth ceases.

Further insights into the behavior of Eq. (B.26) can be derived from its first integral (a conserved quantity), which we obtain by dividing the two equations:

$$\frac{dn_{\rm W}}{dn_{\rm M}} = \frac{\left(1-\alpha\frac{n_{\rm M}}{n_{\rm W}+n_{\rm M}}\right)n_{\rm W}}{\left(1-s+\alpha\frac{n_{\rm W}}{n_{\rm W}+n_{\rm M}}\right)n_{\rm M}}. \tag{B.27}$$

The equation above can be integrated after both sides are multiplied by $dn_{\rm M}(1-s+\alpha n_{\rm W}/(n_{\rm W}+n_{\rm M}))/n_{\rm W}$. This procedure yields the following conserved quantity:

$$C = \frac{(n_{\rm W}+n_{\rm M})^{\alpha} n_{\rm W}^{1-s}}{n_{\rm M}}, \tag{B.28}$$

which we can use to understand the temporal dynamics of the two types. It is convenient to recast Eq. (B.28) in terms of total population density $n = n_{\rm W} + n_{\rm M}$ and mutant frequency $f = n_{\rm M}/n$:

$$\frac{f}{(1-f)^{1-s}} = \frac{n^{\alpha-s}}{C}. \tag{B.29}$$

The left-hand side is a monotonically increasing function of f, and the right hand-side is a monotonic function of n, which is increasing for $\alpha > s$ and decreasing otherwise. Thus, f increases with n for $\alpha > s$ and decreases for $\alpha < s$. Since n is always increasing (assuming it is less than one initially), we conclude that the relative abundance of the mutant increases when $\alpha > s$ and decreases otherwise. Numerical simulations confirm this conclusion; see Fig. B-13A.

In the spatial model, $u = \sqrt{\alpha - s}$, so the mutant can invade only when $s < \alpha$, which is consistent with the local well-mixed competition that we just described.

B.3.2 Growth-dispersal tradeoff model

The well-mixed limit for the growth-dispersal tradeoff model reads

$$\begin{aligned} \frac{n_{\text{W}}}{dt} &= r n_{\text{W}}(1 - n_{\text{W}} - n_{\text{M}}), \\ \frac{n_{\text{M}}}{dt} &= r(1+s) n_{\text{M}}(1 - n_{\text{W}} - n_{\text{M}}). \end{aligned} \tag{B.30}$$

The qualitative behavior of this system of equations is identical to that of the cheater-cooperator model. Any population below the carrying capacity with positive densities of the two types evolves to one of the neutral fixed points on $n_{\text{M}} + n_{\text{W}} = 1$. The change of the mutant fraction can be determined from the following first integral

$$\frac{n_{\text{W}}^{1+s}}{n_{\text{M}}} = n^s \frac{(1-f)^{1+s}}{f} = C. \tag{B.31}$$

The analysis, identical to the one we just described, shows that the frequency of the mutant increases as long as $s > 0$. This is consistent both with the expansion velocity $u = 2\sqrt{Ds}$ and numerical simulations (Fig. B-13).

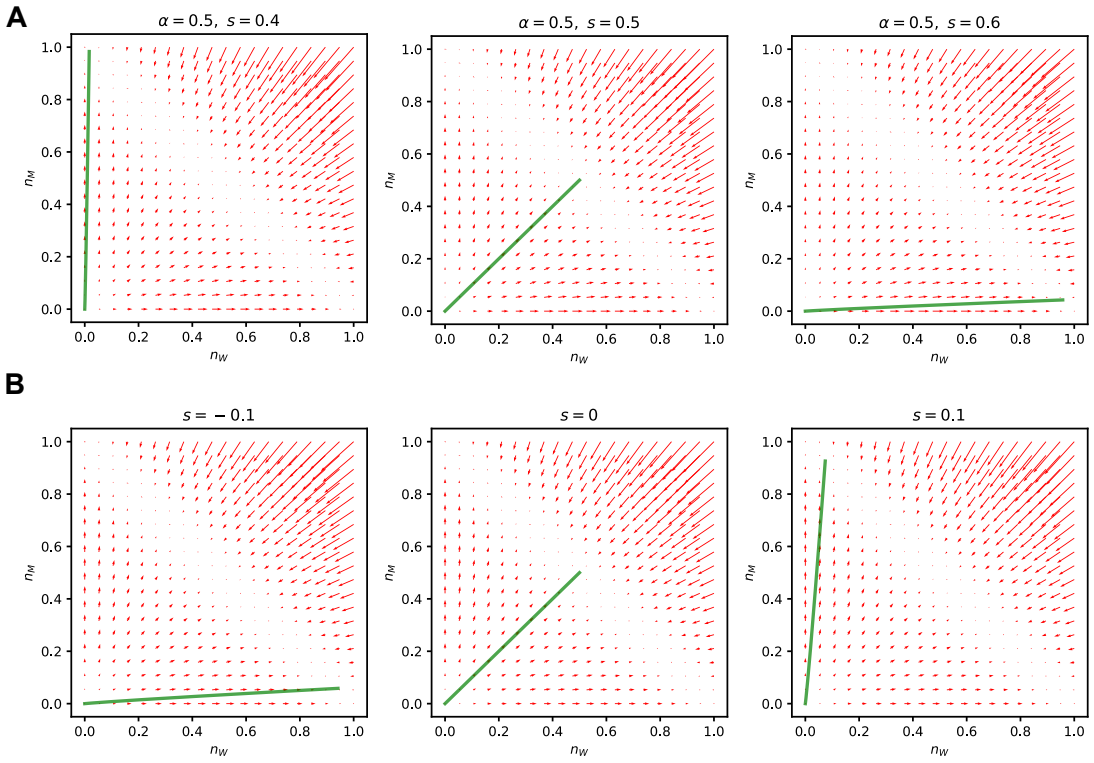

Figure B-13: Phase portraits of ODE dynamics. In each panel, red arrows represent $(dn_{\mathrm{W}}/dt, dn_{\mathrm{M}}/dt)$ and green curve shows the trajectory from small initial population $(n_{\mathrm{W}}, n_{\mathrm{M}}) = (10^{-12}, 10^{-12})$. (A) Phase portraits for cheater-cooperator interaction model. (B) Phase portraits for growth-dispersal tradeoff model.

Bibliography

[1] Edward R Abraham. The generation of plankton patchiness by turbulent stirring. *Nature*, 391(6667):577–580, 1998.

[2] Clare Abreu, Anthony Ortiz Lopez, and Jeff Gore. Pairing off: a bottom-up approach to the human gut microbiome. *Molecular Systems Biology*, 14(6):e8425, 2018.

[3] Clare I Abreu, Vilhelm L Andersen Woltz, Jonathan Friedman, and Jeff Gore. Microbial communities display alternative stable states in a fluctuating environment. *PLoS computational biology*, 16(5):e1007934, 2020.

[4] Clare I Abreu, Jonathan Friedman, Vilhelm L Andersen Woltz, and Jeff Gore. Mortality causes universal changes in microbial community composition. *Nature communications*, 10(1):1–9, 2019.

[5] Benjamin Allen, Jeff Gore, and Martin A Nowak. Spatial dilemmas of diffusible public goods. *Elife*, 2:e01169, 2013.

[6] Stefano Allesina and Jonathan M Levine. A competitive network theory of species diversity. *Proceedings of the National Academy of Sciences*, 108(14):5638–5642, 2011.

[7] Philip W Anderson. More is different: broken symmetry and the nature of the hierarchical structure of science. *Science*, 177(4047):393–396, 1972.

[8] Marco Tulio Angulo, Aaron Kelley, Luis Montejano, Chuliang Song, and Serguei Saavedra. Coexistence holes characterize the assembly and disassembly of multispecies systems. *Nature Ecology & Evolution*, pages 1–11, 2021.

[9] Robert A Armstrong and Richard McGehee. Competitive exclusion. *The American Naturalist*, 115(2):151–170, 1980.

[10] Nicholas H Barton and Brian Charlesworth. Genetic revolutions, founder effects, and speciation. *Annual review of ecology and systematics*, 15(1):133–164, 1984.

[11] Marianne Bauer and Erwin Frey. Multiple scales in metapopulations of public goods producers. *Physical Review E*, 97(4):042307, 2018.

[12] Eshel Ben-Jacob, Inon Cohen, and Herbert Levine. Cooperative self-organization of microorganisms. *Advances in Physics*, 49(4):395–554, 2000.

[13] Olivier Bénichou, Vincent Calvez, Nicolas Meunier, and Raphael Voituriez. Front acceleration by dynamic selection in fisher population waves. *Physical Review E*, 86(4):041908, 2012.

[14] Roeland L Berendsen, Corné MJ Pieterse, and Peter AHM Bakker. The rhizosphere microbiome and plant health. *Trends in plant science*, 17(8):478–486, 2012.

[15] Ian Billick and Ted J Case. Higher order interactions in ecological communities: what are they and how can they be detected? *Ecology*, 75(6):1529–1543, 1994.

[16] Gabriel Birzu, Oskar Hallatschek, and Kirill S Korolev. Fluctuations uncover a distinct class of traveling waves. *Proceedings of the National Academy of Sciences*, 115(16):E3645–E3654, 2018.

[17] Gabriel Birzu, Sakib Matin, Oskar Hallatschek, and Kirill S Korolev. Genetic drift in range expansions is very sensitive to density dependence in dispersal and growth. *Ecology Letters*, 22(11):1817–1827, 2019.

[18] Blox Bloxham, Hyunseok Lee, and Jeff Gore. Diauxic lags explain unexpected coexistence in multi-resource environments. *Molecular Systems Biology*, 18(5):e10630, 2022.

[19] Dries Bonte, Hans Van Dyck, James M Bullock, Aurélie Coulon, Maria Delgado, Melanie Gibbs, Valerie Lehouck, Erik Matthysen, Karin Mustin, Marjo Saastamoinen, et al. Costs of dispersal. *Biological reviews*, 87(2):290–312, 2012.

[20] Max Born and Emil Wolf. *Principles of optics: electromagnetic theory of propagation, interference and diffraction of light*. Elsevier, 2013.

[21] Lars Bosshard, Isabelle Dupanloup, Olivier Tenaillon, Rémy Bruggmann, Martin Ackermann, Stephan Peischl, and Laurent Excoffier. Accumulation of deleterious mutations during bacterial range expansions. *Genetics*, 207(2):669–684, 2017.

[22] Alberto Bressan. Differential inclusions and the control of forest fires. *Journal of Differential Equations*, 243(2):179–207, 2007.

[23] Jonathan M Chase and Mathew A Leibold. *Ecological niches*. University of Chicago Press, 2009.

[24] Peter Chesson. Mechanisms of maintenance of species diversity. *Annual review of Ecology and Systematics*, 31(1):343–366, 2000.

[25] Human Microbiome Project Consortium et al. Structure, function and diversity of the healthy human microbiome. *nature*, 486(7402):207, 2012.

[26] Franck Courchamp, Tim Clutton-Brock, and Bryan Grenfell. Inverse density dependence and the allee effect. *Trends in ecology & evolution*, 14(10):405–410, 1999.

[27] Katharine Z Coyte, Chitong Rao, Seth Rakoff-Nahoum, and Kevin R Foster. Ecological rules for the assembly of microbiome communities. *PLoS biology*, 19(2):e3001116, 2021.

[28] Jonas Cremer, Tomoya Honda, Ying Tang, Jerome Wong-Ng, Massimo Vergassola, and Terence Hwa. Chemotaxis as a navigation strategy to boost range expansion. *Nature*, 575(7784):658–663, 2019.

[29] Jonas Cremer, Anna Melbinger, Karl Wienand, Tania Henriquez, Heinrich Jung, and Erwin Frey. Cooperation in microbial populations: theory and experimental model systems. *Journal of molecular biology*, 431(23):4599–4644, 2019.

[30] Martina Dal Bello, Hyunseok Lee, Akshit Goyal, and Jeff Gore. Resource–diversity relationships in bacterial communities reflect the network structure of microbial metabolism. *Nature Ecology & Evolution*, 5(10):1424–1434, 2021.

[31] Manoshi S Datta, Elzbieta Sliwerska, Jeff Gore, Martin F Polz, and Otto X Cordero. Microbial interactions lead to rapid micro-scale successions on model marine particles. *Nature communications*, 7(1):1–7, 2016.

[32] Manoshi Sen Datta, Kirill S Korolev, Ivana Cvijovic, Carmel Dudley, and Jeff Gore. Range expansion promotes cooperation in an experimental microbial metapopulation. *Proceedings of the National Academy of Sciences*, 110(18):7354–7359, 2013.

[33] Maxime Deforet, Carlos Carmona-Fontaine, Kirill S Korolev, and Joao B Xavier. Evolution at the edge of expanding populations. *The American Naturalist*, 194(3):291–305, 2019.

[34] Jared M Diamond. Assembly of species communities. *Ecology and evolution of communities*, pages 342–444, 1975.

[35] James A Drake. Community-assembly mechanics and the structure of an experimental species ensemble. *The American Naturalist*, 137(1):1–26, 1991.

[36] M Drancourt, C Bollet, A Carta, and P Rousselier. Phylogenetic analyses of klebsiella species delineate klebsiella and raoultella gen. nov., with description of raoultella ornithinolytica comb. nov., raoultella terrigena comb. nov. and raoultella planticola comb. nov. *International journal of systematic and evolutionary microbiology*, 51(3):925–932, 2001.

[37] Rick Durrett and Simon Levin. Spatial aspects of interspecific competition. *Theoretical population biology*, 53(1):30–43, 1998.

[38] A Ershadi, E Weiss, E Verduzco, D Chia, and M Sadigh. Emerging pathogen: a case and review of raoultella planticola. *Infection*, 42(6):1043–1046, 2014.

[39] Laurent Excoffier, Matthieu Foll, and Rémy J Petit. Genetic consequences of range expansions. *Annual Review of Ecology, Evolution, and Systematics*, 40:481–501, 2009.

[40] Paul G Falkowski, Tom Fenchel, and Edward F Delong. The microbial engines that drive earth's biogeochemical cycles. *science*, 320(5879):1034–1039, 2008.

[41] FDC Farrell, Oskar Hallatschek, D Marenduzzo, and B Waclaw. Mechanically driven growth of quasi-two-dimensional microbial colonies. *Physical review letters*, 111(16):168101, 2013.

[42] Frank Xavier Ferrer-González, Brittany Widner, Nicole R Holderman, John Glushka, Arthur S Edison, Elizabeth B Kujawinski, and Mary Ann Moran. Resource partitioning of phytoplankton metabolites that support bacterial heterotrophy. *The ISME journal*, 15(3):762–773, 2021.

[43] Ronald Aylmer Fisher. The wave of advance of advantageous genes. *Annals of eugenics*, 7(4):355–369, 1937.

[44] Harry J Flint, Karen P Scott, Petra Louis, and Sylvia H Duncan. The role of the gut microbiota in nutrition and health. *Nature reviews Gastroenterology & hepatology*, 9(10):577–589, 2012.

[45] David T Fraebel, Harry Mickalide, Diane Schnitkey, Jason Merritt, Thomas E Kuhlman, and Seppe Kuehn. Environment determines evolutionary trajectory in a constrained phenotypic space. *Elife*, 6:e24669, 2017.

[46] James K Fredrickson. Ecological communities by design. *Science*, 348(6242):1425–1427, 2015.

[47] Jonathan Friedman, Logan M Higgins, and Jeff Gore. Community structure follows simple assembly rules in microbial microcosms. *Nature ecology & evolution*, 1(5):1–7, 2017.

[48] Michel Fruchart, Ryo Hanai, Peter B Littlewood, and Vincenzo Vitelli. Non-reciprocal phase transitions. *Nature*, 592(7854):363–369, 2021.

[49] He Fu, Mario Uchimiya, Jeff Gore, and Mary Ann Moran. Ecological drivers of bacterial community assembly in synthetic phycospheres. *Proceedings of the National Academy of Sciences*, 117(7):3656–3662, 2020.

[50] Tadashi Fukami. Historical contingency in community assembly: integrating niches, species pools, and priority effects. *Annual Review of Ecology, Evolution, and Systematics*, 46:1–23, 2015.

[51] Joshua E Goldford, Nanxi Lu, Djordje Bajić, Sylvie Estrela, Mikhail Tikhonov, Alicia Sanchez-Gorostiaga, Daniel Segrè, Pankaj Mehta, and Alvaro Sanchez. Emergent simplicity in microbial community assembly. *Science*, 361(6401):469–474, 2018.

[52] Alison L Gould, Vivian Zhang, Lisa Lamberti, Eric W Jones, Benjamin Obadia, Nikolaos Korasidis, Alex Gavryushkin, Jean M Carlson, Niko Beerenwinkel, and William B Ludington. Microbiome interactions shape host fitness. *Proceedings of the National Academy of Sciences*, 115(51):E11951–E11960, 2018.

[53] Hans-Peter Grossart, Thomas Kiørboe, Kam Tang, and Helle Ploug. Bacterial colonization of particles: growth and interactions. *Applied and environmental microbiology*, 69(6):3500–3509, 2003.

[54] Tobias Großkopf and Orkun S Soyer. Synthetic microbial communities. *Current opinion in microbiology*, 18:72–77, 2014.

[55] Sebastian Gude, Erçağ Pinçe, Katja M Taute, Anne-Bart Seinen, Thomas S Shimizu, and Sander J Tans. Bacterial coexistence driven by motility and spatial competition. *Nature*, 578(7796):588–592, 2020.

[56] Oskar Hallatschek and Daniel S Fisher. Acceleration of evolutionary spread by long-range dispersal. *Proceedings of the National Academy of Sciences*, 111(46):E4911–E4919, 2014.

[57] Oskar Hallatschek, Pascal Hersen, Sharad Ramanathan, and David R Nelson. Genetic drift at expanding frontiers promotes gene segregation. *Proceedings of the National Academy of Sciences*, 104(50):19926–19930, 2007.

[58] Oskar Hallatschek and David R Nelson. Gene surfing in expanding populations. *Theoretical population biology*, 73(1):158–170, 2008.

[59] Luh Hang-Kwang and Stuart L Pimm. The assembly of ecological communities: a minimalist approach. *Journal of Animal Ecology*, pages 749–765, 1993.

[60] Ilkka Hanski. Metapopulation dynamics. *Nature*, 396(6706):41–49, 1998.

[61] Alan Hastings, Kim Cuddington, Kendi F Davies, Christopher J Dugaw, Sarah Elmendorf, Amy Freestone, Susan Harrison, Matthew Holland, John Lambrinos, Urmila Malvadkar, et al. The spatial spread of invasions: new developments in theory and evidence. *Ecology Letters*, 8(1):91–101, 2005.

[62] Jordan M Horowitz and Mehran Kardar. Bacterial range expansions on a growing front: Roughness, fixation, and directed percolation. *Physical Review E*, 99(4):042134, 2019.

[63] Jiliang Hu, Daniel R Amor, Matthieu Barbier, Guy Bunin, and Jeff Gore. Emergent phases of ecological diversity and dynamics mapped in microcosms. *Science*, 378(6615):85–89, 2022.

[64] Stephen P Hubbell. The unified neutral theory of biodiversity and biogeography (mpb-32). In *The Unified Neutral Theory of Biodiversity and Biogeography (MPB-32)*. Princeton University Press, 2011.

[65] Jef Huisman and Franz J Weissing. Biodiversity of plankton by species oscillations and chaos. *Nature*, 402(6760):407–410, 1999.

[66] G Evelyn Hutchinson. Homage to santa rosalia or why are there so many kinds of animals? *The American Naturalist*, 93(870):145–159, 1959.

[67] Jonathan M Jeschke and Tina Heger. *Invasion biology: hypotheses and evidence*, volume 9. CABI, 2018.

[68] Eric W Jones, Jean M Carlson, David A Sivak, and William B Ludington. Stochastic microbiome assembly depends on context. *Proceedings of the National Academy of Sciences*, 119(7):e2115877119, 2022.

[69] Brandon L Jutras, Robert B Lochhead, Zachary A Kloos, Jacob Biboy, Klemen Strle, Carmen J Booth, Sander K Govers, Joe Gray, Peter Schumann, Waldemar Vollmer, et al. Borrelia burgdorferi peptidoglycan is a persistent antigen in patients with lyme arthritis. *Proceedings of the National Academy of Sciences*, 116(27):13498–13507, 2019.

[70] Daniel B Kearns. A field guide to bacterial swarming motility. *Nature Reviews Microbiology*, 8(9):634–644, 2010.

[71] Jared Kehe, Anthony Kulesa, Anthony Ortiz, Cheri M Ackerman, Sri Gowtham Thakku, Daniel Sellers, Seppe Kuehn, Jeff Gore, Jonathan Friedman, and Paul C Blainey. Massively parallel screening of synthetic microbial communities. *Proceedings of the National Academy of Sciences*, 116(26):12804–12809, 2019.

[72] Evelyn F Keller and Lee A Segel. Model for chemotaxis. *Journal of theoretical biology*, 30(2):225–234, 1971.

[73] Benjamin Kerr, Margaret A Riley, Marcus W Feldman, and Brendan JM Bohannan. Local dispersal promotes biodiversity in a real-life game of rock–paper–scissors. *Nature*, 418(6894):171–174, 2002.

[74] Seraina Klopfstein, Mathias Currat, and Laurent Excoffier. The fate of mutations surfing on the wave of a range expansion. *Molecular biology and evolution*, 23(3):482–490, 2006.

[75] Andreï N Kolmogorov. A study of the equation of diffusion with increase in the quantity of matter, and its application to a biological problem. *Moscow University Bulletin of Mathematics*, 1:1–25, 1937.

[76] Kirill S Korolev. The fate of cooperation during range expansions. *PLoS Comput Biol*, 9(3):e1002994, 2013.

[77] Kirill S Korolev. Evolution arrests invasions of cooperative populations. *Physical review letters*, 115(20):208104, 2015.

[78] Kirill S Korolev, Mikkel Avlund, Oskar Hallatschek, and David R Nelson. Genetic demixing and evolution in linear stepping stone models. *Reviews of modern physics*, 82(2):1691, 2010.

[79] Kirill S Korolev, Melanie J I Müller, Nilay Karahan, Andrew W Murray, Oskar Hallatschek, and David R Nelson. Selective sweeps in growing microbial colonies. *Physical Biology*, 9(2):026008, 2012.

[80] Kirill S Korolev, Joao B Xavier, and Jeff Gore. Turning ecology and evolution against cancer. *Nature Reviews Cancer*, 14(5):371–380, 2014.

[81] Kirill S Korolev, Joao B Xavier, David R Nelson, and Kevin R Foster. A quantitative test of population genetics using spatiogenetic patterns in bacterial colonies. *The American Naturalist*, 178(4):538–552, 2011.

[82] Mark Kot, Mark A Lewis, and Pauline van den Driessche. Dispersal data and the spread of invading organisms. *Ecology*, 77(7):2027–2042, 1996.

[83] Nathan JB Kraft, Peter B Adler, Oscar Godoy, Emily C James, Steve Fuller, and Jonathan M Levine. Community assembly, coexistence and the environmental filtering metaphor. *Functional ecology*, 29(5):592–599, 2015.

[84] Simon Lax, Clare I Abreu, and Jeff Gore. Higher temperatures generically favour slower-growing bacterial species in multispecies communities. *Nature ecology & evolution*, 4(4):560–567, 2020.

[85] Hyunseok Lee, Jeff Gore, and Kirill S Korolev. Slow expanders invade by forming dented fronts in microbial colonies. *Proceedings of the National Academy of Sciences*, 119(1):e2108653119, 2022.

[86] Donald A Levin and Harold W Kerster. The dependence of bee-mediated pollen and gene dispersal upon plant density. *Evolution*, 23(4):560–571, 1969.

[87] Simon A Levin. Dispersion and population interactions. *The American Naturalist*, 108(960):207–228, 1974.

[88] Jonathan M Levine, Jordi Bascompte, Peter B Adler, and Stefano Allesina. Beyond pairwise mechanisms of species coexistence in complex communities. *Nature*, 546(7656):56–64, 2017.

[89] Zhiyuan Li, Bo Liu, Sophia Hsin-Jung Li, Christopher G King, Zemer Gitai, and Ned S Wingreen. Modeling microbial metabolic trade-offs in a chemostat. *PLoS computational biology*, 16(8):e1008156, 2020.

[90] Gipsi Lima-Mendez, Karoline Faust, Nicolas Henry, Johan Decelle, Sébastien Colin, Fabrizio Carcillo, Samuel Chaffron, J Cesar Ignacio-Espinosa, Simon Roux, Flora Vincent, et al. Determinants of community structure in the global plankton interactome. *Science*, 348(6237), 2015.

[91] Yen Ting Lin, Hyejin Kim, and Charles R Doering. Demographic stochasticity and evolution of dispersion i. spatially homogeneous environments. *Journal of mathematical biology*, 70(3):647–678, 2015.

[92] Ariel Lipson, Stephen G Lipson, and Henry Lipson. *Optical physics*. Cambridge University Press, 2010.

[93] Jaime G Lopez and Ned S Wingreen. Noisy metabolism can promote microbial cross-feeding. *Elife*, 11:e70694, 2022.

[94] Robert MacArthur. Species packing and competitive equilibrium for many species. *Theoretical population biology*, 1(1):1–11, 1970.

[95] Hafiz Maherali and John N Klironomos. Influence of phylogeny on fungal community assembly and ecosystem functioning. *science*, 316(5832):1746–1748, 2007.

[96] Christopher P Mancuso, Hyunseok Lee, Clare I Abreu, Jeff Gore, and Ahmad S Khalil. Environmental fluctuations reshape an unexpected diversity-disturbance relationship in a microbial community. *Elife*, 10:e67175, 2021.

[97] Robert Marsland, Wenping Cui, Joshua Goldford, and Pankaj Mehta. The community simulator: A python package for microbial ecology. *PloS one*, 15(3):e0230430, 2020.

[98] Robert Marsland III, Wenping Cui, and Pankaj Mehta. The minimum environmental perturbation principle: A new perspective on niche theory. *The American Naturalist*, 196(3):291–305, 2020.

[99] Katsuyoshi Matsuoka and Takanori Kanai. The gut microbiota and inflammatory bowel disease. In *Seminars in immunopathology*, volume 37, pages 47–55. Springer, 2015.

[100] Erik Matthysen. Density-dependent dispersal in birds and mammals. *Ecography*, 28(3):403–416, 2005.

[101] Robert M May and Warren J Leonard. Nonlinear aspects of competition between three species. *SIAM journal on applied mathematics*, 29(2):243–253, 1975.

[102] Nittay Meroz, Nesli Tovi, Yael Sorokin, and Jonathan Friedman. Community composition of microbial microcosms follows simple assembly rules at evolutionary timescales. *Nature communications*, 12(1):1–9, 2021.

[103] Sara Mitri, Ellen Clarke, and Kevin R Foster. Resource limitation drives spatial organization in microbial groups. *The ISME journal*, 10(6):1471–1482, 2016.

[104] Babak Momeni, Kristen A Brileya, Matthew W Fields, and Wenying Shou. Strong inter-population cooperation leads to partner intermixing in microbial communities. *elife*, 2:e00230, 2013.

[105] Babak Momeni, Li Xie, and Wenying Shou. Lotka-volterra pairwise modeling fails to capture diverse pairwise microbial interactions. *Elife*, 6:e25051, 2017.

[106] Harold A Mooney and Elsa E Cleland. The evolutionary impact of invasive species. *Proceedings of the National Academy of Sciences*, 98(10):5446–5451, 2001.

[107] RP Moore, WD Robinson, IJ Lovette, and TR Robinson. Experimental evidence for extreme dispersal limitation in tropical forest birds. *Ecology letters*, 11(9):960–968, 2008.

[108] Melanie JI Müller, Beverly I Neugeboren, David R Nelson, and Andrew W Murray. Genetic drift opposes mutualism during spatial population expansion. *Proceedings of the National Academy of Sciences*, 111(3):1037–1042, 2014.

[109] James D. Murray. *Mathematical Biology*. Berlin: Springer, 2003.

[110] Carey D Nadell, Knut Drescher, and Kevin R Foster. Spatial structure, cooperation and competition in biofilms. *Nature Reviews Microbiology*, 14(9):589–600, 2016.

[111] Carey D Nadell, Kevin R Foster, and Joao B Xavier. Emergence of spatial structure in cell groups and the evolution of cooperation. *PLoS Comput Biol*, 6(3):e1000716, 2010.

[112] Bin Ni, Bhaswar Ghosh, Ferencz S Paldy, Remy Colin, Thomas Heimerl, and Victor Sourjik. Evolutionary remodeling of bacterial motility checkpoint control. *Cell reports*, 18(4):866–877, 2017.

[113] Lori Niehaus, Ian Boland, Minghao Liu, Kevin Chen, David Fu, Catherine Henckel, Kaitlin Chaung, Suyen Espinoza Miranda, Samantha Dyckman, Matthew Crum, et al. Microbial coexistence through chemical-mediated interactions. *Nature communications*, 10(1):1–12, 2019.

[114] Anthony Ortiz, Nicole M Vega, Christoph Ratzke, and Jeff Gore. Interspecies bacterial competition regulates community assembly in the c. elegans intestine. *The ISME Journal*, 15(7):2131–2145, 2021.

[115] James P O'Dwyer. Whence lotka-volterra? *Theoretical Ecology*, 11(4):441–452, 2018.

[116] Alan R Pacheco, Melisa L Osborne, and Daniel Segrè. Non-additive microbial community responses to environmental complexity. *Nature communications*, 12(1):1–11, 2021.

[117] Stephan Peischl and Kimberly J Gilbert. Evolution of dispersal can rescue populations from expansion load. *The American Naturalist*, 195(2):349–360, 2020.

[118] Benjamin L Phillips, Gregory P Brown, Jonathan K Webb, and Richard Shine. Invasion and the evolution of speed in toads. *Nature*, 439(7078):803–803, 2006.

[119] Philippe Piccardi, Björn Vessman, and Sara Mitri. Toxicity drives facilitation between 4 bacterial species. *Proceedings of the National Academy of Sciences*, 116(32):15979–15984, 2019.

[120] Simone Pigolotti, Roberto Benzi, Mogens H Jensen, and David R Nelson. Population genetics in compressible flows. *Physical review letters*, 108(12):128102, 2012.

[121] Anna Posfai, Thibaud Taillefumier, and Ned S Wingreen. Metabolic trade-offs promote diversity in a model ecosystem. *Physical review letters*, 118(2):028103, 2017.

[122] William H Press, Saul A Teukolsky, William T Vetterling, and Brian P Flannery. *Numerical recipes 3rd edition: The art of scientific computing*. Cambridge university press, 2007.

[123] Arthur Prindle, Jintao Liu, Munehiro Asally, San Ly, Jordi Garcia-Ojalvo, and Gürol M Süel. Ion channels enable electrical communication in bacterial communities. *nature*, 527(7576):59–63, 2015.

[124] Lionel Roques, Jimmy Garnier, François Hamel, and Etienne K Klein. Allee effect promotes diversity in traveling waves of colonization. *Proceedings of the National Academy of Sciences*, 109(23):8828–8833, 2012.

[125] James Rosindell, Stephen P Hubbell, and Rampal S Etienne. The unified neutral theory of biodiversity and biogeography at age ten. *Trends in ecology & evolution*, 26(7):340–348, 2011.

[126] Serguei Saavedra, Rudolf P Rohr, Jordi Bascompte, Oscar Godoy, Nathan JB Kraft, and Jonathan M Levine. A structural approach for understanding multispecies coexistence. *Ecological Monographs*, 87(3):470–486, 2017.

[127] Ann K Sakai, Fred W Allendorf, Jodie S Holt, David M Lodge, Jane Molofsky, Kimberly A With, Syndallas Baughman, Robert J Cabin, Joel E Cohen, Norman C Ellstrand, et al. The population biology of invasive species. *Annual review of ecology and systematics*, 32(1):305–332, 2001.

[128] Joshua Schimel and Sean Michael Schaeffer. Microbial control over carbon cycling in soil. *Frontiers in microbiology*, 3:348, 2012.

[129] Rudolf O. Schlechter, Hyunwoo Jun, Michał Bernach, Simisola Oso, Erica Boyd, Dian A. Muñoz-Lintz, Renwick C. J. Dobson, Daniela M. Remus, and Mitja N. P. Remus-Emsermann. Chromatic bacteria – a broad host-range plasmid and chromosomal insertion toolbox for fluorescent protein expression in bacteria. *Frontiers in Microbiology*, 9:3052, 2018.

[130] Sebastian J Schreiber and Seth Rittenhouse. From simple rules to cycling in community assembly. *Oikos*, 105(2):349–358, 2004.

[131] Erwin Schrödinger et al. *What is life?: With mind and matter and autobiographical sketches*. Cambridge University Press, 1992.

[132] Carlos A Serván and Stefano Allesina. Tractable models of ecological assembly. *Ecology Letters*, 24(5):1029–1037, 2021.

[133] Hong-Yan Shih, Harry Mickalide, David T Fraebel, Nigel Goldenfeld, and Seppe Kuehn. Biophysical constraints determine the selection of phenotypic fluctuations during directed evolution. *Physical biology*, 15(6):065003, 2018.

[134] Richard Shine, Gregory P Brown, and Benjamin L Phillips. An evolutionary process that assembles phenotypes through space rather than through time. *Proceedings of the National Academy of Sciences*, 108(14):5708–5711, 2011.

[135] Adam D Simmons and Chris D Thomas. Changes in dispersal during species' range expansions. *The American Naturalist*, 164(3):378–395, 2004.

[136] John Gordon Skellam. Random dispersal in theoretical populations. *Biometrika*, 38(1/2):196–218, 1951.

[137] Montgomery Slatkin and Laurent Excoffier. Serial founder effects during range expansion: a spatial analog of genetic drift. *Genetics*, 191(1):171–181, 2012.

[138] Richard R Stein, Vanni Bucci, Nora C Toussaint, Charlie G Buffie, Gunnar Rätsch, Eric G Pamer, Chris Sander, and Joao B Xavier. Ecological modeling from time-series inference: insight into dynamics and stability of intestinal microbiota. *PLoS computational biology*, 9(12):e1003388, 2013.

[139] Ofer Stempler, Amit K Baidya, Saurabh Bhattacharya, Ganesh Babu Malli Mohan, Elhanan Tzipilevich, Lior Sinai, Gideon Mamou, and Sigal Ben-Yehuda. Interspecies nutrient extraction and toxin delivery between bacteria. *Nature communications*, 8(1):1–9, 2017.

[140] Shinichi Sunagawa, Luis Pedro Coelho, Samuel Chaffron, Jens Roat Kultima, Karine Labadie, Guillem Salazar, Bardya Djahanschiri, Georg Zeller, Daniel R Mende, Adriana Alberti, et al. Structure and function of the global ocean microbiome. *Science*, 348(6237):1261359, 2015.

[141] Caz M Taylor and Alan Hastings. Allee effects in biological invasions. *Ecology Letters*, 8(8):895–908, 2005.

[142] Chris D Thomas, EJ Bodsworth, Robert J Wilson, Adam D Simmons, Zoe G Davies, Martin Musche, and Larissa Conradt. Ecological and evolutionary processes at expanding range margins. *Nature*, 411(6837):577–581, 2001.

[143] David Tilman. Resources: a graphical-mechanistic approach to competition and predation. *The American Naturalist*, 116(3):362–393, 1980.

[144] David Tilman. Competition and biodiversity in spatially structured habitats. *Ecology*, 75(1):2–16, 1994.

[145] David Tilman. *Resource Competition and Community Structure.(MPB-17), Volume 17*. Princeton university press, 2020.

[146] Justin MJ Travis and Calvin Dytham. Dispersal evolution during invasions. *Evolutionary Ecology Research*, 4(8):1119–1129, 2002.

[147] Naomi Iris van den Berg, Daniel Machado, Sophia Santos, Isabel Rocha, Jeremy Chacón, William Harcombe, Sara Mitri, and Kiran R Patil. Ecological modelling approaches for predicting emergent properties in microbial communities. *Nature Ecology & Evolution*, pages 1–11, 2022.

[148] Stéfan van der Walt, Johannes L. Schönberger, Juan Nunez-Iglesias, François Boulogne, Joshua D. Warner, Neil Yager, Emmanuelle Gouillart, Tony Yu, and the scikit-image contributors. scikit-image: image processing in Python. *PeerJ*, 2:e453, 2014.

[149] Dave Van Ditmarsch, Kerry E Boyle, Hassan Sakhtah, Jennifer E Oyler, Carey D Nadell, Éric Déziel, Lars EP Dietrich, and Joao B Xavier. Convergent evolution of hyperswarming leads to impaired biofilm formation in pathogenic bacteria. *Cell reports*, 4(4):697–708, 2013.

[150] J David Van Dyken, Melanie JI Müller, Keenan ML Mack, and Michael M Desai. Spatial population expansion promotes the evolution of cooperation in an experimental prisoner's dilemma. *Current Biology*, 23(10):919–923, 2013.

[151] John H Vandermeer. The competitive structure of communities: an experimental approach with protozoa. *Ecology*, 50(3):362–371, 1969.

[152] Ophelia S Venturelli, Alex V Carr, Garth Fisher, Ryan H Hsu, Rebecca Lau, Benjamin P Bowen, Susan Hromada, Trent Northen, and Adam P Arkin. Deciphering microbial interactions in synthetic human gut microbiome communities. *Molecular systems biology*, 14(6):e8157, 2018.

[153] Mya R Warren, Hui Sun, Yue Yan, Jonas Cremer, Bo Li, and Terence Hwa. Spatiotemporal establishment of dense bacterial colonies growing on hard agar. *Elife*, 8:e41093, 2019.

[154] Philip H Warren, Richard Law, and Anita J Weatherby. Mapping the assembly of protist communities in microcosms. *Ecology*, 84(4):1001–1011, 2003.

[155] Jonathan M Waters, Ceridwen I Fraser, and Godfrey M Hewitt. Founder takes all: density-dependent processes structure biodiversity. *Trends in ecology & evolution*, 28(2):78–85, 2013.

[156] Robert H Whittaker. A consideration of climax theory: the climax as a population and pattern. *Ecological monographs*, 23(1):41–78, 1953.

[157] Stefanie Widder, Rosalind J Allen, Thomas Pfeiffer, Thomas P Curtis, Carsten Wiuf, William T Sloan, Otto X Cordero, Sam P Brown, Babak Momeni, Wenying Shou, et al. Challenges in microbial ecology: building predictive understanding of community function and dynamics. *The ISME journal*, 10(11):2557–2568, 2016.

[158] J Bastow Wilson, Elly Spijkerman, and Jef Huisman. Is there really insufficient support for tilman's r* concept? a comment on miller et al. *The american naturalist*, 169(5):700–706, 2007.

[159] J Timothy Wootton. The nature and consequences of indirect effects in ecological communities. *Annual review of ecology and systematics*, 25(1):443–466, 1994.

[160] Erik S Wright and Kalin H Vetsigian. Inhibitory interactions promote frequent bistability among competing bacteria. *Nature communications*, 7(1):1–7, 2016.

[161] Yandong Xiao, Marco Tulio Angulo, Jonathan Friedman, Matthew K Waldor, Scott T Weiss, and Yang-Yu Liu. Mapping the ecological networks of microbial communities. *Nature communications*, 8(1):1–12, 2017.

[162] Liyang Xiong, Yuansheng Cao, Robert Cooper, Wouter-Jan Rappel, Jeff Hasty, and Lev Tsimring. Flower-like patterns in multi-species bacterial colonies. *Elife*, 9:e48885, 2020.

[163] Jing Yan, Carey D Nadell, Howard A Stone, Ned S Wingreen, and Bonnie L Bassler. Extracellular-matrix-mediated osmotic pressure drives vibrio cholerae biofilm expansion and cheater exclusion. *Nature communications*, 8(1):1–11, 2017.

[164] Xiao Yi and Antony M Dean. Phenotypic plasticity as an adaptation to a functional trade-off. *Elife*, 5:e19307, 2016.

[165] Mary Lou Zeeman. Hopf bifurcations in competitive three-dimensional lotka–volterra systems. *Dynamics and stability of systems*, 8(3):189–216, 1993.